# Illuminating Molecular Mechanisms of Serotonin Transporter Regulation with Quantum Dot Single Particle Tracking

By

Danielle M. Bailey

Dissertation

Submitted to the Faculty of the

Graduate School of Vanderbilt University

in partial fulfillment of the requirements

for the degree of

Doctor of Philosophy

in

Interdisciplinary Materials Science

February 28, 2019

Nashville, Tennessee

Approved:

Professor Sandra Rosenthal

Professor Qi Zhang

Professor John McLean

Professor John Wilson

Professor Yaqiong Xu

## DEDICATION

Dedicated to my children, Daniel and William, for inspiring me in new ways every day; and to my loving husband, Stephen, for your unwavering support and patience throughout this journey.

## ACKNOWLEDGMENTS

Thank you to my advisor, Sandy, for taking a chance on me. I showed up at your door as a 5th grade science teacher asking to do this research, and you said yes. You have given me the space and freedom to pursue the research I am passionate about, and I appreciate the trust it takes to allow a graduate student to do that. Thank you for supporting me through both of my pregnancies during my time in graduate school and for making your lab a space where I felt comfortable being both a mom and a scientist. I am forever grateful for that.

Thank you to my co-advisor, Qi, for accepting me into your lab from day 1. You encouraged me to think critically about my work, kept me reading the literature consistently, and always pushed me to keep questioning. I appreciate everything you did for me during my time in your lab.

Thank you to the rest of my committee – John Wilson, John McLean, and Yaqiong Xu – for your time and insights. Thank you to the entire Rosenthal lab for the constant support, jokes, and fun. Nathaniel, I loved being your desk buddy; thanks for having all the answers to my questions and for the sticky note reminders. Ian, I always appreciated your conversation and sense of humor. Louie, thank you for the couch conversations and for being a thought partner. Kemar, thanks for always being open for advice (and for being my marathon buddy!). James, you were there for me so many times when I needed it – you encouraged me through the tough times in graduate school and also when I found out I was going to be a mom! Thank you for always helping me find and keep perspective on what is most important. Oleg – thank you for everything. You always kept me laughing, edited just about everything I wrote, helped me whiteboard ideas, taught me what to do with data – the ways you've helped me navigate grad school are endless. I appreciate your brutal honesty and how you are always true to yourself. It really was always a pleasure.

Kristina, thank you for always being available to talk about anything and everything – experiments, papers, ideas, life. We spent many, many hours together working through

QDs, doing dissections, and doing day to day tasks, and I am so glad I had you by my side for that. Sarah, I could NOT have gotten through this program without you, both professionally and personally! You have become such a dear friend to me, and I am so lucky to have you in my life. Thanks for loving me and my kiddos so well! Alisha, thank you for all the emergency snacks and letting me chat with you when I needed breaks. Janet, thank you for being there for me when I had no idea what I was doing as a first time mom. Your open door gave me peace on many occasions. Thank you for all the advice, stories, solidarity, and mentorship.

Thank you, Jake, for your friendship. You were the best study partner I could have hoped for, were endlessly patient and always positive. You make the people around you better, and I am so glad I got to know you during this experience. Stephanie, I am so glad I had you to keep me laughing throughout grad school. Thanks for all the good conversation, encouragement, and love! To the tribal council, Alex and Alice – I will always miss the special time we had together. Thanks for loving me for who I am and for being my safe space. Alice, you have become family. Thank you for loving my kids so well and for your friendship. Auvy and Nausheen – thank you for taking Daniel on so many occasions so I could get this dissertation done! It takes a village. And to my parents – Mom, Dad, Dan, and Janine – thank you for being endlessly supportive.

The biggest thank you goes to my husband, Stephen. You are the reason I am now at the finish line. You are the best partner, best friend, and father to our babies, and I will never be able to tell you how much your encouragement and faith in me means. Daniel (my qual baby) and Will (my dissertation baby) – it was a joy going on this adventure with you. You remind me what is most important and keep me moving forward. I hope I make you proud.

This work was supported financially by the IMS program at Vanderbilt University, NSF Graduate Research Fellowship Program under Grant No. DGE-1445197, and VINSE.

## TABLE OF CONTENTS

## LIST OF TABLES

## LIST OF FIGURES

## LIST OF ABBREVIATIONS

| | |
|---|---|
| 5-HT | Serotonin |
| 8-Br-cGMP | 8-Bromo-cyclic GMP |
| BG-DNA-QD | Benzylguanine-DNA-QD |
| DAT | Dopamine transporter protein |
| G56A | Gly56Ala |
| K-S Test | Kolmogorov-Smirnov Test |
| M$\beta$CD | Methyl-$\beta$-cyclodextrin |
| MSD | Mean square displacement |
| NET | Norepinephrine transporter protein |
| NTT | Neurotransmitter transporter |
| PEG | Polyethylene glycol |
| PKG | Protein kinase G |
| ptDNA | phosphorothioate DNA |
| QD | Quantum dot |
| SERT | Serotonin transporter protein |
| SPT | Single particle tracking |
| Thr276 | Threonine 276 |

# CHAPTER 1

## Introduction

> "New directions in science are launched by new tools much more often than by new concepts. The effect of a concept-driven revolution is to explain old things in new ways. The effect of a tool-driven revolution is to discover new things that have to be explained."
>
> *Imagined Worlds*, Freeman Dyson

Mood disorders, including major depression and bipolar disorder, affect almost 20 percent of the U.S. population. Additionally, depression is the leading cause of disability worldwide. These disorders place a huge burden on our global society, both economically and socially, and cost America over $193 billion in lost earnings every year (Insel, 2008). Individuals with mental disorders are also much more likely to develop chronic medical conditions, further accruing costs due to medical bills over time. Among adults who have serious mental illness, their life expectancies are on average 25 years shorter than individuals without serious mental illness. Beyond the physical implications of mental illness, individuals also suffer lower quality of life, educational struggles, poverty, and social problems, including homelessness (National Institute of Mental Health).

We still have a long way to go in understanding the underlying mechanisms of many neuropsychiatric disorders; so much so, that in 2014 the National Institutes of Health (NIH) launched the Brain Research through Advancing Innovative Neurotechnologies (BRAIN) Initiative to begin to tackle understanding these mechanisms. This initiative has devoted over 100 million dollars to discover new approaches to understanding the brain, both at

a large scale and single cell level. A key aspect of this initiative is to bring together researchers from a broad spectrum of fields – neuroscientists, engineers, chemists, biologists, physicists, pharmacologists – to work together to unravel the mystery that is the brain. As Professor Paul Alivisatos, a pioneer in the quantum dot community, puts it, "Understanding the brain is arguably one of the greatest scientific challenges of our time" (Alivisatos et al., 2012).

The Rosenthal lab is leading the charge in the intersection of nanoscience with neuroscience through probing individual neurotransmitter transporters with semiconductor nanocrystals called quantum dots (QDs). These transporters, specifically serotonin transporter (SERT) and dopamine transporter (DAT), are at the heart of many neuropsychiatric disorders, and QDs have allowed us to view these transporters behaving, both normally and in disease states, in real-time. QDs have the potential to revolutionize how we do neuroscience at the single particle level. This introduction will provide an overview of the basic properties and characteristics of QDs, their applications in biology and single particle tracking experiments, and the general motivation for the research presented in this dissertation.

## 1.1 Introduction to quantum dots

### 1.1.1 Quantum confinement in quantum dots

Quantum dots (QDs) are nanometer-sized semiconductor nanocrystals made of hundreds to thousands of atoms with sizes ranging from 2-10 nm. Cadmium selenide (CdSe) is one of the most common materials used commercially and is the material used throughout this work. To synthesize CdSe QDs with narrow size distributions, Cd and Se organometallic precursors are injected into hot trioctylphosphine oxide (TOPO) in a glove box to begin nucleation of the nanocrystals. The temperature is immediately dropped to allow growth until the desired size is achieved, at which point the reaction is stopped by pulling it from heat (Kippeny et al., 2002).

While the CdSe nanocrystals have the same wurtzite crystal structure as the bulk mate-

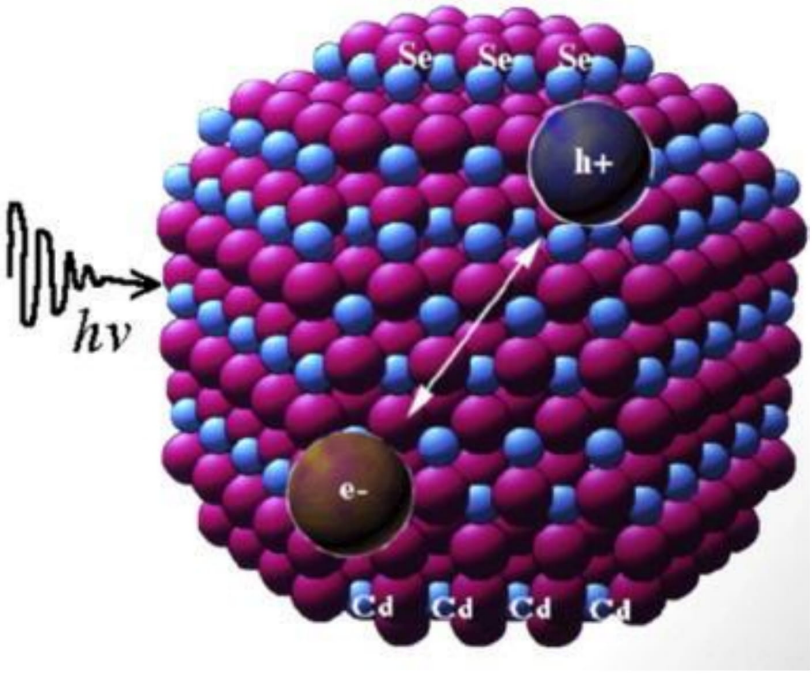


Figure 1.1: When a CdSe QD absorbs a photon, an electron hole pair is produced. The electron and hole cannot achieve the desired Bohr exciton radius, thus leading to quantum confinement. Quantum confinement of the electron and hole generates size-dependent emission wavelengths. Figure reproduced with permission from Elsevier (Rosenthal et al., 2011).

rial, their small size leads to unique optical and electronic properties. In the bulk material, absorption of a photon generates an electron-hole pair, where the electron orbits the hole at an average distance known as the Bohr exciton radius. For CdSe, this distance is about 56 angstroms. If the synthesized CdSe is less than 112 angstroms in diameter, the electron-hole pair becomes confined and cannot reach the desired distance, leading to quantum confinement (Figure 1.1). This quantum confinement shifts the energy states to higher levels. Energy levels become discrete and dependent on the diameter of the QD. As the diameter gets smaller, the band gap energy increases. For example, bulk CdSe has a band gap energy of 1.85 eV, while a 605 nm-emitting CdSe QD has a band gap energy of about 2.5 eV. The

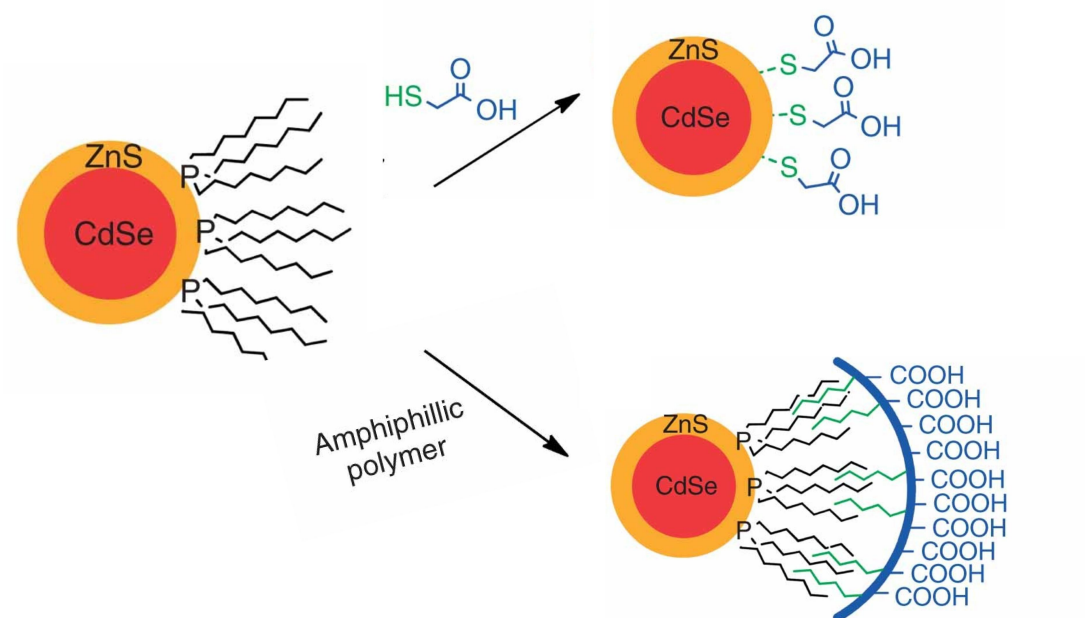


Figure 1.2: As synthesized, QDs are inorganic in nature, with hydrophobic ligands on the surface. For use in biological applications, QDs must be phase transferred to be aqueous. Two common strategies include ligand exchange (top panel) and polymer encapsulation (bottom panel). In the ligand exchange approach, native ligands are replaced with water soluble ligands. In the polymer encapsulation method, native ligands are kept, but water soluble ligands intercalate into the original ligands. Figure reproduced with permission from John Wiley and Sons (Chang et al., 2012a).

quantized energy states lead to differences in emission wavelength upon absorbance of a photon (Kippeny et al., 2002). QDs can thus be tuned to emit different wavelengths, which becomes useful in applications ranging from brighter, more vivid color in televisions and tablets to multiplexing during biological imaging experiments.

### 1.1.2 Generation of biocompatible QDs

As synthesized, QDs of a single core material were not efficient or photostable for meaningful applications. With just a core, dangling bonds exist on the surface due to undercoordinated surface atoms (Rosenthal et al., 2011). Hines et al. developed a way to overcome this by passivating the core QD material with a shell of wider band gap material, thus generating ”core/shell QDs”(Hines and Guyot-Sionnest, 1996). These QDs are used

today in applications ranging from lighting and televisions to biological labeling. The QDs used in this dissertation are commercially available CdSe/CdS/ZnS. Because the lattice mismatch between CdSe and ZnS is 14%, leading to preferential shell growth on the ZnS atoms, Cd atoms are included between the CdSe and ZnS layers to alleviate the mismatch and generate monodisperse core/shell structures with quantum yields of up to 95% (Rosenthal et al., 2011).

Upon synthesis, the core/shell QDs are capped with hydrophobic organic ligands that are not water-soluble. For use in biological systems, the QDs must be solubilized, which can happen in a couple of key ways. The two most popular methods are ligand exchange and polymer encapsulation. With ligand exchange, native hydrophobic ligands from the original synthesis are exchanged for bifunctional ligands containing a hydrophilic endgroup (Figure 1.2, top panel) (Medintz et al., 2005). This approach can decrease the overall size of the QD, which is advantageous when tagging receptors and transporters on a cell surface. However, ligand exchange can decrease the stability and quantum yield of the QD once the native ligands are removed. The preferred method for solubilization is polymer encapsulation. Water-soluble ligands intercalate into the native hydrophobic ligands, effectively coating the QD in an extra polymer layer (Figure 1.2, bottom panel) (Rosenthal et al., 2011). This method retains the native, as-synthesized ligands, which maintains stability and quantum yields, although it does increase overall size. These polymer-coated QDs also achieve excellent stability in physiologically relevant solutions, which is ideal for long-term tracking experiments. Once QDs are water soluble, they are then made to target a protein. Targeting molecules can include DNA, aptamers, peptides, small molecules, antibodies, and streptavidin/biotin (Medintz et al., 2005). Of these options, streptavidin-conjugated QDs are most widely used with biotinylated molecules, as streptavidin has a very high binding affinity for biotin. Commercial kits are available to biotinylate molecules, especially antibodies (protocol discussed in Chapter 2).

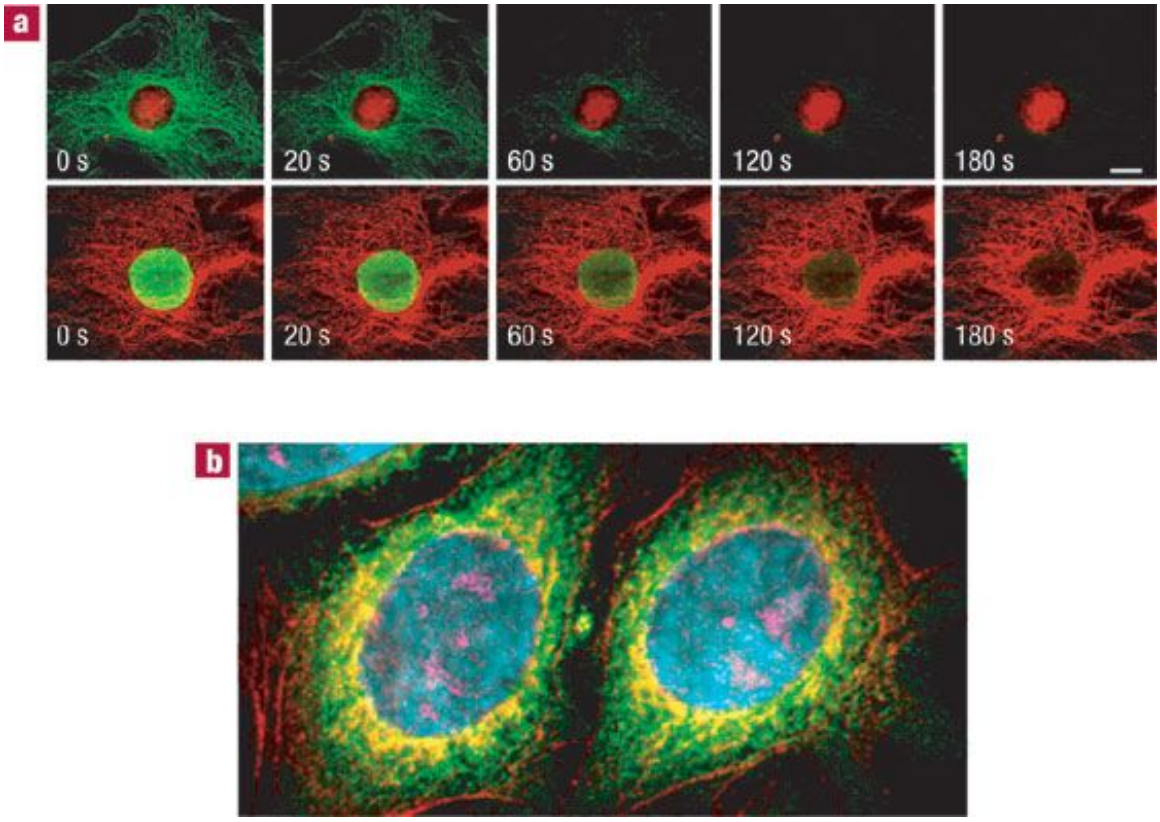


Figure 1.3: Quantum dots have superior photostability compared to dyes. (A) Over a 180 second time frame, Streptavidin QDs (red) maintain their brightness while AlexaFluor 488 (green) photobleach rapidly. (B) Fixed human epithelial cells are stained with five different QD colors, demonstrating the multiplexing potential due to narrow emission spectra. (QD size corresponds to colors as follows: Cyan, 655 QD; Magenta, 605 QDs; Orange, 525 QDs; Green, 565 QDs; and Red, 705 QDs.) Figure reprinted by permission from Springer Nature (Medintz et al., 2005).

## 1.2 Quantum dot applications in biology

### 1.2.1 Quantum dots compared to organic dyes as fluorescent labels

When choosing a fluorescent probe for biological applications, many factors should be considered: photostability, specificity to the target of interest, overall size, potential for multiplexing, absorption/emission properties, and detection limit. For decades, we were limited to dyes for visualizing events in neuroscience, but these probes come with significant downsides. While dyes do offer small size, which is important when tracking certain targets such as synaptic or overexpressed proteins, the main downside is their tendency to photobleach

rapidly, limiting the experimental applications to the short term (Figure 1.3). Additionally, dyes have smaller Stokes shift, limiting potential for multiplexing experiments, especially for live cell single particle tracking (Resch-Genger et al., 2008). The main advantages QDs have over dyes include their resistance to photobleaching, large Stokes shift, broad absorption and narrow emission, and size-tunability. QDs have broad absorption spectra but narrow emission based on the size of the dot, which allows for more precise multiplexing with proper microscope filters (Figure 1.4). The QD surface is easy to functionalize, so a diversity of biomolecules can be used in conjunction with QDs for imaging. QDs are much larger in size than a dye, typically around 15-20 nm once the biomolecules are included, compared to dyes which are 1-2 nm, but this limitation is not as relevant in lower expressing systems. QDs have become the probe of choice for long-term imaging and single particle tracking (SPT) experiments (Resch-Genger et al., 2008).

### 1.2.2 Drug delivery applications using QD-FRET-based nanosensors

Developing more efficient and precise disease detection and drug delivery systems leads to timely and accurate diagnoses and subsequent treatments. Recently, nanomedicine, and specifically QDs, has emerged as an exciting alternative to traditional drug delivery and sensing approaches that exploits QD properties such as brightness, photostability, size-tunability, and multi-functionality (Probst et al., 2013). One popular QD-based approach includes using QDs in conjunction with Forster resonance energy transfer (FRET) as a nanosensor system. FRET involves the transfer of electronic energy from a donor chromophore to an acceptor chromophore (Clegg, 1995). This transfer occurs through intermolecular dipole-dipole interactions over distances as small as 10 to 100 angstroms, making it an ideal tool for determining distances between biological molecules, for acting as a sensor when two fluorophores are present and interacting, and for confirming that drugs have reached their target locations (Clegg, 1995). QDs are typically used as donors in FRET interactions, as emission intensity changes can easily be quantitated in the presence

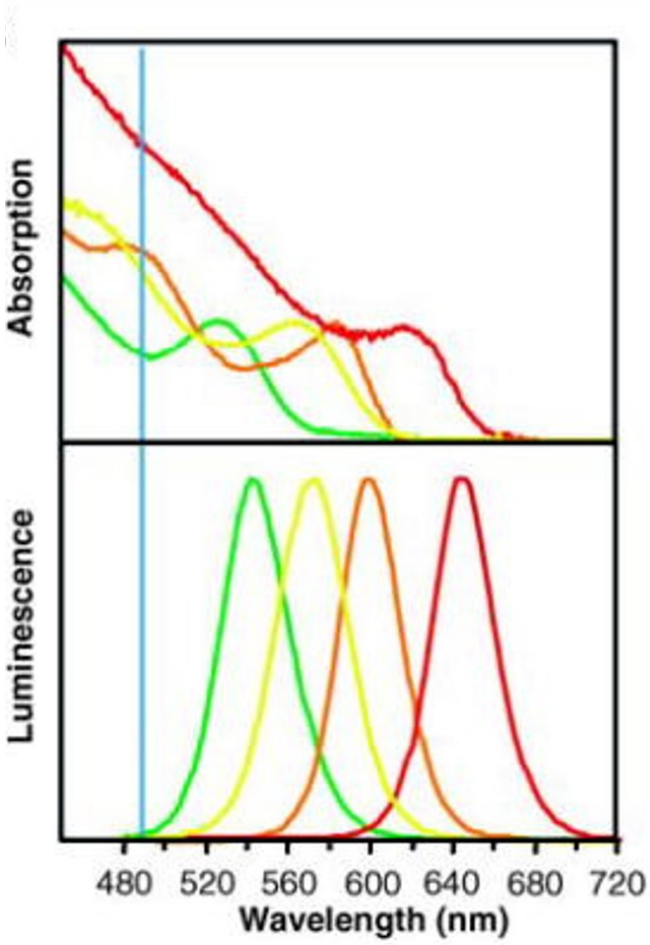


Figure 1.4: Quantum dots exhibit broad absorption and narrow emission. The narrow emission allows for multiplexing within the same experiment with proper microscope filters. Figure reproduced with permission from (Michalet, 2005). Reprinted with permission from AAAS.

of acceptor molecules (Kovtun et al., 2013). The narrow emission spectra, the diverse surface functionalization capabilties, small size, and brightness of QDs have made them ideal donor molecules for use in FRET-nanomedicine applications.

Zhang et.al. used single quantum dots conjugated to DNA probes to detect DNA implicated in genetic diseases (Zhang et al., 2005). They took advantage of a single-strand DNA capture probe labeled with biotin that binds to a streptavidin-coated QD, and the target DNA sequence became sandwiched between this sequence and another single-strand DNA reporter probe, which also included a fluorophore (Figure 1.5). When the DNA target was

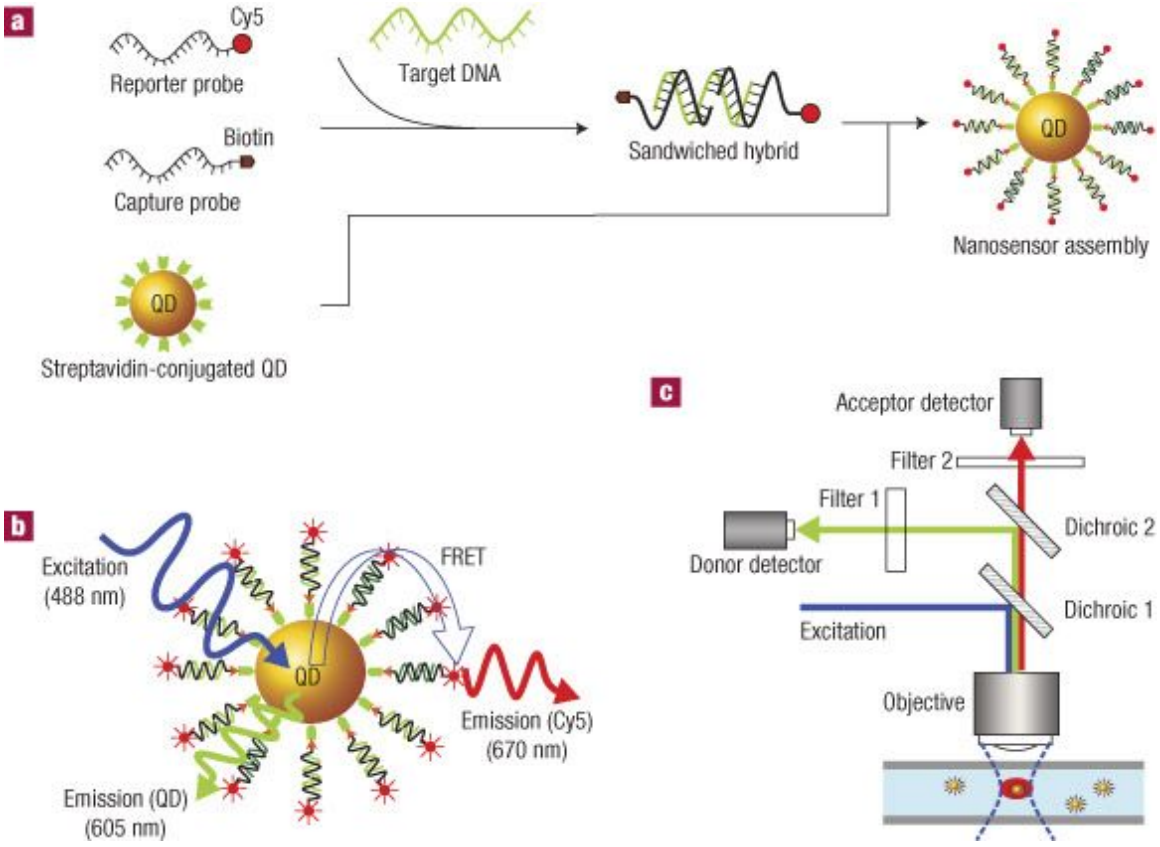


Figure 1.5: (A) Zhang et al. designed a QD nanosensor using a fluorescent reporter probe that has a FRET interaction with the QD when the target DNA is present. (B) Schematic showing the FRET interaction between the Cy5 acceptors and QD donors. (C) Schematic showing the experimental microscopy setup. Figure reproduced with permission from Springer Nature (Zhang et al., 2005).

present, the QD, which acted as a donor, was brought into close proximity with the acceptor, which was the reporter probe. The QD then non-radiatively transferred energy to the acceptor, and the acceptor emitted a photon, allowing for easy confirmation that the DNA target was present. As expected, in the absence of the acceptor, the FRET efficiency was zero, since all of the fluorescence was from the donor. As acceptor/donor ratios increased, so did the FRET efficiency, confirming the presence of the DNA target of interest (Zhang et al., 2005). In another application, Bagalkot et.al. used a QD-aptamer with a fluorescent drug loaded into the aptamer (Bagalkot et al., 2007). When the drug was loaded onto the QD, both the QD and drug were in the off state due to a FRET interaction. The aptamer

served to specifically target the cancer cells, and the particle then underwent endocytosis. Once the drug was released from the QD, both the QD and the drug were fluorescent again, as the FRET interaction could no longer take place. This fluorescence confirmed that the drug had reached its target (Bagalkot et al., 2007). This design offers the potential to revolutionize the way specific diseases, including cancer, are treated. Prasuhn et al. took advantage of two QD-conjugated dye-labeled peptides to detect caspase 3, a protease of interest in cancer research, and calcium ions, which are critical in many biological pathways (Prasuhn et al., 2010). When caspase 3 was present, the peptide was cleaved from the QD, disturbing the FRET interaction, resulting in QD emission. Alternatively, when calcium was present, it increased dye emission of the peptide. These applications utilized straightforward chemistries that can be applied to other molecules and ions of interest, offering diverse and relevant methods.

QDs will continue to be a material of choice for biosensing applications. Their large surface area allows for multivalent functionalization, increasing FRET signal and allowing for widespread applications. Unique QD functionalization and chemistries will continue to evolve, offering widespread applications as nanosensors.

### 1.2.3 Specific in vivo targeting for precise imaging

Another medically relevant application of specifically-targeted QDs includes targeted tumor imaging. In vivo targeting is advantageous to in vitro targeting as it provides more complex information about the natural environment of the protein of interest. Zhang et al. synthesized specific CdTe:$Zn^{2+}$ QDs functionalized with a phosphorothioate DNA aptamer with a targeting sequence (Zhang et al., 2013). These QDs targeted lung cancer tumors in vivo for easy and specific tumor identification. Non-aptamer QDs showed no signal, further confirming specificity. These QDs offered exciting possibilities for advancements in disease detection and eventual treatments. Han et al. conjugated tetrazine-modified antibodies to quantum dots passivated with a polyimidazole ligand including norbornene, which main-

tains an overall neutral charge, decreasing nonspecific binding (Han et al., 2015). Using their design, they targeted a rare cell population in bone marrow at the single cell level in live animals using multiphoton microscopy. The advantages to their QD design included high stability and quantum yield in vivo, low nonspecific binding, compact size, and being easily adaptable for a variety of targeting antibodies.

These new technologies described above will allow scientists to target problems at the molecular level. Though the scope of this research is aimed at specialized drug delivery, more efficient disease discovery, and more precise imaging for diagnoses, this technology will provide for many more exciting uses and advancements in the future.

### 1.2.4 Single particle tracking with quantum dots

Single particle tracking (SPT) experiments have provided the scientific community with invaluable single-molecule information about the dynamic regulation of individual receptors, transporters, kinases, lipids, and molecular motors. The goal of SPT trajectory analysis is to extract quantitative parameters of motion and consequently illuminate the type of motion and diffusive behavior each particle undergoes. In a typical QD-based SPT experiment, QDs are bound to the target of interest and imaged for seconds to minutes via fluorescence video microscopy to create time-series image stacks (Figure 1.6 A). The individual QD spot intensity values are fitted into two-dimensional Gaussian distributions, with localization accuracy as low as 10 nm. Single QD spots in individual frames are then linked from frame to frame to form trajectories ((Figure 1.6 B). The x and y positions from each trajectory are generated and used to determine mean square displacement, diffusion coefficient, confinement index, and instantaneous velocity (Figure 1.6 C) (Bailey et al., 2017).

In contrast to ensemble averaging approaches, the use of SPT has led to the discovery of heterogeneous modes of motion of membrane proteins. The most common targeting molecules used for these experiments are antibodies that recognize an extracellular epitope of the protein and small molecule ligands that typically bind to the protein binding pockets.

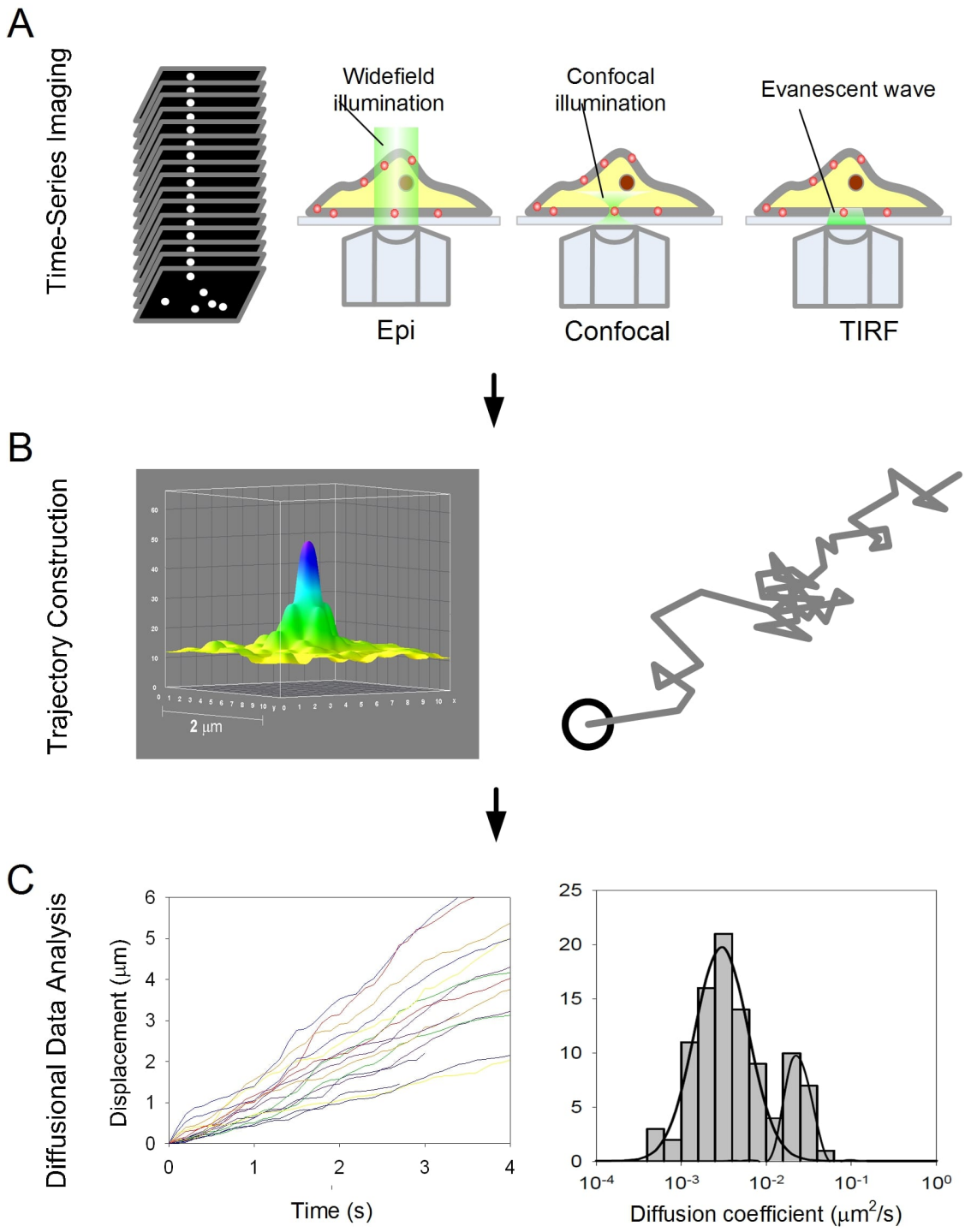


Figure 1.6: In a typical SPT experiment, time series images at video rates through a fluorescence microscope. Trajectories are reconstructed throughout the time series and analyzed. Example displacement and diffusion coefficient graphs are shown. Figure reproduced with permission from Elsevier (Chang et al., 2012a).

Both of these approaches typically are used in two-step labeling experiments: the antibody or ligand is bound to the target of interest first, followed by labeling with QDs (Bailey et al., 2017). No matter which method is chosen, ensuring probe specificity during SPT experiments is of crucial importance. Not only should the targeting molecule only bind to the target of interest, the QDs themselves should be sufficiently passivated to eliminate nonspecific binding. This is a huge experimental limitation, as nonspecific QDs are hard to distinguish from specifically bound ones during analysis. To alleviate potential nonspecific binding in SPT experiments, blocking agents, such as casein or serum, are usually included to further passivate the QD surface. To ensure that the targeting molecules are specific, thorough controls should be run that include a blocking agent specific to the targeting site. For example, for an antibody-based approach, a blocking peptide can be purchased that binds the same sequence as the antibody. If the antibody is specific for the protein, no labeling should be seen when the peptide is present.

One major hurdle that remains with the use of QDs for SPT experiments is the multivalency of the QD probes due to the large QD surface area. Most of the research done with QD SPT utilizes streptavidin- or antibody-coated QDs, both of which have many binding sites that could lead to crosslinking of tagged proteins. For example, commercial streptavidin-QDs have 4-10 streptavidin molecules per QD, and each streptavidin has 4 binding sites (Howarth et al., 2008). For many proteins, if crosslinking occurs, signaling pathways can be activated, internalization can occur, or diffusion of the proteins can slow down (Saxton and Jacobson, 1997). To address these concerns, recent research has focused on QD probe development, specifically on generating smaller, monovalent probes that can be generalized for many different proteins of interest. In 2008, Howarth et al. described a method that led to monovalency by using monovalent streptavidin, eliminating the multiple binding sites that could lead to crosslinking. They also decreased the overall size of the final QD products by passivating with a smaller carboxy-polyethylene glycol (PEG). They purified their conjugates with gel electrophoresis to eliminate the multivalent

QDs and confirmed monovalency in live cells by labeling ephrin receptors (Howarth et al., 2008). Uddayasankar and colleagues used a different purification method for obtaining monovalent probes. In this study, hexahistidine-functionalized DNA was attached to the QD surface. To isolate products that had a single DNA strand attached, DNA-QDs were incubated with diethylaminoethyl (DEAE) functionalized magnetic beads and captured onto the beads by electrostatic interactions. Before isolation, 67% of DNA-QDs were monovalent (Uddayasankar et al., 2014). While the majority of QD-SPT experiments still use probes that can be considered multivalent, the work towards easy to synthesize monovalent, smaller QD probes continues.

### 1.2.5 Quantum dot single particle tracking examples

QDs have been utilized in a myriad of applications, including drug delivery, biosensing, tissue and organ imaging in small animals, and single particle tracking (Medintz et al., 2008; Pinaud et al., 2010; Delehanty et al., 2009). In 2002, the Rosenthal group first reported the use of serotonin-conjugated nanocrystals to target serotonin transporter in living cells (Rosenthal et al., 2002), demonstrating the potential for utilizing QDs in SPT applications. In 2003, Dahan and co-workers carried out the first SPT experiment with QDs in living neurons. They tracked glycine receptors with antibody-conjugated QDs and observed site-specific differences in lateral diffusion in different neuronal compartments, with the lowest diffusion rates happening in the synapse and increasing as the proteins moved out of synaptic regions. This first report of QD SPT demonstrated the importance of membrane protein mobility, especially as the proteins diffused in and out of synaptic, perisynaptic, and extrasynaptic domains (Dahan et al., 2003). Dahan and Triller also investigated the role of $\gamma$-aminobutyric acid ($GABA_A$) receptors in chemotactic signaling, concluding that QD-labeled GABA receptors redistribute asymmetrically along the growth cone of neurons (Bouzigues et al., 2007).

In 2005, Lidke et al. demonstrated for the first time simultaneous two-color QD track-

ing. In this elegant paper, they proposed a novel mechanism of retrograde transport by which filopodia detect effector molecules and mediate cellular responses through active transport of receptors. They utilized two colors of epidermal growth factor (EGF)- conjugated QDs to achieve single molecule resolution of these processes (Lidke et al., 2005). Zhang and colleagues first used QD tracking in presynaptic neuronal vesicles to further understand modes of vesicular fusion. By loading small, pH-sensitive amphililic polymer-coated QDs into synaptic vesicles, they discovered that both kiss-and-run (K&R) and full collapse fusion (FCF) events can be preferred depending on how the neuron was stimulated. The readily releasable pool of synaptic vesicles were predominately released by K&R (Zhang et al., 2009).

In 2012, Chang et al. from the Rosenthal lab first reported SPT of a monoamine neurotransmitter transporter, specifically SERT, in an immortalized serotonergic cell line. One of the most significant findings of this work was that SERT mobility is bimodal, with a faster, more freely diffusing population and a slower, confined population. These modes of mobility were sensitive to cholesterol depletion and SERT activation (Rosenthal et al., 2011). In 2015, Kovtun et al. from the Rosenthal group investigated the mobility dynamics of a DAT mutant, Arg615Cys, associated with attention-deficit/hyperactivity disorder (ADHD). QD tracking analysis showed that the mutant DATs had significantly increased lateral mobility compared to the wild type, and that this increased mobility was insensitive to further DAT activation or cholesterol depletion (Kovtun et al., 2015). As demonstrated by this work, QD SPT has the potential to unravel key mechanisms underlying many neuropsychiatric disorders.

While QD SPT in transfected systems or neuronal cultures provides real-time insight into how these proteins behave, the goal is to be in systems that are most physiologically relevant. In recent years, attention has shifted to QD SPT in more complex systems, such as brain slices. Limitations to this goal have included both optical resolution as well as ability of QDs to penetrate throughout the tissue. Biermann and co-workers presented an

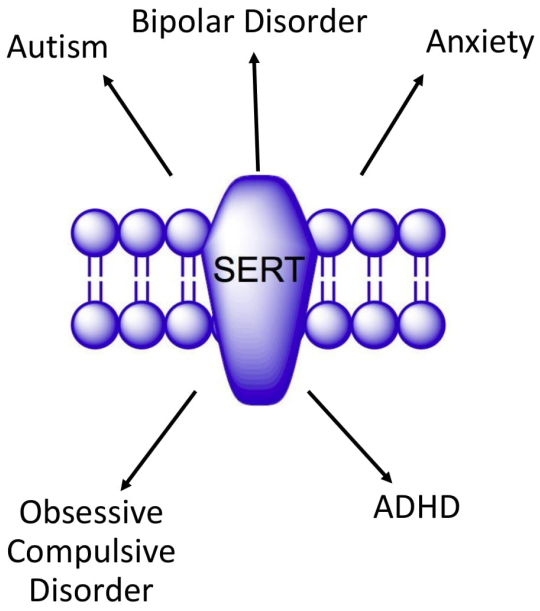


Figure 1.7: SERT is associated with a variety of mental disorders and is the pharmacological target for treating many of these disorders.

impressive account of the feasibility of QD SPT in organotypic hippocampal brain slices. They were able to image QDs at depths up to 60 µm with temporal resolution for SPT at depths of 20 µm (Biermann et al., 2014). This exciting advancement demonstrated that not only can QDs penetrate more complex environments like brain tissue, they can also be tracked with high specificity, spatial localization accuracy of about 50 nm, and temporal resolution in milliseconds. Building on these studies, work from the Groc lab showed that QDs can be utilized for SPT in living acute brain slices after being injected in vivo (Varela et al., 2016). While much information is still to be gleaned from tracking proteins in culture, SPT in these more native environments is a direction the field is moving towards.

## 1.3 Serotonin transporter: research motivation

### 1.3.1 Serotonin transporter 5-HT transport

The Rosenthal lab pioneered the use of QDs in tracking individual neurotransmitter transporters, including dopamine transporter and serotonin transporter, and specializes in ligand-conjugated QDs for neurotransmitter transporter single particle tracking. The protein that the bulk of this dissertation focuses on is the monoamine serotonin transporter protein (SERT). SERT is an important target for treating a myriad of mental illnesses, including major depressive disorder, bipolar disorder, and anxiety (Figure 1.7) (Murphy et al., 2004). SERT is an important pharmacological target, as it is sensitive to antidepressants, cocaine, and 3,4-methamphetamine (Steiner et al., 2008). SERT is the critical protein in the brain that terminates serotonin signaling. It is responsible for the removal of serotonin, or 5-hydroxytryptamine (5-HT), which is a tryptophan-derived indoleamine that is an important signaling molecule implicated in mental illness, as well as in sleep, mood regulation, and appetite. 5-HT is released presynaptically and received by the postsynaptic serotonin receptors. The serotonin that does not gets trafficked get recycled back into the presynaptic neuron through SERT (Figure 1.8 A). This reuptake occurs through a secondary active, ion-coupled transport, as transporting 5-HT independently would be energetically unfavorable. The energy for the influx of 5-HT primarily comes from the transmembrane sodium gradient. Typically, 5-HT influx depends on the co-transport of a 5-HT molecule with a sodium and a chloride ion, with the efflux of potassium also contributing in a separate process (Figure 1.8 B) (Steiner et al., 2008).

Two conformations seem to exist that allow this transport to take place. One conformation results in the substrate binding site facing extracellularly so that the binding of 5-HT or an ion can take place. For the protein to conformationally change, both the substrate and the necessary ions must be bound or alternatively the sites must be empty. Once this happens, the protein can then shift back to face the extracellular side so that more transport can occur. If potassium ions are also required, the coupling would happen in a separate

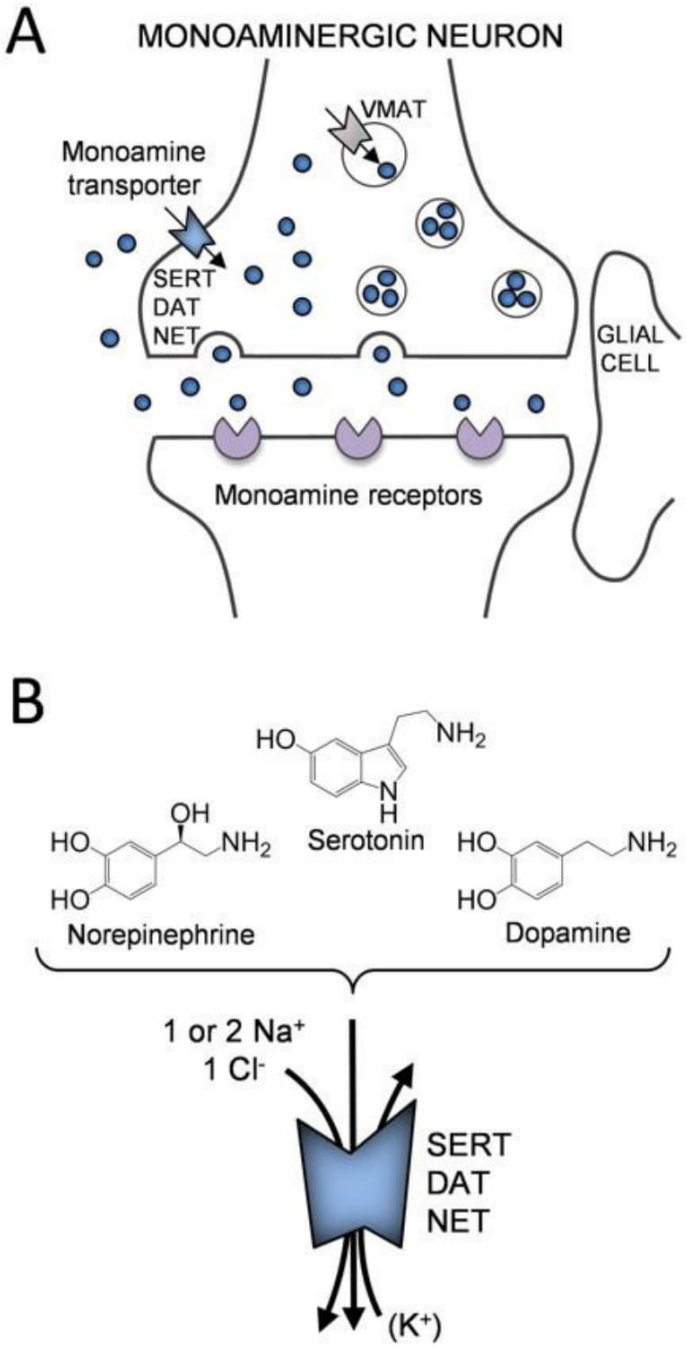


Figure 1.8: (A) In a monoaminergic neuron, neurotransmitter is released from the presynaptic neuron and recieved by the postsynaptic monoamine receptors. The neurotransmitter left in the synaptic cleft gets recycled by the presynaptic monoamine transporters. (B) Transport of neurotransmitter is an ion-coupled process, where the influx of neuotransmitter is accompanied by sodium and chloride ions. Figure reprinted with permission from American Society for Pharmacology and Experimental Therapeutics (ASPET) (Kristensen et al., 2011).

step. Potassium binds when the binding site is facing intracellularly, triggering transition to the other conformation where the extracellular molecules can then bind (Rudnick et al., 2014).

### 1.3.2 Serotonin transporter structure and localization

Structurally, SERT is encoded by a single gene, SLC6A4, in humans and rodent models. SERT is an integral membrane protein with twelve transmembrane spanning domains (Andersen et al., 2009). SERT is also a phosphoprotein, meaning that phosphorylation is an important post-translational regulatory mechanism for activating, deactivating, or internalizing the protein (Ramamoorthy et al., 1998). SERT is localized both on the plasma membrane and in the cytoplasm and is distributed along axonal projections, as well as within cell bodies and dendrites. SERT is found primarily in the raphe nuclei in the brain but is also seen throughout fibers in certain regions of the forebrain (Qian et al., 1995). Some SERT may also be present in glial cells (Pickel and Chan, 1999). SERT is typically located along the axons in the plasma membrane and not typically in the active zones (Tao-Cheng and Zhou, 1999). SERT has also been found to localize within cholesterol-rich membrane microdomains along the plasma membrane. When cholesterol was depleted, SERT exhibited a decrease in maximal transport velocity and an increase in lateral diffusion (Magnani et al., 2004; Chang et al., 2012b).

### 1.3.3 Serotonin transporter conformation and phosphorylation dynamics

Research over the past few decades has shown that SERT function and expression is under tight regulation through a variety of mechanisms, including kinase activity (Bermingham and Blakely, 2016), membrane microdomain localization (Magnani et al., 2004; Chang et al., 2012a), and conformation shifts (Zhang et al., 2016). Investigating SERT structure and function at the single protein level remains a challenge and presents an exciting opportunity to better understand underlying molecular mechanisms of these mood disorders. While a significant amount of research has been done to better understand SERT function

in the central nervous system, how SERT behaves at the single protein level in endogenous systems is not well-known.

Exciting new evidence suggests that intracellular SERT regulatory mechanisms, such as cGMP-dependent phosphorylation, are modulated by shifts in conformation from outward to inward facing, and vice versa (Zhang et al., 2016). During phosphorylation, a phosphate group is added to a protein by a kinase, which can either activate or deactivate proteins depending on where the event occurs. Threonine 276 (Thr276), which lies at the cytoplasmic end of SERT transmembrane helix 5, has recently been identified as the phosphorylation site for the cGMP-stimulated PKG pathway (Ramamoorthy et al., 2007). Recent evidence suggests that, because this site is not easily accessible, conformation shifts may unwind that transmembrane helix to increase the level of Thr276 phosphorylation. Zhang et al. found that when SERT is stabilized facing inward, phosphorylation at this site increases, while agents that stabilize the outward-facing conformation decrease phosphorylation (Zhang et al., 2007).

Membrane cholesterol plays an important role in regulating a variety of receptors and transporters and can affect both the membrane fluidity as well as specific protein conformations (Scanlon et al., 2001; Pucadyil and Chattopadhyay, 2005; Hong and Amara, 2010). Several studies have shown that SERT exists within membrane microdomains that are rich in cholesterol, affecting SERT mobility in the membrane (Chang et al., 2012a). While it was originally thought that cholesterol depletion reduces SERT activity (Scanlon et al., 2001), new evidence from the past two years suggests that there may be another role of cholesterol in SERT regulation. Recently Coleman et al. determined the crystal structure of human SERT (hSERT) and revealed a cholesterol binding site near transmembrane domain 12, providing the first evidence of direct binding (Figure 1.9) (Coleman et al., 2016). Importantly, the depletion of membrane cholesterol induces a more inward-facing conformation of SERT (Bjerregaard et al., 2015). Our lab has previously shown that SERT exhibits two main modes of mobility, a fast and slow population, and that the majority of

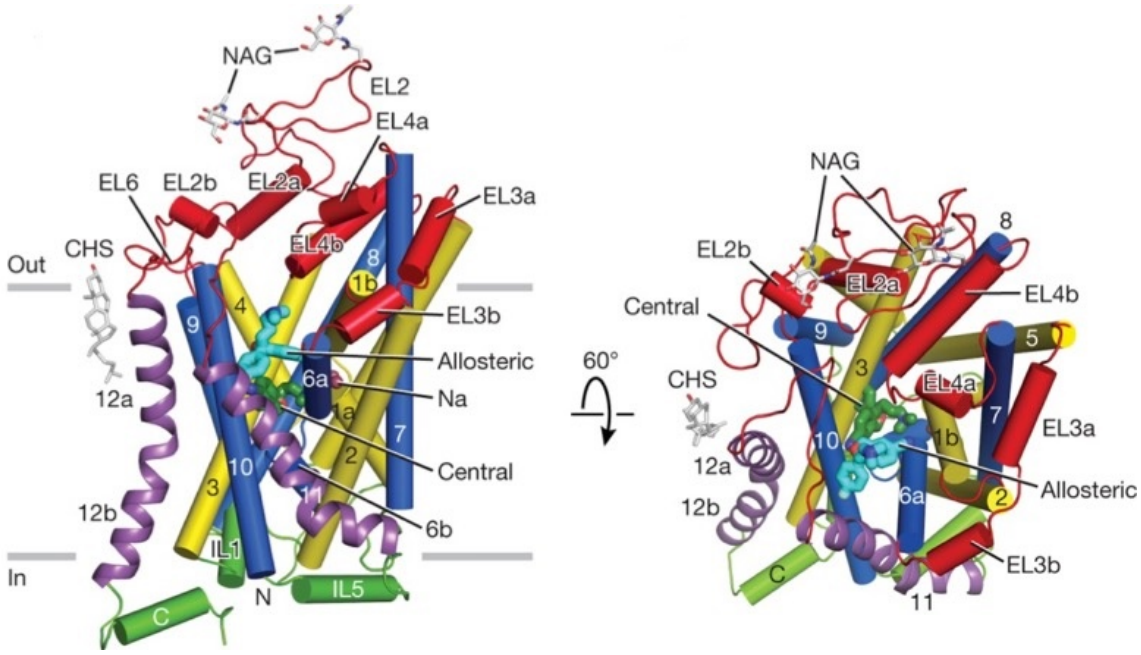


Figure 1.9: The first schematic depicts SERT structure parallel to the membrane. (S)-citalopram molecules are shown in dark green and cyan at the central and allosteric cites. Also of note is the cholesteryl hemisuccinate molecule interacting with transmembrane domain 12. The second schematic shows the view of SERT from the extracellular side of the membrane. Figure reprinted with permission from Springer Nature (Coleman et al., 2016).

basal SERT is localized to membrane microdomains, displaying confined motion (Chang et al., 2012b).

Transporters have been visualized in heterologous cell lines using QDs, but they have not yet been utilized in endogenously expressing primary neuronal systems. In my dissertation, I am building on these studies by using a similar approach in a more physiologically relevant system – primary neuronal cultures from rat brain. These studies provide new insights about how SERT behaves in an endogenous neuronal system and how surface dynamics modulate activity. I am also probing the interplay between mobility and phosphorylation using a hyperphosphorylated mutant model. I then build upon those findings by revealing a new mechanism for the role of cholesterol in Thr276 phosphorylation. These studies shed light on how SERT is organized and regulated in the dynamic membrane in an endogenous neuronal system.

## 1.4 Dissertation outline

This dissertation focuses on the development and utilization of quantum dot probes for single particle tracking applications. I begin with an overview of the methods I have developed in SPT of both stably-expressed SERT in a cell line and endogenous SERT in primary midbrain cultures (Chapter 2). This chapter discusses both ligand-based and antibody-based quantum dot tracking methods. I then detail the advances made with generating monovalent aptamer-conjugated QDs (Chapter 3). These probes offer the potential for tracking GFP-encoded proteins at a 1:1 ratio and are generalizable to other proteins by changing the aptamer.

After thoroughly discussing these methods, I subsequently focus on the role of cholesterol and phosphorylation in SERT mobility in endogenous SERT and a disease-associated mutant model (Chapters 4 and 5). These chapters utilize the methods outlined in Chapter 2 to shed light on serotonin transporter function in primary midbrain neurons and a stably-transfected cell line. I conclude this dissertation with a summary and future directions for the work presented here (Chapter 6).

## 1.5 Bibliography


Alivisatos, A. P., Chun, M., Church, G. M., Greenspan, R. J., Roukes, M. L., and Yuste, R. (2012). The Brain Activity Map Project and the Challenge of Functional Connectomics. *Neuron*, 74:970–974.

Andersen, J., Kristensen, A. S., Bang-Andersen, B., and Stromgaard, K. (2009). Recent advances in the understanding of the interaction of antidepressant drugs with serotonin and norepinephrine transporters. *Chemical Communications*, (25):3677–3692.

Bagalkot, V., Zhang, L., Levy-Nissenbaum, E., Jon, S., Kantoff, P. W., Langery, R., and Farokhzad, O. C. (2007). Quantum dot-aptamer conjugates for synchronous cancer imaging, therapy, and sensing of drug delivery based on Bi-fluorescence resonance energy transfer. *Nano Letters*, 7(10):3065–3070.

Bailey, D. M., Kovtun, O., and Rosenthal, S. J. (2017). Antibody-Conjugated Single Quantum Dot Tracking of Membrane Neurotransmitter Transporters in Primary Neuronal Cultures. In *Biomedical Nanotechnology: Methods and Protocols*, volume 726, pages 165–177.

Bermingham, D. P. and Blakely, R. D. (2016). Kinase-dependent Regulation of Monoamine Neurotransmitter Transporters. *Pharmacol. Rev.*, 35559(October):888–953.

Biermann, B., Sokoll, S., Klueva, J., Missler, M., Wiegert, J. S., Sibarita, J. B., and Heine, M. (2014). Imaging of molecular surface dynamics in brain slices using single-particle tracking. *Nature Communications*, 5(3024).

Bjerregaard, H., Severinsen, K., Said, S., Wiborg, O., and Sinning, S. (2015). A dualistic conformational response to substrate binding in the human serotonin transporter reveals a high affinity state for serotonin. *Journal of Biological Chemistry*, 290(12):7747–7755.

Bouzigues, C., Morel, M., Triller, A., and Dahan, M. (2007). Asymmetric redistribution of GABA receptors during GABA gradient sensing by nerve growth cones analyzed by single quantum dot imaging. *Proceedings of the National Academy of Sciences*, 104(27):11251–11256.

Chang, J. C., Kovtun, O., Blakely, R. D., and Rosenthal, S. J. (2012a). Labeling of neuronal receptors and transporters with quantum dots. *Wiley Interdisciplinary Reviews: Nanomedicine and Nanobiotechnology*, 4(6):605–619.

Chang, J. C., Tomlinson, I. D., Warnement, M. R., Ustione, A., Carneiro, A. M. D., Piston, D. W., Blakely, R. D., and Rosenthal, S. J. (2012b). Single Molecule Analysis of Serotonin Transporter Regulation Using Antagonist-Conjugated Quantum Dots Reveals Restricted, p38 MAPK-Dependent Mobilization Underlying Uptake Activation. *Journal of Neuroscience*, 32(26):8919–8929.

Clegg, R. M. (1995). Fluorescence resonance energy transfer. *Current Opinion in Biotechnology*, 6(1):103–110.

Coleman, J. A., Green, E. M., and Gouaux, E. (2016). X-ray structures and mechanism of the human serotonin transporter. *Nature*, 532(7599):334–339.

Dahan, M., Lévi, S., Luccardini, C., Rostaing, P., Riveau, B., and Triller, A. (2003). Diffusion Dynamics of Glycine Receptors Revealed by Single-Quantum Dot Tracking. *Science*, 302(5644):442–445.

Delehanty, J. B., Mattoussi, H., and Medintz, I. L. (2009). Delivering quantum dots into cells: strategies, progress and remaining issues. *Anal. Bioanal. Chem*, 393:1091–1105.

Frecker, T., Bailey, D., Arzeta-Ferrer, X., McBride, J., and Rosenthal, S. J. (2016). Review: Quantum Dots and Their Application in Lighting, Displays, and Biology. *ECS Journal of Solid State Science and Technology*, 5(1):R3019–R3031.

Han, H.-S., Niemeyer, E., Huang, Y., Kamoun, W. S., Martin, J. D., Bhaumik, J., Chen, Y., Roberge, S., Cui, J., Martin, M. R., Fukumura, D., Jain, R. K., Bawendi, M. G., and Duda, D. G. (2015). Quantum dot/antibody conjugates for in vivo cytometric imaging in mice. *Proceedings of the National Academy of Sciences*, 112(5):1350–1355.

Hines, M. A. and Guyot-Sionnest, P. (1996). Synthesis and Characterization of Strongly Luminescing ZnS-Capped CdSe Nanocrystals. *Journal of Physical Chemistry*, 100(2):468–471.

Hong, W. C. and Amara, S. G. (2010). Membrane cholesterol modulates the outward facing conformation of the dopamine transporter and alters cocaine binding. *Journal of Biological Chemistry*, 285(42):32616–32626.

Howarth, M., Liu, W., Puthenveetil, S., Zheng, Y., Marshall, L. F., Schmidt, M. M., Wittrup, K. D., Bawendi, M. G., and Ting, A. Y. (2008). Monovalent, reduced-size quantum dots for imaging receptors on living cells. *Nature Methods*, 5(5):397–399.

Insel, T. (2008). Assessing the Economic Costs of Serious Mental Illness. *American Journal of Psychiatry*, 165(6):663–665.

Kippeny, T., Swafford, L. A., and Rosenthal, S. J. (2002). Semiconductor Nanocrystals: A Powerful Visual Aid for Introducing the Particle in a Box. *Journal of Chemical Education*, 79(9):1094.

Kovtun, O., Arzeta-Ferrer, X., and Rosenthal, S. J. (2013). Quantum dot approaches for target-based drug screening and multiplexed active biosensing. *Nanoscale*, 5(24):12072–12081.

Kovtun, O., Sakrikar, D., Tomlinson, I. D., Chang, J. C., Arzeta-Ferrer, X., Blakely, R. D., and Rosenthal, S. J. (2015). Single-Quantum-Dot Tracking Reveals Altered Membrane Dynamics of an Attention-Deficit/Hyperactivity-Disorder-Derived Dopamine Transporter Coding Variant. *ACS Chemical Neuroscience*, 6(4):526–534.

Kristensen, A. S., Andersen, J., Jørgensen, T. N., Sorensen, L., Eriksen, J., Loland, C. J., Stromgaard, K., and Gether, U. (2011). SLC6 Neurotransmitter Transporters: Structure, Function, and Regulation. *Pharmacological Reviews*, 63(3):585–640.

Lidke, D. S., Lidke, K. A., Rieger, B., Jovin, T. M., and Arndt-Jovin, D. J. (2005). Reaching out for signals: filopodia sense EGF and respond by directed retrograde transport of activated receptors. *The Journal of Cell Biology*, 170(4):619–626.

Magnani, F., Tatell, C. G., Wynne, S., Williams, C., and Haase, J. (2004). Partitioning of the serotonin transporter into lipid microdomains modulates transport of serotonin. *Journal of Biological Chemistry*, 279(37):38770–38778.

Medintz, I. L., Mattoussi, H., and Clapp, A. R. (2008). Potential clinical applications of quantum dots. *International Journal of Nanomedicine*, 3(2):151–167.

Medintz, I. L., Uyeda, H. T., Goldman, E. R., and Mattoussi, H. (2005). Quantum dot bioconjugates for imaging, labelling and sensing. *Nature Materials*, 4(6):435–446.

Michalet, X. (2005). Quantum Dots for Live Cells, in Vivo Imaging, and Diagnostics. *Science*, 307(5709):538–544.

Murphy, D. L., Lerner, A., Rudnick, G., and Klaus-Peter, L. (2004). Serotonin Transporter: Gene, Genetic Disorders, and Pharmacogenetics. *Molecular Interventions*, 4(2):109–123.

Pickel, V. M. and Chan, J. (1999). Ultrastructural localization of the serotonin transporter in limbic and motor compartments of the nucleus accumbens. *Journal of Neuroscience*, 19(17):7356–66.

Pinaud, F., Clarke, S., Sittner, A., and Dahan, M. (2010). Probing cellular events, one quantum dot at a time. *Nature Methods*, 7(4):275–285.

Prasuhn, D. E., Feltz, A., Blanco-Canosa, J. B., Susumu, K., Stewart, M. H., Mei, B. C., Yakovlev, A. V., Loukou, C., Mallet, J.-M., Oheim, M., Dawson, P. E., and Medintz, I. L. (2010). Quantum Dot Peptide Biosensors for Monitoring Caspase 3 Proteolysis and Calcium Ions. *ACS Nano*, 4(9):5487–5497.

Probst, C. E., Zrazhevskiy, P., Bagalkot, V., and Gao, X. (2013). Quantum dots as a platform for nanoparticle drug delivery vehicle design. *Advanced Drug Delivery Reviews*, 65(5):703–718.

Pucadyil, T. J. and Chattopadhyay, A. (2005). Cholesterol modulates the antagonist-binding function of hippocampal serotonin1Areceptors. *Biochimica et Biophysica Acta - Biomembranes*, 1714(1):35–42.

Qian, Y., Melikian, E., Rye, B., Levey, I., and Blakely, D. (1995). Identification and Characterization of Antidepressant-Sensitive Serotonin Transporter Proteins Using Site-Specific Antibodies. *Journal of Neuroscience*, 15(2):1261–74.

Ramamoorthy, S., Giovanetti, E., Qian, Y., and Blakely, R. D. (1998). Phosphorylation and regulation of antidepressant-sensitive serotonin transporters. *Journal of Biological Chemistry*, 273(4):2458–2466.

Ramamoorthy, S., Samuvel, D. J., Buck, E. R., Rudnick, G., and Jayanthi, L. D. (2007). Phosphorylation of threonine residue 276 is required for acute regulation of serotonin transporter by cyclic GMP. *Journal of Biological Chemistry*, 282(16):11639–11647.

Resch-Genger, U., Grabolle, M., Cavaliere-Jaricot, S., Nitschke, R., and Nann, T. (2008). Quantum dots versus organic dyes as fluorescent labels. *Nature Methods*, 5(9):763–775.

Rosenthal, S. J., Chang, J. C., Kovtun, O., McBride, J. R., and Tomlinson, I. D. (2011). Biocompatible quantum dots for biological applications. *Chemistry and Biology*, 18(1):10–24.

Rosenthal, S. J., Tomlinson, I., Adkins, E. M., Schroeter, S., Adams, S., Swafford, L., McBride, J., Wang, Y., DeFelice, L. J., and Blakely, R. D. (2002). Targeting cell surface receptors with ligand-conjugated nanocrystals. *Journal of the American Chemical Society*, 124(17):4586–4594.

Rudnick, G., Krämer, R., Blakely, R. D., Murphy, D. L., and Verrey, F. (2014). The SLC6 transporters: Perspectives on structure, functions, regulation, and models for transporter dysfunction. *Pflugers Archiv European Journal of Physiology*, 466(1):25–42.

Saxton, M. J. and Jacobson, K. (1997). SINGLE-PARTICLE TRACKING:Applications to Membrane Dynamics. *Annual Review of Biophysics and Biomolecular Structure*, 26(1):373–399.

Scanlon, S. M., Williams, D. C., and Schloss, P. (2001). Membrane cholesterol modulates serotonin transporter activity. *Biochemistry*, 40(35):10507–10513.

Steiner, J. A., Carneiro, A. M. D., and Blakely, R. D. (2008). Going with the flow: Trafficking-dependent and -independent regulation of serotonin transport. *Traffic*, 9(9):1393–1402.

Tao-Cheng, J. H. and Zhou, F. C. (1999). Differential polarization of serotonin transporters in axons versus soma-dendrites: An immunogold electron microscopy study. *Neuroscience*, 94(3):821–830.

Uddayasankar, U., Zhang, Z., Shergill, R. T., Gradinaru, C. C., and Krull, U. J. (2014). Isolation of Monovalent Quantum DotNucleic Acid Conjugates Using Magnetic Beads. *Bioconjugate Chemistry*, 25(7):1342–1350.

Varela, J. A., Dupuis, J. P., Etchepare, L., Espana, A., Cognet, L., and Groc, L. (2016). Targeting neurotransmitter receptors with nanoparticles in vivo allows single-molecule tracking in acute brain slices. *Nature Communications*, 7:10947.

Zhang, C., Ji, X., Zhang, Y., Zhou, G., Ke, X., Wang, H., Tinnefeld, P., and He, Z. (2013). One-pot synthesized aptamer-functionalized CdTe:Zn2+quantum dots for tumor-targeted fluorescence imaging in vitro and in vivo. *Analytical Chemistry*, 85(12):5843–5849.

Zhang, C. Y., Yeh, H. C., Kuroki, M. T., and Wang, T. H. (2005). Single-quantum-dot-based DNA nanosensor. *Nature Materials*, 4(11):826–831.

Zhang, Q., Li, Y., and Tsien, R. W. (2009). The dynamic control of kiss-and-run and vesicular reuse probed with single nanoparticles. *Science*, 323(5920):1448–1453.

Zhang, Y.-W., Gesmonde, J., Ramamoorthy, S., and Rudnick, G. (2007). Serotonin Transporter Phosphorylation by cGMP-Dependent Protein Kinase Is Altered by a Mutation Associated with Obsessive Compulsive Disorder. *Journal of Neuroscience*, 27(40):10878–10886.

Zhang, Y.-W., Turk, B. E., and Rudnick, G. (2016). Control of serotonin transporter phosphorylation by conformational state. *Proceedings of the National Academy of Sciences*, 113(20):E2776–E2783.

# CHAPTER 2

## Methods for tracking neurotransmitter transporters using quantum dots

Single particle tracking (SPT) applications have continued to expand in the field of molecular biology, shedding light on how individual proteins are organized and regulated. SPT has allowed for individual molecules to be visualized at sub-diffraction limited spatial resolutions, providing critical information about targets in the entire cell (Fig. 2.1) (Chang and Rosenthal, 2013a). In contrast to ensemble averaging approaches, the use of SPT has led to the discovery of heterogeneous modes of motion of membrane proteins. Since nanoscience has been implemented into biomedical research, SPT in endogenous systems is now a useful tool to elucidate underlying mechanisms related to disease states.

As described in the introduction, quantum dots (QDs), semiconductor nanocrystals that have a core nanocrystal passivated with a wider bandgap shell, make excellent fluorescent probes for SPT applications (Rosenthal et al., 2002). Commercially available QDs with CdSe/CdS/ZnS core/shell configurations are most commonly used in biological applications (Valizadeh et al., 2012); they are capped with native nonpolar surface ligands that are solubilized. For example, an amphiphilic polymer can be intercalated into nonpolar ligands to preserve the original architecture and photoluminescence properties of the particles. Once the QDs are solubilized, streptavidin, antibodies, peptides, single-stranded DNA, and small molecule ligands can be incorporated onto the surface for biological targeting and SPT experiments (Bilan et al., 2015). The core/shell design gives QDs their excellent fluorescent properties, including high brightness that increases their signal-to-noise ratios, excellent photostabilities, narrow emission spectra, and large Stokes shifts (Rosenthal et al., 2002). One unique feature of QDs is their characteristic blinking, or fluorescence fluctuations, which can be used to confirm single QDs are being analyzed, although trajectory reconstruction is necessary during analysis (Chang et al., 2012a).

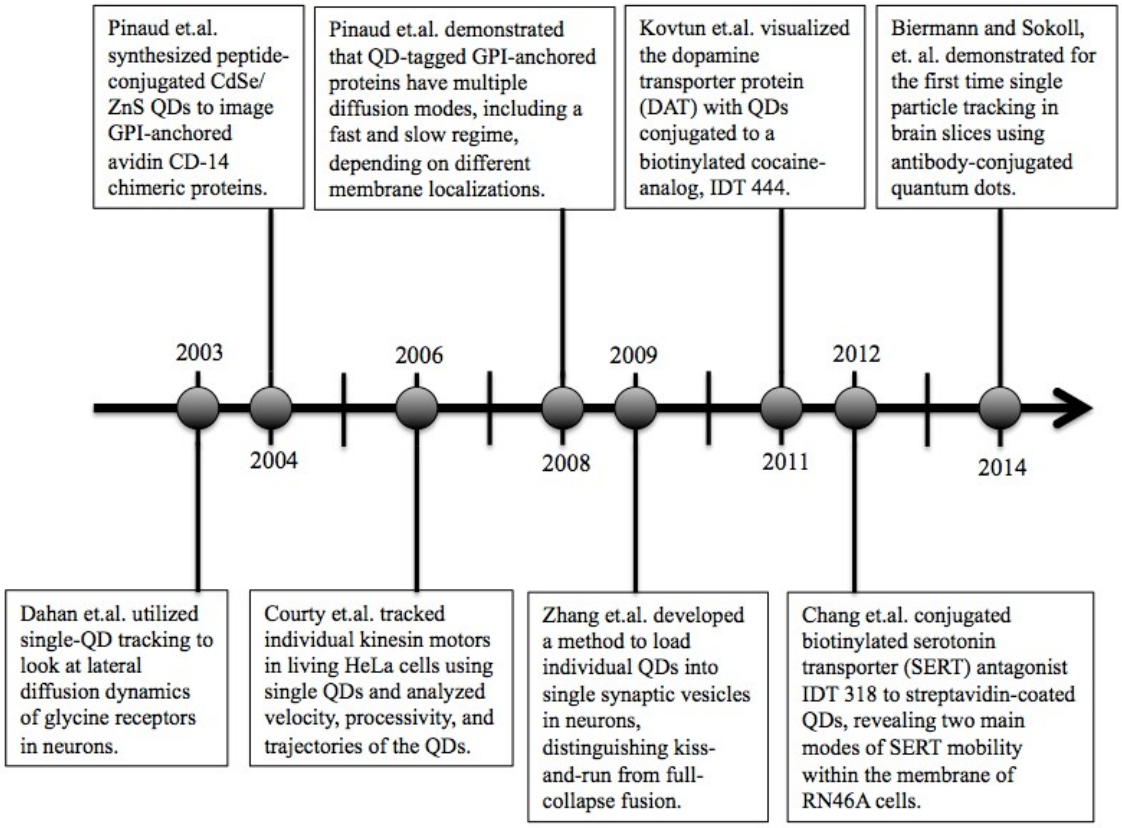


Figure 2.1: Literature examples of QD SPT applications starting with the first single-QD tracking experiment in neurons and ending with the first single-QD tracking experiment in brain slices (Dahan et al., 2003; Pinaud et al., 2004; Courty et al., 2006; Pinaud et al., 2009; Zhang et al., 2009; Kovtun et al., 2011; Chang et al., 2012b; Biermann et al., 2014)

In a typical SPT experiment, QD probes are first bound to their targets, and a time-lapse image series is then acquired with a fluorescence microscope at video rates as the probe is shuttled around the cell membrane by the neurotransmitter transporter. Next, the images are processed in an image analysis program, such as Image-J, IDL, or MATLAB, using tracking algorithms that are readily available (Chang et al., 2012a; Blair and Dufresne, 2017). The density of QD labeling should be sufficiently low so that each QD spot is spatially separated further than the diffraction limit. The localization of each centroid is estimated by fitting individual bright spots to a 2D Gaussian distribution (Chang and Rosenthal, 2013b). Localization data (x,y) are then used to generate trajectories, and multiple parameters can be determined, such as mean square displacement (MSD), diffusion coef-

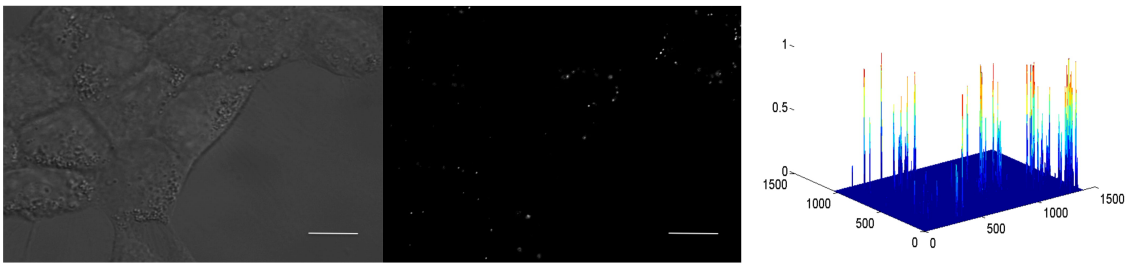


Figure 2.2: In a two step labeling protocol, biotinylated SERT-specific ligands are first bound to SERT followed by streptavidin-conjugated QDs. QDs act as point emitters that can then be characterized by a point spread function. Each centroid is fitted to a 2D Gaussian distribution. Localization data are then used for analysis. Scale bar, 10 μm.

ficient, confinement index, and instantaneous velocity. This chapter details how to carry out SPT experiments using ligands, antibodies, and streptavidin-conjugated or antibody-conjugated QDs targeted to membrane neurotransmitter transporters in heterologous cell lines or primary neuronal cultures. Basic analysis of the single particle trajectory data will also be discussed.

## 2.1 Ligand-based QD tracking

SPT permits real-time observation of neurotransmitter transporters (NTT) in the plasma membrane at a subdiffraction-limited spatial resolution and imaging rates at 10 Hz. As surface NTT trafficking appears to be an important post-translational regulatory mechanism, SPT analysis can provide invaluable information about NTT lateral diffusion dynamics, membrane compartmentalization, and dynamic interactions with its binding partners. QDs are bright, robust point-like emitters characterized by a narrow, well-defined point-spread function (PSF) and therefore an ideal probe choice in SPT studies (Fig. 2.2) (Chang and Rosenthal, 2013a). The point emitters must be separated farther than the diffraction-limited regime and thus must be in sufficiently low concentration. The centroid positions can then be localized with subpixel accuracy by fitting the intensity distribution to a 2D Gaussian

function:

$$I_{xy} = A_0 + A \times e^{\frac{(x-x_0)^2+(y-y_0)^2}{w^2}} \tag{2.1}$$

where $I_{xy}$ is the pixel intensity, A is signal amplitude, $A_0$ is local background, $x_0$ and $y_0$ are the local maximum coordinates of the Gaussian fit, and w is the width of the curve (Chang and Rosenthal, 2013b). The accuracy of the fit depends on the signal-to-noise ratio (SNR):

$$SNR = \frac{I_0}{\sqrt{\sigma_{bg}^2 + \sigma_{I_0}^2}} \tag{2.2}$$

where $I_0$ is the signal intensity, $\sigma_{bg}$ is the variance of the background intensity, and $\sigma_{I_0}$ is the variance of the signal intensity (Chang and Rosenthal, 2013b). QDs significantly increase the SNR compared to common organic fluorophores, providing another advantage as single molecule imaging probes. Once precise localization data (x, y) is determined, QD positions in successive frames must be linked to construct trajectories. We previously described in detail basic analysis using ImageJ (Chang and Rosenthal, 2013b). Once trajectories are constructed, net displacement and velocities can be determined, as well as mean square displacement (MSD). Our recent group efforts focused on visualizing and analyzing NTT membrane dynamics using antagonist-conjugated QDs. We first utilized a biotinylated serotonin transporter protein (SERT) antagonist, IDT 318, to specifically label individual SERT proteins within the membranes of serotonergic RN46A cells. We observed two distinct populations, one that freely diffused across the membrane and one that displayed restricted mobility and was confined to membrane microdomains. Upon SERT stimulation, individual proteins remained confined within microdomains but displayed untethering from cytoskeletons that allowed for increased mobility through a p38 MAPK pathway (Chang et al., 2012b). Next we visualized the dynamics of wild-type and ADHD-associated mutant (R615C) dopamine transporter protein (DAT) using a high affinity biotinylated cocaine analogue, IDT 444, and streptavidin-conjugated QDs in living transfected cells. From QD trajectory analysis, the R615C mutant showed increased

mobility and diffusion rates across the membrane compared to the wild type and lacked response to cholesterol depletion and amphetamine stimulation (Kovtun et al., 2015). These findings demonstrated, for the first time, how a disease-associated mutation affects the surface dynamics of single DAT proteins, which opens possibilities for future studies linking disease states with individual protein behavior. This protocol outlines QD labeling using a SERT-specific ligand, IDT 357, in NTT-expressing adherent cell lines and provides a set of common troubleshooting tips.

### 2.1.1 SERT-specific IDT 357 synthesis

For the ligand-based studies described in Chapter 5, a high affinity SERT-selective antagonist was biotinylated and PEGylated so that it could be used in conjunction with streptavidin-coated QDs. A homotryptamine-based SERT antagonist, 3-(1,2,3,6-tetrahydro pyridin-4-yl)-1H-indole, with a half-maximal inhibition ($IC_{50}$) of 80 nM was chosen as the drug molecule due to its high SERT specificity and basic nitrogen in the tetrahydropyridine ring that allowed for further conjugation. The full synthesis has been described previously (Tomlinson et al., 2011). An alkyl spacer arm with 11 methylene units was attached to the basic nitrogen and unprotected to obtain a primary amine terminus, which was then coupled to biotin PEG5000-succinimidyl NHS ester (Figure 2.3). Crude products of IDT 357 were then purified by high performance liquid chromatography (HPLC) and characterized by mass spectrometry. The biological activity of this ligand was then confirmed with the two-step labeling protocol described below. IDT 357 successfully labeled SERT-expressing HEK293T cells as evidenced by fluorescence along the membrane. When SERT was pre-blocked with paroxetine, a SERT inhibitor, fluorescence was eliminated (Figure 2.4).

### 2.1.2 Materials

The following materials are needed to carry out SPT experiments with a biotinylated NTT-specific ligand and streptavidin-coated QDs, from labeling the target to imaging.

1. No. 1.5 35-mm MatTek glass-bottom dishes (14 mm coverslip)

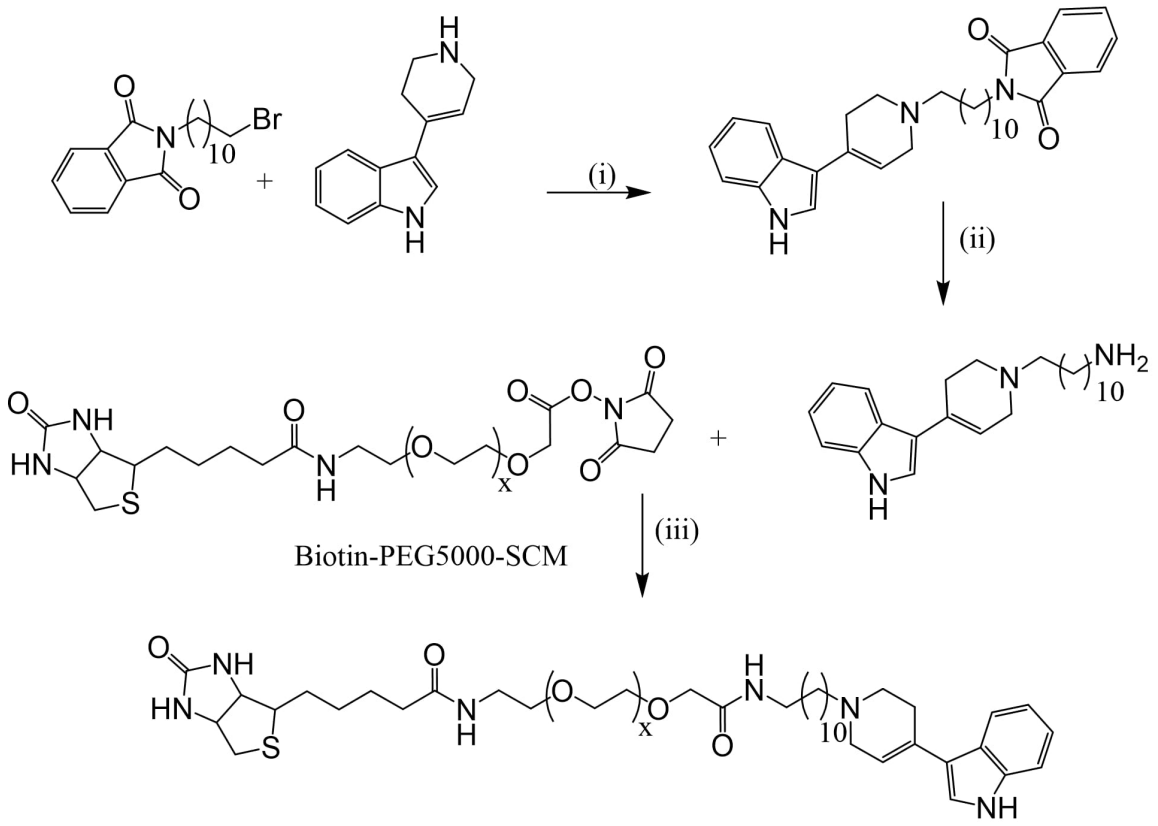


Figure 2.3: Synthesis of SERT-selective IDT357. (i) acetonitrile, triethylamine, reflux for 18 hours; (ii) ethanol, hydrazine monohydrate, ambient temperature, 1 hour; (iii) $CH_2Cl_2$, ambient temperature, 18 hours. Figure reproduced from (Kovtun et al., 2018).

2. Poly-D-lysine (working concentration of 0.01 mg/mL) to pre-coat glass-bottom dishes

3. Fluorobrite DMEM

4. Biotinylated NTT-specic ligand, like IDT357 (1 mM stock in phosphate buffered saline (PBS))

5. Streptavidin-conjugated QDs, prepared as a 1 M stock QD imaging solution (0.1 nM QD solution in Fluorobrite with 1-5% bovine serum albumin (BSA) and/or 1-2% fetal bovine serum (FBS))

6. Adherent cells expressing NTT of interest, in this case stably transfected SERT Flp-In Chinese Hamster Ovary (CHO) Cells

7. Analysis software (Microsoft Excel, ImageJ, MATLAB)

8. Fluorescence microscope, such as the Carl Zeiss LSM 5 Live, congured with a 63X 1.4NA oil immersion objective, solid-state laser diode (488 nm, 100 mW), and a linear array charge-coupled device (CCD) camera

### 2.1.3 Methods

This method is generalizable for any NTT in any cell line. The crucial factor is that the ligand is specific to the target of interest and that specificity is validated prior to SPT experiments.

1. Culture NTT-expressing cells in glass-bottom dishes until they are 50-60% confluent.

2. Prepare a solution of 0.01-0.1 nM streptavidin-conjugated QDs in warm DMEM Fluorobrite media containing 2-5% BSA or 1-2% dialyzed FBS. Vortex for 5 seconds to break up aggregates.

3. Add 0.1-0.5 nM biotinylated ligand directly to culture media and incubate for 5 minutes.

4. Wash cells gently 3-5 times with phenol-red free DMEM or DMEM Fluorobrite.

5. Add QD solution to cells and incubate at 37°C for 5 minutes.

6. Wash cells gently 3-5 times with warm DMEM Fluorobrite.

7. Place the dish on a heated (37°C) microscope stage and acquire time-lapse images.

The following experimental considerations should be taken into account, especially when troubleshooting common problems:

- A frame rate of 10 frames per second or faster is recommended using an appropriate filter for the type of QD. A 600/30 bandpass filter is used for 605 QDs.

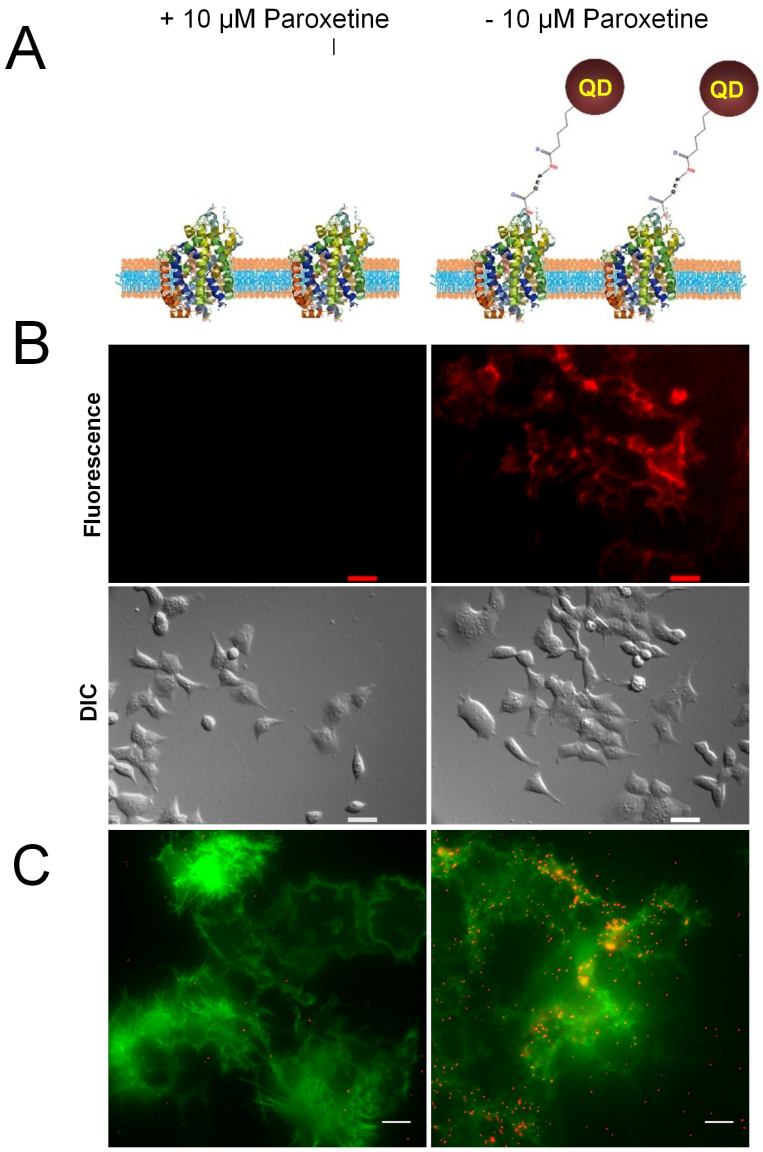


Figure 2.4: IDT357 labels SERT specifically. (A) Schematic showing the experimental design for the Paroxetine block. SERT-expressing HEK293T cells were labeled with 500 nM biotinylated IDT357 for 10 minutes followed by 1 nM streptavidin-conjugated QDs for 5 minutes. When paroxetine was included, no QD fluorescence was observed, indicating specific binding. (B) Widefield fluorescence and DIC images showing specific labeling of IDT357. Scale bar, 40 μm. (C) Widefield fluorescence images showing specific labeling of YFP-SERT. Scale bar, 10 μm. Figure reprinted from (Kovtun et al., 2018).

- Image in a low-background buffer, like DMEM Fluorobrite, to improve signal-to-noise ratio.

- Include a blocking reagent, such as BSA, dialyzed FBS, or casein, to decrease non-

specific labeling of QDs.

- Avoid QD internalization by imaging immediately after labeling.
- Decrease QD incubation time if QDs are internalizing.
- Determine ligand specificity using controls.

## 2.2 Antibody-based quantum dot tracking of endogenous transporters

Transporters have been visualized in heterologous cell lines using QDs, but they have not yet been utilized in endogenously-expressing primary neuronal systems, making this protocol a valuable resource. Our method is generalizable as many extracellular antibodies are already commercially available. In our method, biotinylated and unmodified antibody probes are used with streptavidin-functionalized and antibody-conjugated QDs, respectively, to detect individual neurotransmitter transporters. Monoclonal extracellular antibodies are more specific to the target of interest than polyclonal antibodies thus they are preferred for use in SPT experiments (AbCam Inc., 2014).

### 2.2.1 Materials

These materials cover what is needed for neuronal culture, QD labeling, and imaging.

**Neuronal culture**

1. Sprague-Dawley rats, postnatal day 0-2.
2. 24-well plates.
3. No. 0 bottom glass coverslips.
4. Forceps.
5. 70% ethanol for sterilization.
6. Fire-polished Pasteur pipettes.

7. Matrigel.

8. Trypsin.

9. HEPES buffer.

10. DNase.

11. Hanks buffer salt solution (HBSS).

12. Plating media: Minimum essential media (MEM, 500 mL), glucose (2.5 g), $NaHCO_3$ (1 M), transferrin (50 mg), L-glutamine (0.2 M), insulin (12.5 mg/mL), fetal bovine serum (FBS) (50 mL).

13. 4-AraC: MEM (500 mL), glucose (2.5 g), $NaHCO_3$ (1 M), transferrin (50 mg), L-glutamine (0.2 M), B-27 (10 mL), AraC stock (1.12 mg/mL), FBS (25 mL).

14. H+20: HBSS + 20% FBS.

15. Dissociation solution: HBSS + 12 mM $MgSO_4$ + DNase (1 kilo-unit/mL)

**QD labeling**

1. Streptavidin-conjugated 605 or 655 quantum dots.

2. Secondary antibody-conjugated 605 or 655 quantum dots.

3. Extracellular monoclonal antibody.

4. EZ-Link micro sulfo-NHS-LC biotinylation kit.

5. Bovine serum albumin (BSA) or dialyzed FBS.

6. Fluorobrite live-cell imaging media (to reduce background).

7. Tyrodes solution: 150 mM NaCl, 4 mM KCl, 2 mM $MgCl_2$, 2 mM $CaCl_2$, 10 mM HEPES buffer, 10 mM glucose in a final volume of 1 L deionized water, pH 7.35

8. 1.5 mL microcentrifuge tubes.

9. 15 mL conicals.

**Instruments and analysis software**

1. Fluorescence microscope with frame rate $\geq$ 10 frames per second (custom-built epi-fluorescence, Andor EMCCD camera, 600/30 bandpass filter).

2. Microscope heating chamber.

3. Microscope software (MetaMorph, Micromanager, or similar).

4. Image analysis software (Image-J or FIJI).

5. Data analysis software (Excel or MATLAB).

### 2.2.2 Methods

This protocol gives a general outline of neuronal culture dissociation and plating.

1. Dissect the midbrain or hippocampus from postnatal day 0 - 2 Sprague-Dawley rats. Cut tissue into 4-6 small pieces for further dissociation and place in 5 mL H+20.

2. Wash the tissue three times with HBSS. Add trypsin with DNase to the tissue and incubate for 10 minutes to digest the tissue and degrade the released DNA.

3. Fire-polish three glass Pasteur pipettes so that the diameters get progressively smaller. The largest diameter should have rounded edges but should not decrease in size. The next two should be smaller in diameter, with the smallest being around 0.5 mm.

4. Wash the tissue three times with 5 mL of H+20 to block the trypsin. Wash the tissue three more times with 5 mL of HBSS. Add 3 mL of the dissociation solution to prepare for the titration of the tissue.

5. Manually titrate the dissociation solution with tissue 5 times with the largest pipette to begin breaking up tissue. Repeat for the two other pipette sizes to dissociate the tissue into cells, keeping the tissue in the same dissociation solution. Do not attempt to wash.

6. Centrifuge the dissociation solution at 1,000 rpm at 4°C for 5 minutes.

7. Aspirate the supernatant and resuspend the cell pellet with warm plating media using the smallest-sized (about 0.5 mm diameter) pipette. Add enough volume to plate 100 µL of the cell solution onto the desired number of coverslips.

8. Plate 100 µL of cell solution onto matrigel-coated glass coverslips in a culture plate. Add 1 mL of plating media after 1-2 hours.

9. Add 1 mL 4-AraC the following day after cell plating to inhibit glial growth.

**Antibody biotinylation**

Streptavidin/biotin binding has long been utilized in biological studies due to its formation affinity constant of $10^{15}$ L mol$^{-1}$, making it one of the strongest noncovalent interactions reported (Christopoulos, 1991). In cases where the biotinylation of antibodies is possible, this protocol can be used in conjunction with streptavidin-conjugated QDs for labeling. Antibodies have numerous primary amino (NH2) groups available that are ideal for coupling reactions involving sulfo-N-hydroxysulfosuccinimide (sulfo-NHS). The EZ-Link Sulfo-NHS-LC-Biotin kit from Thermo Scientific makes the linking chemistry easy, quick, and straightforward. For all biotinylation reactions, the detailed protocol from Thermo Scientific was followed with no modification:

1. Calculate the millimoles of Sulfo-NHS-Biotin to add using the following formula:

$$\text{mL protein} \times \frac{mg protein}{mL protein} \times \frac{mmol protein}{mg protein} \times \frac{50 mmol biotin}{mmol protein} = \text{mmol biotin}$$

A 50-fold molar excess ensures 1-4 biotin groups per antibody.

2. Calculate the microliters of 9 mM Sulfo-NHS-LC-Biotin to add using the mmol biotin calculated in 1:

$$mmol biotin \times \frac{557mg}{mmol biotin} \times \frac{200\mu L}{1.0mg} = \mu L biotin solution$$

3. Dissolve 50-200 µg of antibody in 200-700 µL of phosphate-buffered saline (PBS).

4. Right before use, puncture one microtube of Sulfo-NHS-LC-Biotin and add 200 µL of water, giving 9 mM biotin, and add the calculated amount (step 2) to the antibody.

5. Incubate on ice for two hours or room temperature for 30-60 minutes.

6. Centrifuge this solution in the Zeba Spin Desalting Column from the kit by placing it in a 15 mL conical at 1000 x g for 2 minutes. Discard the storage buffer and mark the side that has the resin slanted upward. Place this side facing out for all further centrifugation steps.

7. Equilibrate the column with 1 mL of PBS and centrifuge again at 1000 x g for 2 minutes, discarding the buffer. Repeat 2-3 times.

8. Place the column in a new 15 mL conical and add antibody solution to the center of resin the until absorbed. Centrifuge again at 1000 x g for 2 minutes. The collected solution is the purified antibody.

9. Store the final product in microcentrifuge tubes in 5 µL aliquots at -20 ° C.

### 2.2.3 Single quantum dot labeling of neurotransmitter transporters in live neuronal cultures

These protocols are optimized for a two-step labeling procedure utilizing unmodified primary antibody and secondary antibody-conjugated QDs (Method A) or a biotinylated anti-

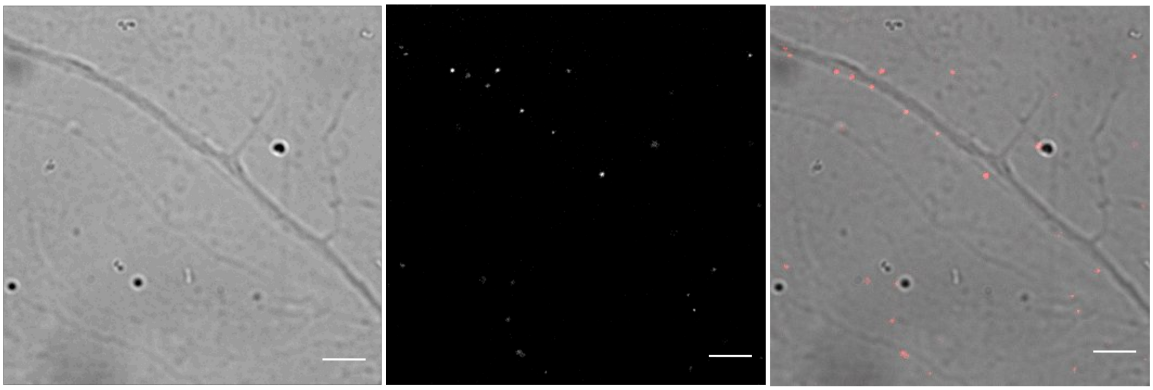

Figure 2.5: QD labeling of neurotransmitter transporters in cultured primary neurons. Primary antibody is bound to the transporters first followed by secondary antibody-conjugated QDs. Bright field, fluorescence, and overlay are shown. Scale bar, 10 μm.

body and streptavidin-functionalized QDs (Method B). In both methods, the antibodies are incubated with the neurons, washed and finally incubated with a 0.01-0.1 nM QD solution. After washing multiple times, the QDs are imaged using a custom-built epifluorescence microscope with an oil-immersion 60X or 100X objective lens (Fig. 2.5). Video-microscopy rates ($\geq$ 10 frames per second) and nanometer QD localization accuracy ($<$ 20 nm) are achieved with an electron multiplying charge-coupled device (EMCCD) camera (Andor). Single particles are then localized using imaging software, such as Image-J, to map trajectories (Fig. 2.6). These protocols are generalizable for any protein associated with a specific, extracellular antibody, including the GABAa receptor (Bannai et al., 2009), the glycine receptor (Dahan et al., 2003), the Dopamine D1 receptor (Ladepeche et al., 2013), and the glutamate transporter (Murphy-Royal et al., 2015). While this protocol is optimized for primary neuronal cultures, it is also applicable to heterologous expression systems.

**Method A: Unmodified primary extracellular antibody and secondary antibody conjugated QDs**

1. Culture dissociated neurons for two weeks on No. 0 glass coverslips.

2. Prepare a solution of 5-10 μg/mL primary antibody in warm fluorobrite media with

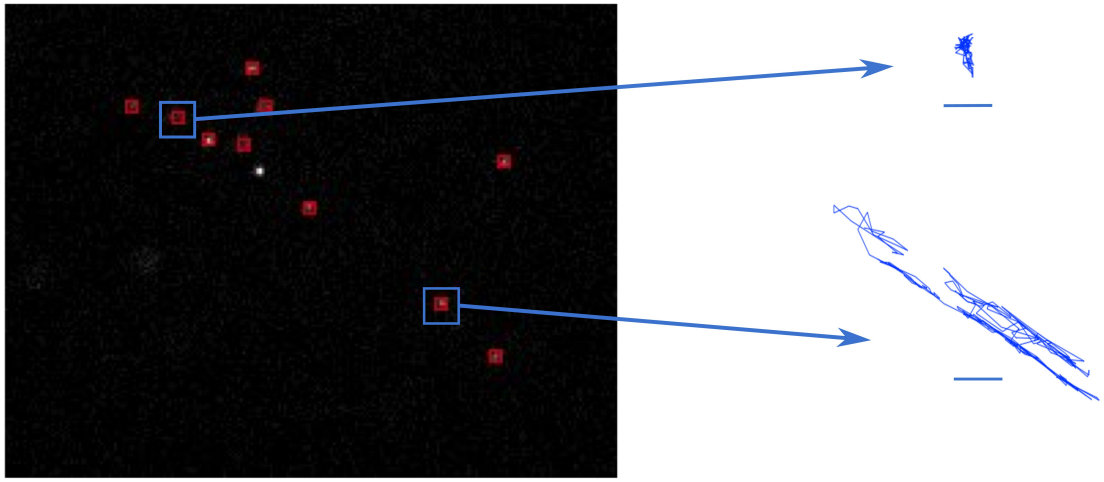

Figure 2.6: Single particles are localized using Image-J and trajectories are subsequently mapped. Single particle tracking reveals the heterogeneity in motion that exists between different proteins. Scale bar, 2 μm.

4% bovine serum albumin (BSA) to be added to cells. Invert multiple times to ensure mixing.

3. Prepare a solution of 0.05 - 0.15 nM secondary antibody-conjugated QDs (depending on desired QD density) in warm 4% BSA fluorobrite media. Invert multiple times to ensure mixing.

4. Remove the culture media and add the antibody solution to the neurons. Incubate at 37°C for 5-10 minutes.

5. Gently wash 2 times with warm fluorobrite media. Add the QD solution and incubate at 37°C for 3-5 min.

6. Gently wash 5 times with Tyrodes solution. Leave in Tyrodes.

7. Mount the coverslip onto a heated (37°C) microscope stage.

8. Acquire time-lapse images at a frame rate of 10 frames per second or faster using an appropriate filter for the QD used. A 600/30 bandpass filter was used for 605 QDs.

**Method B: Biotinylated antibody + streptavidin-conjugated QDs**

This method can be used when biotinylation of the antibody is possible without losing functionality.

1. Culture dissociated neurons for two weeks on No. 0 glass coverslips.

2. Prepare a solution of 5-10 μg/mL biotinylated antibody in warm fluorobrite media with 2-4% dialyzed FBS (dFBS) to be added to cells. Invert multiple times to ensure mixing.

3. Prepare a solution of 0.05 - 0.15 nM streptavidin QDs in warm 2-4% dFBS fluorobrite media. Vortex for 5 seconds to break up aggregates.

4. Remove the culture media and add the antibody solution to the neurons. Incubate at 37°C for 10 - 20 minutes.

5. Gently wash 2 times with warm dFBS fluorobrite. Add the QD solution and incubate at 37°C for 5 min.

6. Gently wash 5 times with Tyrodes solution. Leave in Tyrodes.

7. Mount the coverslip onto a heated (37°C) microscope stage.

8. Acquire time-lapse images at a frame rate of 10 frames per second or faster using an appropriate filter for the QD used. A 600/30 bandpass filter was used for 605 QDs.

The following notes are helpful considerations for troubleshooting during the experimental methods listed above:

- QDs are bound to an extracellular epitope of transporter proteins in an antibody-dependent manner. The motion of the transporter-bound QDs is monitored on the surface of cultured neurons. As cultured neurons are considered a low expression system with less than 1-2 transporters per $\mu m^2$ at the cell membrane, we estimate

QD labeling at 1:1 stoichiometry. However, in a higher expression system antibody-mediated QD labeling might lead to protein crosslinking and promote undesirable target protein internalization. In such cases, we recommend preforming QD-primary antibody complexes at 1:1 stoichiometry and only then labeling target proteins. An alternate route is generating monovalent antibody fragments with a single-antigen binding site.

- Pre-mix the antibody or QD solutions to reduce aggregation of each. Dilute the antibody and QDs in the final volume that will be added to the cells.

If the QDs are internalizing:

- Image immediately after labeling.
- Decrease the incubation time with QDs to 3 minutes.
- Label cells at 4°C to further minimize internalization.

If the QDs are binding nonspecifically:

- Increase the percentage of BSA or dFBS when incubating with the QDs.
- Include an additional blocking reagent (e.g., casein, newborn calf serum, dehydrated fat-free milk).
- Increase the number of wash steps.
- Perform a control experiment with QDs only.
- Perform a control experiment with a blocking agent (e.g., a peptide sequence for the protein).

If signal-to-noise ratio is low:

- Use a low-background buffer, like DMEM Fluorobrite.

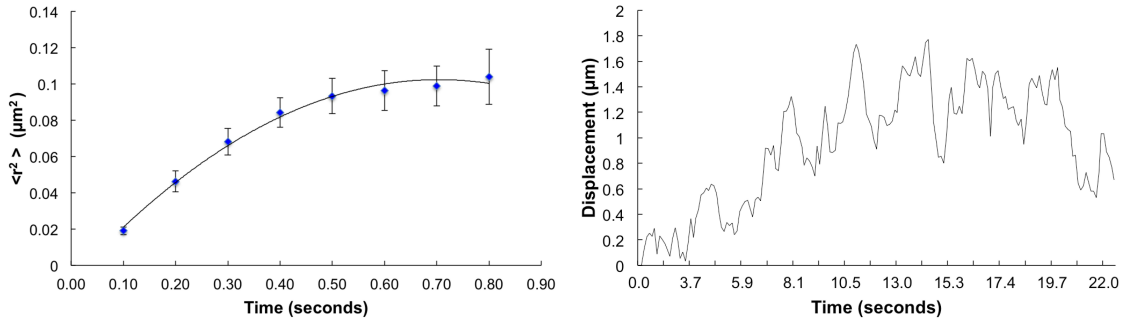


Figure 2.7: Example MSD and displacement plots showing confined motion for a single particle trajectory (see Fig. 2.6).

- Adjust the pinhole size, gain, and amplitude.
- Increase the excitation intensity.

## 2.3 Serotonin transporter-specific drug treatments

One of the aims in this dissertation was to assess whether acute and chronic cholesterol depletion releases neuronal SERT from cholesterol-rich membrane microdomains in primary neurons. We thus employed two main techniques for manipulating cholesterol. Acute cholesterol depletion by methyl-beta-cyclodextrin (M$\beta$CD) is an established method for removing cellular surface cholesterol. M$\beta$CD sequesters membrane cholesterol, efficiently removing it and disrupting potential cholesterol-rich membrane domains (Zidovetzki and Levitan, 2007). Chronic cholesterol depletion, where cholesterol biosynthesis is inhibited, can be accomplished through statins. Statins are used clinically to reduce the risk of cardiovascular disease. They inhibit production of the HMG-CoA reductase in cholesterol synthesis, which reduces overall cholesterol serum levels. Statins have been associated with adverse cognitive effects, including depression. Many statins were found to be blood-brain-barrier permeable, and treatments with statins led to lowered cholesterol levels in the brain (Vevera et al., 2016).

For acute cholesterol depletion, cells were incubated with 5 µM methyl-$\beta$-cyclodextrin (M$\beta$CD, Fisher Scientific) at 37°C for 30 min. Cells were then washed gently with imaging

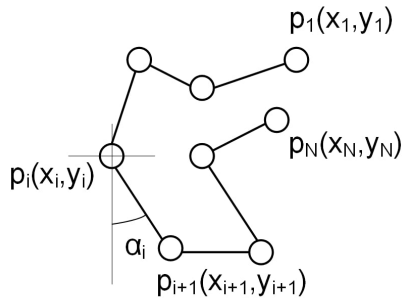


| Parameter | Definition |
|---|---|
| **Total displacement** | $\Delta r_{total} = \sum_{i=1}^{N-1} \Delta r(p_i, p_{i+1})$ |
| **Net displacement** | $\Delta r_{net} = \Delta r(p_i, p_{i+1})$ |
| **Confinement ratio** | $z_{conf} = \Delta r_{net} / \Delta r_{total}$ |
| **Instantaneous angle** | $\alpha_i = \arctan(y_{i+1} - y_i) / (x_{i+1} - x_i)$ |
| **Instantaneous velocity** | $v_i = \Delta r(p_i, p_{i+1}) / \Delta t$ |
| **Mean square displacement** | $MSD(n) = \frac{1}{N-1} \sum_{i=1}^{N-n} \Delta r^2(p_i, p_{i+n})$ |

Table 2.1: Biologically useful quantitative parameters derived from a single particle trajectory. The example 2D trajectory drawn on the left consists of N points ($p_1(x_1,y_1)$ through $p_N(x_N,y_N)$). The table on the right provides mathematical definitions for several quantitative measures commonly encountered in the literature. Δr is defined as the Euclidean norm between two consecutive trajectory points.

buffer before labeling with QDs according to the appropriate protocol listed above. At this concentration, no morphology changes were seen. For chronic cholesterol depletion, cells were incubated with 50 μM mevastatin (Sigma) for 16 hours according to previously published methods (Shrivastava et al., 2010). Cells were then washed gently with imaging buffer followed by QD labeling. Again, at this incubation concentration and time, cell morphology was not compromised.

To assess the effects of PKG activation on SERT mobility, we used 8-Br-cGMP, which stimulates the PKG pathway, increasing Thr276 phosphorylation levels. For PKG activation, cells were incubated with 100 μM 8-Br-cGMP (Sigma) for 30 min to 1 hour followed by washing and labeling with QDs.

## 2.4 Analysis of single particle tracking data

The goal of SPT trajectory analysis is to extract quantitative parameters of motion and consequently elucidate the type of motion and diffusive behavior each particle undergoes. Table 2.1 defines a set of particularly useful motion parameters associated with each trajectory. As the protein diffusion is a stochastic process, a pool of multiple displacements,

| Diffusion Model | MSD Definition | Parameters |
|---|---|---|
| **Linear** | $4Dt$ | $D$ (diffusion coefficient) |
| **Anomalous** | $4D_\alpha t^\alpha$ | $D_\alpha, \alpha$ (confinement coefficient) |
| **Directed** | $4Dt + (Vt)^2$ | $D, V$ (velocity) |
| **Restricted** | $L^2(1 - A_1 e^{-4A_2 Dt/L^2})$ | $D, L$ (length of the confinement domain) |

Table 2.2: Different modes of diffusion defined by the analytical forms of the MSD versus time curves (Saxton and Jacobson, 1997).

$\Delta r_{(pi,pi+1)}$, is necessary to attain a more complete understanding of the particle dynamic behavior. The most popular means of analyzing a pool of multiple displacements within a single trajectory is by computing the MSD, which gives a measure of the area explored by a particle at any given time interval. By fitting the MSD curve over time with the appropriate equations, it is thus possible to identify the mode of motion the particle undergoes. Table 2.2 provides analytical forms of the MSD curve that describe linear (free) diffusion, anomalous subdiffusion, directed motion, and restricted (corralled) diffusion (Saxton and Jacobson, 1997). Once x and y positions have been identified from a single trajectory, MSD can be calculated using the following formula (19):

$$MSD(n\Delta t) = \frac{1}{N-n} \sum_{i=1}^{N-n} (x_{i+n} - x_i)^2 + (y_{i+n} - y_i)^2 \tag{2.3}$$

where N is the total number of frames, n Δ t is the time interval in which the MSD is calculated, and $x_i$ and $y_i$ are the positions of the particles in the trajectories (Fig 2.7). Here, we provide a stepwise protocol for calculating the MSD:

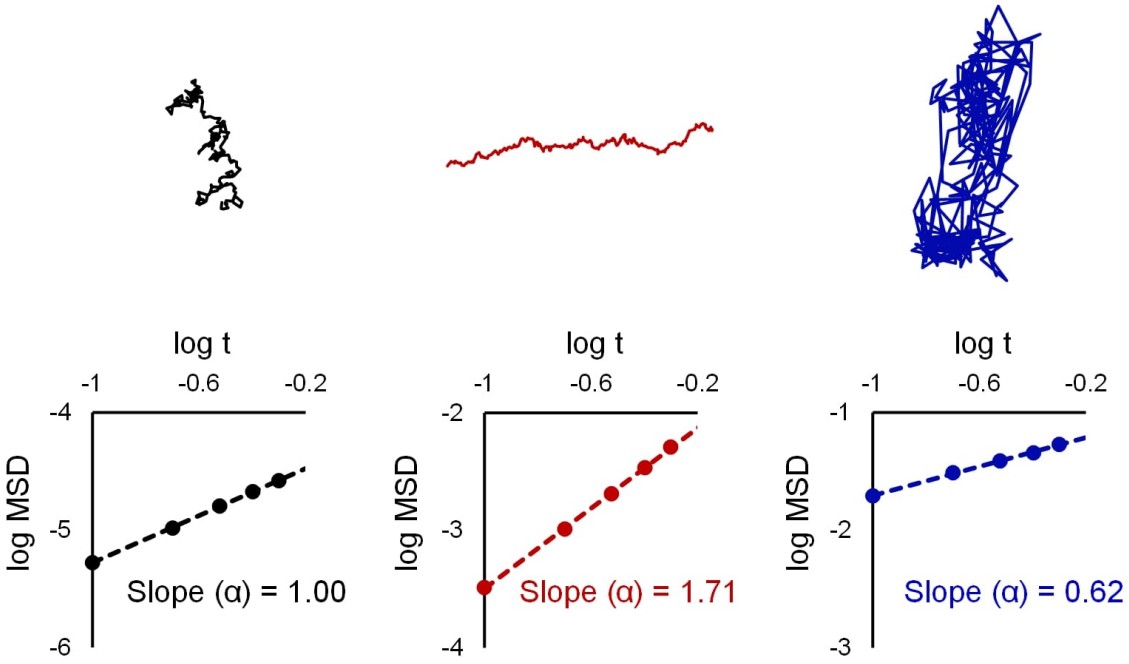


Figure 2.8: Graphical guide for determining the trajectory motion type based on the $\alpha$ parameter. Individual MSD versus time curves are transformed to the log-log plot; the $\alpha$ parameter, i.e., the slope of the linear regression line (dashed) of the resulting plot, is then used to classify the motion type of each trajectory as restricted ( $\alpha < 1$), Brownian ($\alpha = 1$), Brownian + directed ($1 < \alpha < 2$), or "pure" active transport ($\alpha = 2$).

1. Display the trajectory data as a numeric array of particle xy-position over time t:

| | | |
|---|---|---|
| $x_1$ | $y_1$ | $t_1$ |
| $x_2$ | $y_2$ | $t_2$ |
| $x_3$ | $y_3$ | $t_3$ |
| $x_4$ | $y_4$ | $t_4$ |
| $x_5$ | $y_5$ | $t_5$ |

2. Determine the minimum lag time as $\Delta t = t_2 - t_1$ (i.e., temporal resolution of acquisition).

3. Extract from the trajectory the following displacements at a lag time of Δt:

$$\Delta r_{21} = (\Delta x_{21} = x_2 - x_1, \Delta y_{21} = y_2 - y_1)$$

$$\Delta r_{32} = (\Delta x_{32} = x_3 - x_2, \Delta y_{32} = y_3 - y_2)$$

$$\Delta r_{43} = (\Delta x_{43} = x_4 - x_3, \Delta y_{43} = y_4 - y_3)$$

$$\Delta r_{54} = (\Delta x_{54} = x_5 - x_4, \Delta y_{54} = y_5 - y_4)$$

4. Extract the following displacements at a lag time of 2Δt:

$$\Delta r_{31} = (\Delta x_{31} = x_3 - x_1, \Delta y_{31} = y_3 - y_1)$$

$$\Delta r_{42} = (\Delta x_{42} = x_4 - x_2, \Delta y_{42} = y_4 - y_2)$$

$$\Delta r_{53} = (\Delta x_{53} = x_5 - x_3, \Delta y_{53} = y_5 - y_3)$$

5. Repeat this calculation for a given trajectory at increasing lag times that are multiples of Δt. Square and average individual displacements to yield MSD values for each lag time. For convenience, the example MATLAB code for implementing this calculation is provided in Fig. 2.9.

6. To determine the motion type a tagged molecule undergoes, transform the MSD versus Δt curve to its log-log form:

$$logMSD(t) = log4D + \alpha logt \tag{2.4}$$

7. Calculate the $\alpha$ value from the slope of the log-log curve and determine the mode of motion:

```
%   x: vector of x positions converted from pixels to microns;
%   y: vector of y positions converted from pixels to microns;
%   code below is applicable to trajectories without gaps due to blinking;

tau = 0.1; % time in s between trajectory points, i.e. temporal resolution of acquisition
data = sqrt(x.^2 + y.^2);
N = length(data); % number of data points in the trajectory
ndt = floor(N/4); % ndt should be up to 25% of number of data points

msd = zeros(ndt, 1); % vector storing a pool of MSD values calculated for each dt
msdpts = zeros(ndt, 1); % vector with calculated MSD values
dt = zeros(ndt, 1); % dt lag time vector
sem = zeros(ndt, 1); % vector with SEM values for each MSD point

% calculate msd for all dt's

for i = 1:ndt;
  msd = (data(1+i:end) - data(1:end-i)).^2;
  dt(i) = i * tau;
  sem(i) = std(msd) / sqrt(length(msd));
  msdpts(i) = mean(msd);
end
```

Figure 2.9: Example MATLAB code demonstrating how to calculate MSD from individual x and y positions.

$\alpha < 1$ anomalous subdiffusion

$\alpha = 1$ Brownian motion

$\alpha > 1$ anomalous superdiffusion

$\alpha = 2$ active transport

The $\alpha$ exponent gives a measure of the degree the motion of a QD-tagged molecule is influenced by the local environment (Fig. 2.8). Smaller values of the exponent correspond to either increased binding or a higher density of obstacles (organelles, lipid rafts, or cytoskeleton) in the diffusion path. Larger $\alpha$ values are usually indicative of active cellular transport events.

In summary, the protocols outlined in this chapter included QD labeling techniques for both ligand- and antibody-conjugated QDs, as well as basic analysis for SPT experi-

ments. Additionally, the primary midbrain culture protocol was detailed. For the rest of the dissertation, these methods were used unless otherwise noted.

**Copyright Permissions**

## 2.5 Bibliography

AbCam Inc. (2014). Polyclonal and monoclonal: A comparison. pages 1–2.

Bailey, D. M., Kovtun, O., and Rosenthal, S. J. (2017). Antibody-Conjugated Single Quantum Dot Tracking of Membrane Neurotransmitter Transporters in Primary Neuronal Cultures. In *Biomedical Nanotechnology: Methods and Protocols*, volume 726, pages 165–177.

Bannai, H., Lévi, S., Schweizer, C., Inoue, T., Launey, T., Racine, V., Sibarita, J. B., Mikoshiba, K., and Triller, A. (2009). Activity-Dependent Tuning of Inhibitory Neurotransmission Based on GABAAR Diffusion Dynamics. *Neuron*, 62(5):670–682.

Biermann, B., Sokoll, S., Klueva, J., Missler, M., Wiegert, J. S., Sibarita, J. B., and Heine, M. (2014). Imaging of molecular surface dynamics in brain slices using single-particle tracking. *Nature Communications*, 5(3024).

Bilan, R., Fleury, F., Nabiev, I., and Sukhanova, A. (2015). Quantum dot surface chemistry and functionalization for cell targeting and imaging. *Bioconjugate Chemistry*, 26(4):609–624.

Blair, D. and Dufresne, E. (2017). The Matlab Particle Tracking Code Repository.

Chang, J. C., Kovtun, O., Blakely, R. D., and Rosenthal, S. J. (2012a). Labeling of neuronal receptors and transporters with quantum dots. *Wiley Interdisciplinary Reviews: Nanomedicine and Nanobiotechnology*, 4(6):605–619.

Chang, J. C. and Rosenthal, S. J. (2013a). A bright light to reveal mobility: Single quantum dot tracking reveals membrane dynamics and cellular mechanisms. *Journal of Physical Chemistry Letters*, 4(17):2858–2866.

Chang, J. C. and Rosenthal, S. J. (2013b). Quantum Dot-Based Single-Molecule Microscopy for the Study of Protein Dynamics. *NanoBiotechnology Protocols, Methods in Molecular Biology*, 1026:71–84.

Chang, J. C., Tomlinson, I. D., Warnement, M. R., Ustione, A., Carneiro, A. M. D., Piston, D. W., Blakely, R. D., and Rosenthal, S. J. (2012b). Single Molecule Analysis of Serotonin Transporter Regulation Using Antagonist-Conjugated Quantum Dots Reveals Restricted, p38 MAPK-Dependent Mobilization Underlying Uptake Activation. *Journal of Neuroscience*, 32(26):8919–8929.

Christopoulos, K. (1991). The Biotin-(Strept)Avidin System: Principles and Applicationsin Biotechnology. *Clinical chemistry*, 37(5):625–636.

Courty, S., Luccardini, C., Bellaiche, Y., Cappello, G., and Dahan, M. (2006). Tracking individual kinesin motors in living cells using single quantum-dot imaging. *Nano Letters*, 6(7):1491–1495.

Dahan, M., Lévi, S., Luccardini, C., Rostaing, P., Riveau, B., and Triller, A. (2003). Diffusion Dynamics of Glycine Receptors Revealed by Single-Quantum Dot Tracking. *Science*, 302(5644):442–445.

Kovtun, O., Sakrikar, D., Tomlinson, I. D., Chang, J. C., Arzeta-Ferrer, X., Blakely, R. D., and Rosenthal, S. J. (2015). Single-Quantum-Dot Tracking Reveals Altered Membrane Dynamics of an Attention-Deficit/Hyperactivity-Disorder-Derived Dopamine Transporter Coding Variant. *ACS Chemical Neuroscience*, 6(4):526–534.

Kovtun, O., Tomlinson, I. D., Bailey, D. M., Thal, L. B., Ross, E. J., Harris, L., Frankland, M. P., Ferguson, R. S., Glaser, Z., Greer, J., and Rosenthal, S. J. (2018). Single quantum dot tracking illuminates neuroscience at the nanoscale. *Chemical Physics Letters*, 706:741–752.

Kovtun, O., Tomlinson, I. D., Sakrikar, D. S., Chang, J. C., Blakely, R. D., and Rosenthal, S. J. (2011). Visualization of the cocaine-sensitive dopamine transporter with ligand-conjugated quantum dots. *ACS Chemical Neuroscience*, 2(7):370–378.

Ladepeche, L., Dupuis, J. P., Bouchet, D., Doudnikoff, E., Yang, L., Campagne, Y., Bezard, E., Hosy, E., and Groc, L. (2013). Single-molecule imaging of the functional crosstalk between surface NMDA and dopamine D1 receptors. *Proceedings of the National Academy of Sciences*, 110(44):18005–18010.

Murphy-Royal, C., Dupuis, J. P., Varela, J. A., Panatier, A., Pinson, B., Baufreton, J., Groc, L., and Oliet, S. H. R. (2015). Surface diffusion of astrocytic glutamate transporters shapes synaptic transmission. *Nature Neuroscience*, 18(2):219–226.

Pinaud, F., King, D., Moore, H. P., and Weiss, S. (2004). Bioactivation and Cell Targeting of Semiconductor CdSe/ZnS Nanocrystals with Phytochelatin-Related Peptides. *Journal of the American Chemical Society*, 126(19):6115–6123.

Pinaud, F., Michalet, X., Iyer, G., Margeat, E., Moore, H. P., and Weiss, S. (2009). Dynamic partitioning of a glycosyl-phosphatidylinositol-anchored protein in glycosphingolipid-rich microdomains imaged by single-quantum dot tracking. *Traffic*, 10(6):691–712.

Rosenthal, S. J., Tomlinson, I., Adkins, E. M., Schroeter, S., Adams, S., Swafford, L., McBride, J., Wang, Y., DeFelice, L. J., and Blakely, R. D. (2002). Targeting cell surface receptors with ligand-conjugated nanocrystals. *Journal of the American Chemical Society*, 124(17):4586–4594.

Saxton, M. J. and Jacobson, K. (1997). SINGLE-PARTICLE TRACKING:Applications to Membrane Dynamics. *Annual Review of Biophysics and Biomolecular Structure*, 26(1):373–399.

Shrivastava, S., Pucadyil, T. J., Paila, Y. D., Ganguly, S., and Chattopadhyay, A. (2010). Chronic cholesterol depletion using statin impairs the function and dynamics of human serotonin1A receptors. *Biochemistry*, 49(26):5426–5435.

Thal, L. B., Bailey, D. M., Kovtun, O., and Rosenthal, S. J. (2017). Quantum Dot Toolbox in Membrane Neurotransmitter Transporter Research. In *Membrane Proteins: Chemical and Synthetic Approaches*, pages 219–230.

Tomlinson, I. D., Iwamoto, H., Blakely, R. D., and Rosenthal, S. J. (2011). Biotin tethered homotryptamine derivatives: High affinity probes of the human serotonin transporter (hSERT). *Bioorganic and Medicinal Chemistry Letters*, 21(6):1678–1682.

Valizadeh, A., Mikaeili, H., Samiei, M., Farkhani, S. M., Zarghami, N., Kouhi, M., Akbarzadeh, A., and Davaran, S. (2012). Quantum dots: Synthesis, bioapplications, and toxicity. *Nanoscale Research Letters*, 7(1):480.

Vevera, J., Vales, K., Fisar, Z., Hroudova, J., Singh, N., Stuchlik, A., Kacer, P., and Nekovarova, T. (2016). The effect of prolonged simvastatin application on serotonin uptake, membrane microviscosity and behavioral changes in the animal model. *Physiology and Behavior*, 158:112–120.

Zhang, Q., Li, Y., and Tsien, R. W. (2009). The dynamic control of kiss-and-run and vesicular reuse probed with single nanoparticles. *Science*, 323(5920):1448–1453.

Zidovetzki, R. and Levitan, I. (2007). Use of cyclodextrins to manipulate plasma membrane cholesterol content: Evidence, misconceptions and control strategies. *Biochimica et Biophysica Acta - Biomembranes*, 1768(6):1311–1324.

# CHAPTER 3

## Single molecule imaging with monovalent aptamer- quantum dot conjugates

### 3.1 Introduction

Quantum dots (QDs) are semiconductor nanocrystals that have high brightness, resistance to photobleaching, and size-dependent tunability (Chang and Rosenthal, 2013). Unlike traditional fluorophores, they are able to illuminate protein dynamics in cells in real time at longer time scales, offering broad absorption, narrow emission, and large Stokes shift, leading to the potential for multiplexing within the same single particle tracking experiment (Resch-Genger et al., 2008). One difficulty with QD tracking in live cells includes multivalency, which can cause oligomerization, leading to potential protein activation, internalization, or reorganizing of cell surface proteins, thus altering native protein dynamics along the membrane (Saxton and Jacobson, 1997). Because QDs have the unique multiplexing and photoresistance advantage, probe development has been a huge focus in the nanocrystal and microscopy communities, with monovalency representing just one area of focus. A QD probe is considered monovalent when a single QD has just one point of attachment for the protein of interest. For example, commercially available streptavidin-conjugated QDs have 4-10 streptavidins on the surface, and each of these has 4 potential binding sites that a biotinylated target can bind to (Howarth et al., 2008). In a crowded cellular membrane space, this high number of binding sites greatly increases the chances of binding two proteins to one QD. While monovalency is certainly a goal for QD tracking experiments, monovalent QD synthesis has traditionally proven difficult, as both synthesis and purification methods have resulted in low yields (Farlow et al., 2013). Other monovalent QD syntheses required difficult purification methods, such as gel purification or magnetic bead separation, to separate the monovalent QDs from the multivalent ones (Howarth et al., 2008; Liu and Gao, 2011; Uddayasankar et al., 2014).

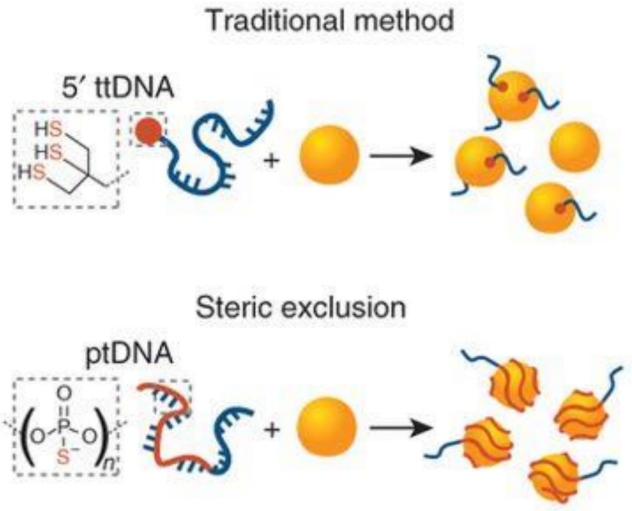


Figure 3.1: Schematic showing traditional versus steric exclusion methods for attaching DNA to QDs. Traditionally, trithiol DNA (ttDNA) attaches to QDs with large valency distributions. The steric exclusion method generates monovalent ptDNA-QDs with one DNA strand per QD. Figure reprinted with permission from Springer Nature. (Farlow et al., 2013)

Single strand DNA and RNA aptamers have both been a recent area of interest for targeted nanoparticle delivery and tracking, especially for drug delivery applications. RNA aptamers are of specific interest due to their high affinity and specificity for their target, acting like a lock and key (Germer et al., 2013). Additionally, RNA aptamers can be synthesized in large quantities and chemically modified for stability, and compared to antibodies, are much smaller in size, which is ideal for single particle tracking applications (Germer et al., 2013). Recently, Farlow et al. designed a novel method to produce monovalent quantum dots with a steric exclusion method using phosphorothioate DNA (ptDNA) (Figure 3.1). Traditional attempts at conjugating DNA to QDs with trithiol DNA (ttDNA) led to a distribution of number of DNA strands attached to the surface of the QD, and attempts at purifying just one DNA per QD proved difficult. For this steric exclusion method, instead of a single attachment point at the end of the DNA strand, ptDNA was synthesized that included 50 adenosines with the phosphorothioate backbone that had the affinity for

the QD surface. Its length was optimized to wrap around the whole surface of 605 nm QDs. This ptDNA strand ended with a sequence that could be targeted to its complement in live cells. The large size of the ptDNA excludes other molecules from reacting with the quantum dot surface, resulting in one polymer per QD (Farlow et al., 2013). Their method can be tailored for many diverse applications, as the protein or target of interest can be genetically encoded to express the DNA complement. The monovalency of these QDs decreases the chance of oligimerization and increases confidence in target specificity. We build upon these methods by incorporating a DNA/RNA aptamer hybrid that can target extracellular green fluorescent protein (GFP), which is a common addition to many surface proteins. The method outlined here allows for ease of targeting, as GFP is both a common and small addition to a protein. Additionally, this method can be altered for any aptamer specific to any protein. We chose GFP as a proof of principle demonstration, but an aptamer specific to the native protein of interest could be used to eliminate protein modification. This chapter includes the generation of the aptamer-QDs, verification of monovalency, and representative live cell imaging.

## 3.2 Experimental techniques

### 3.2.1 Generation of aptamer-QDs

#### Phase transfer of organic QDs

The method from Farlow et al. was followed with a few modifications (Farlow et al., 2013). 605 nm emitting CdSe/ZnS ITK QDs were bought from Life Technologies in the organic phase. 100 µl of a 1 µM solution of organic phase 605 QDs was added to 400 µl chloroform. The QDs were then mixed with 400 µl of a 0.3 M tetrabutylammonium bromide (TBAB) (chloroform) solution with 36 µl of methoxy polyethylene glycol (mPEG) thiol on a shaker overnight. The next day, 800 µL of a 0.2 M NaOH aqueous solution was added and vortexed for 1 minute. The QDs should then be in the aqueous phase as indicated by the color being in the top layer only (Figure 3.2). If phase transfer was not successful, more NaOH and

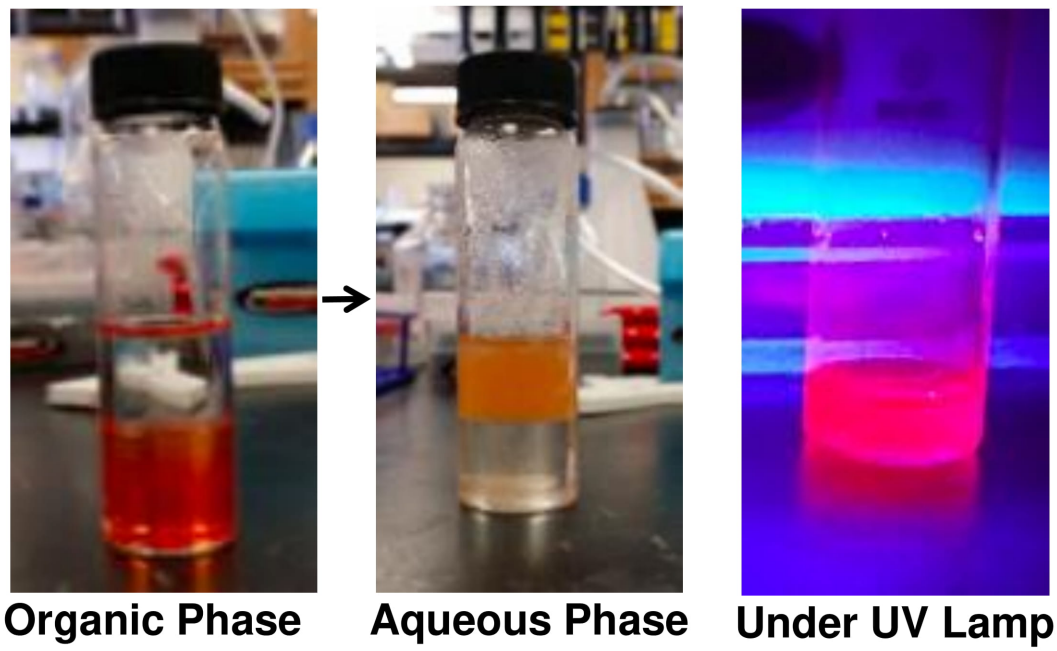


Figure 3.2: Organic phase QDs are transferred to the aqueous phase. QDs are excited under UV lamp.

TBAB was added, and they were then centrifuged at 1,000 g for 1 min. They were vortexed until the phase transfer was complete. The aqueous phase was recovered and transferred to a glass vial. The QDs were concentrated to 1 mL using an Amicon centrifugal spin column (30 kDa cutoff) at 4,000 g for 10 minutes. A Sephadex NAP10 (SNAP10) column (GE Healthcare) was then equilibrated with 10 mM Tris buffer with 30 mM NaCl at a pH of 8.0. The concentrated QDs were then added to the column and eluted with 1.5 mL of the Tris buffer. This step was carried out in a dark room with a UV lamp to aid in seeing when the QDs had all been eluted.

**ptDNA-QD conjugation**

Phosphorothioate DNA (ptDNA) was purchased from Integrated DNA Technologies with the following sequence: 5- AS50 CTC TCT CTC TCT CTC TCT CCC AGA AGA CCC -3. One drop of 200 nM ptDNA was added every 30 minutes to the bare QD solution in a 1:1 ratio while stirring vigorously for at least 9 hours.

### Gel electrophoresis

Gel electrophoresis was used to confirm monovalency. 10 μL QDs were mixed with 2 μL 80% glycerol and run on a 0.8% wt/v agarose gel in sodium borate buffer for 15 minutes at 8 V/cm. Gels were imaged using a MCBR Gel Doc EZ Reader. Bare QDs were confirmed when a single band showed in the well, and ptDNA-conjugated QDs were confirmed by presence of a single migrated band. ptDNA was added until a single band formed out of the well.

### Production of aptamer-QDs

A 150 nM solution of the GFP aptamer hybrid (Integrated DNA Technologies) was added dropwise in the dark while stirring. 10 μL of RNase inhibitor was added at a dilution of 100 units/mL to prevent degradation. To aid in hybridization of the complementary DNA sequences, the solution was then heated on a heat block to 55°C for 10 min and then cooled for 10 min. The QDs were then ready for imaging and used immediately after.

### Alkane PEG-thiol passivation

To better passivate the QD surface for biological imaging, the PEG thiol used for phase transfer was displaced with a longer alkane PEG-thiol. This ligand exchange improved both stability of the QDs as well as nonspecific binding (Farlow et al., 2013). 100 μL of 10 mM carboxy PEG6 alkane thiol ($(CO_2H)CH_2O(CH_2CH_2O)_6C_{11}H_{23}SH$, ProChimia) was added to the aptamer-QDs for 10 min. Excess alkane PEG-thiol was removed by adding 0.5 mL QDs to a SNAP5 column pre-equilibrated with elution buffer as described above. The QDs were collected with 1 mL elution buffer.

### QD immobilization

QDs were diluted to 5 pM in HCl-containing Tris and mixed with 1% agarose sodium borate buffer solution. Before cooling, a thin layer was spread on glass coverslips and imaged as described above. Images were analyzed in Matlab using custom algorithms.

### 3.2.2 Verification of monovalency

#### Generation of TEM construct

To generate the construct for validation of monovalency, aptamer-QDs were generated as described above. 100 μM biotinylated anti-GFP monoclonal antibody (Abcam) was added dropwise to 300 μM Au-Streptavidin (Nanocs) while stirring. The lower concentration of antibody was chosen to eliminate the chance of multiple antibodies binding to the multiple binding sites on streptavidin. 0.104 μM GFP was then added dropwise, followed by 0.150 μM of the aptamer-QDs. This solution was then applied to a copper grid (Ted Pella) for TEM imaging.

#### Transmission electron microscopy

All TEM images were taken using a Tecnai Osiris transmission electron microscope (TEM) at Vanderbilt University. Images were acquired at a voltage of 200 kV. Solutions were applied to an ultrathin carbon type-A, 400 mesh, copper grid (Ted Pella) using the dip-dip method.

#### Denaturing polyacrylamide TBE-urea gel electrophoresis

3 μL aptamer was added to 3 μL tris borate EDTA (TBE) loading buffer (Bio-rad) containing both bromophenol blue and xylene cyanol tracking dyes, and run on 15% TBE-Urea Gels (bio-rad) at 200 V for 60 minutes. Urea was flushed from the wells prior to sample loading. Gels were imaged using a MCBR Gel Doc EZ Reader. For samples incubated with cell culture media, 3 μL stock aptamer was added to either water (stock control) or culture media and placed in the incubator for the indicated time periods. For the fluorobrite samples, 3 μL stock aptamer was added to either water (stock control), fluorobrite, or fluorobrite plus RNase inhibitor for the indicated time periods.

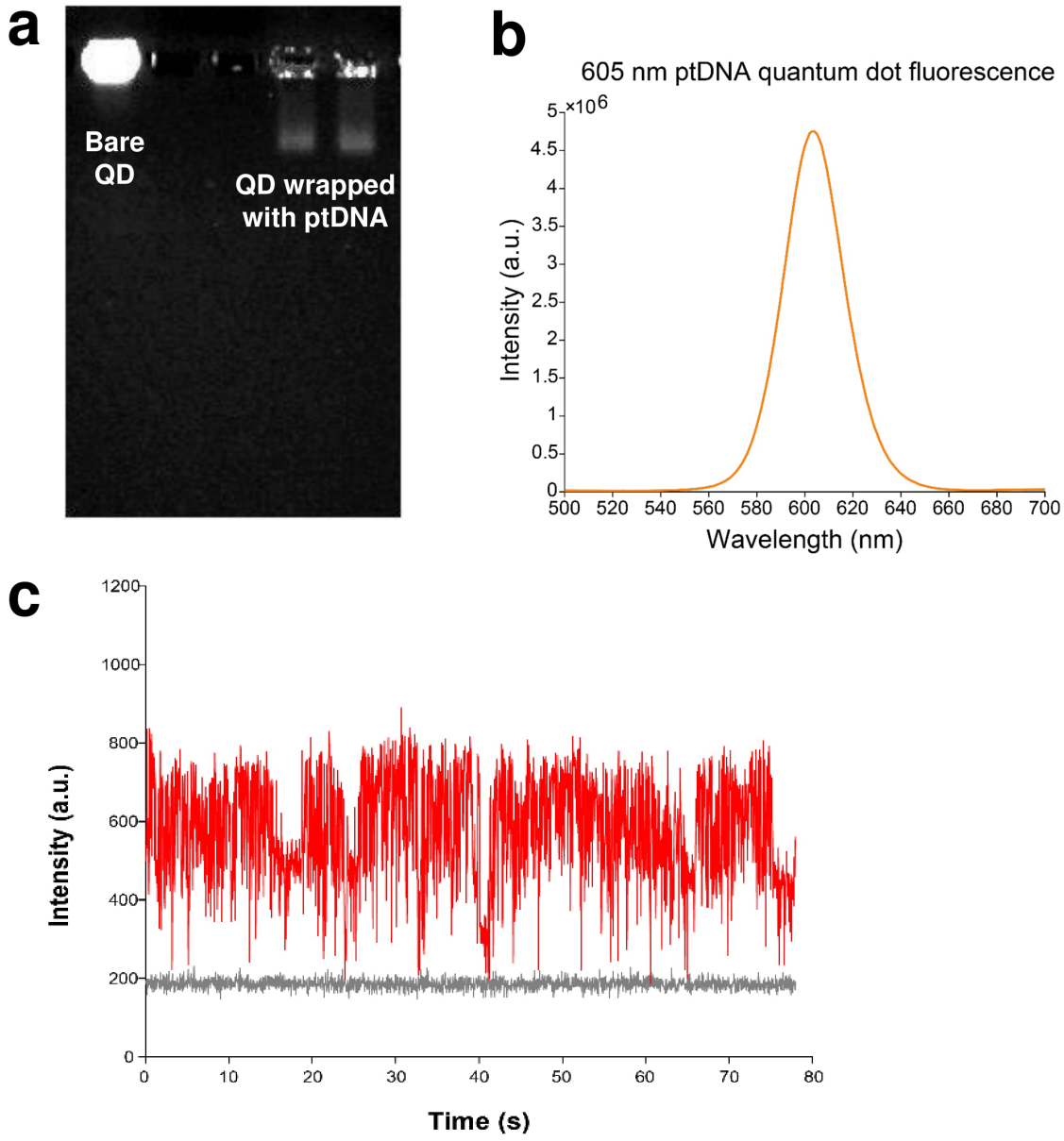


Figure 3.3: (A) Aqueous phase transferred QDs were net neutral, thus they stayed in the well during gel electrophoresis. QD ptDNA wrapping was confirmed by a migration out of the well into a single band. (B) ptDNA-QDs emitted at 605 nm, indicating that the phase transfer process and ptDNA wrapping did not affect fluorescence. (C) Blinking pattern and duration was not affected by ptDNA surface modification. Blinking trace provided by Dr. Kristina E. Kitko.

### 3.2.3 Animal culture and imaging

#### Neuronal culture

All procedures were in accordance with the Vanderbilt University Institutional Animal Care and Use Committee standards. Rat hippocampi were dissected from P0-P1 Sprague-Dawley rats and digested with trypsin-EDTA (Gibco). Tissue was then gently dissociated into single cells in Hanks Buffer Salt Solution (HBSS, Sigma). Dissociated cells were resuspended in Minimal Essential Media (MEM, Life Technologies) containing 27 mM glucose, 2.4 mM $NaHCO_3$, 1.25 μM transferrin, 2 mM L-glutamine, 4.3 μM insulin, and 10% (by volume) fetal bovine serum (FBS, Omega). Neurons were plated onto round 12 mm glass coverslips coated with matrigel (BD Biosciences) and allowed to settle at 37°C with 5% $CO_2$. After 4 hours, 1 mL culture media was added to each coverslip. After 24-48 hours, 1 mL 2% 4-AraC in culture media was added to cell coverslips that also contained 1% (by volume) B27 supplement (Sigma) to prevent astroglia growth. Experiments were performed between DIV 12 and 18.

#### Plasmid transfection

Neurons were transfected with synaptic vesicle glycoprotein 2A (SV2A)-phluorin by a calcium phosphate method when neurons were 7-10 DIV (Sun et al., 2013). SV2a-pHluorin was generously provided by Ed Chapman (University of Wisconsin, Madison).

#### Live cell labeling and imaging

Aptamer-QDs were added to the culture well and incubated for 45 minutes in fluorobrite DMEM with 4% bovine serum albumin (BSA) and 5 μL QDs with RNase inhibitor. QD-labeled cells were immediately imaged in Tyrodes solution with RNase inhibitor added.

#### Widefield epifluorescence microscopy

Images were obtained on an Olympus IX-81 epifluorescence microscope with an Andor EMCCD camera. Images were collected using a 100X oil immersion objective (1.45NA

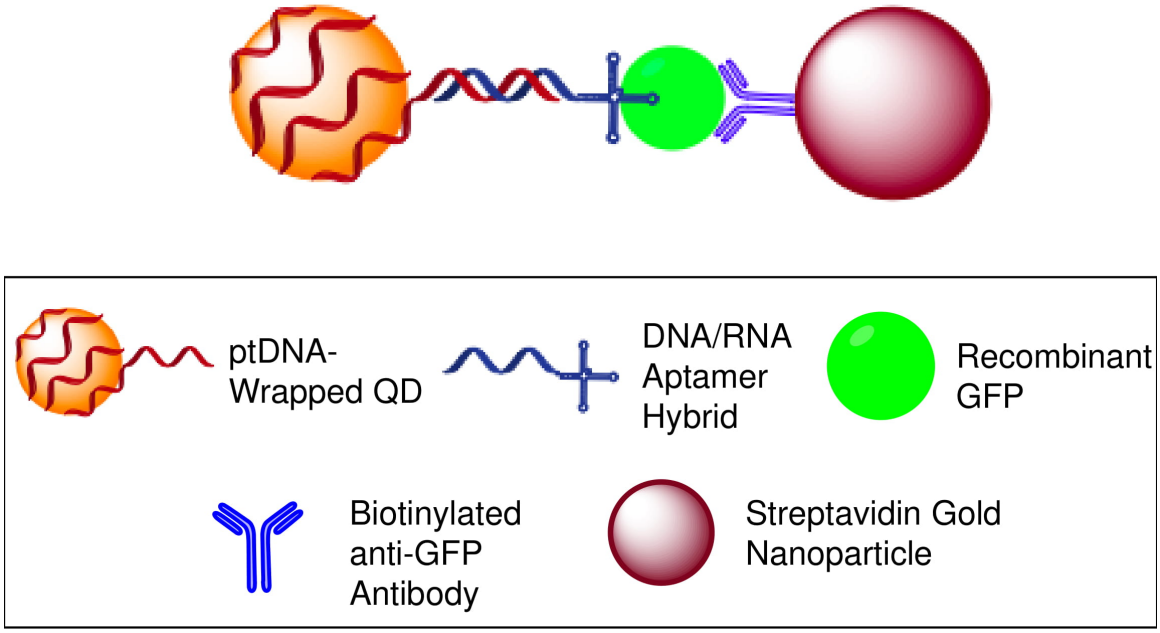


Figure 3.4: To verify monovalency, aptamer-QDs were bound to Au nanoparticles and imaged with TEM. Particle valencies were then quantified. Aptamer-QDs were generated as described. Streptavidin-bound Au nanoparticles were conjugated to biotinylated anti-GFP antibodies. The antibody-Au nanoparticles were then bound to recombinant GFP. The aptamer-QDs were then mixed with the GFP-bound Au and imaged with TEM.

Plan Apo VC). QDs were excited with a 405 nm arc lamp. QD 605 signal was collected with a 600/75 nm Chroma emission filter. Cells on coverslips were mounted in an imaging chamber and imaged at 37°C in Tyrodes solution (150 mM NaCl, 4 mM KCl, 2 mM $MgCl_2$, 2 mM $CaCl_2$, 10 mM HEPES buffer, 10 mM glucose in a final volume of 1 L deionized water, pH 7.35) for the duration of the experiment. QD images were acquired at 10 Hz.

### 3.3 Results and discussion

Here we report the successful generation of a generalizable, monovalent aptamer-QD that can specifically tag extracellular GFP. This approach can be tailored to target different proteins by keeping the complementary DNA sequence to the ptDNA and changing the aptamer sequence. There are several advantages to this method. First, the size of the overall QD remained small, around 12 nm, which is significantly smaller than commer-

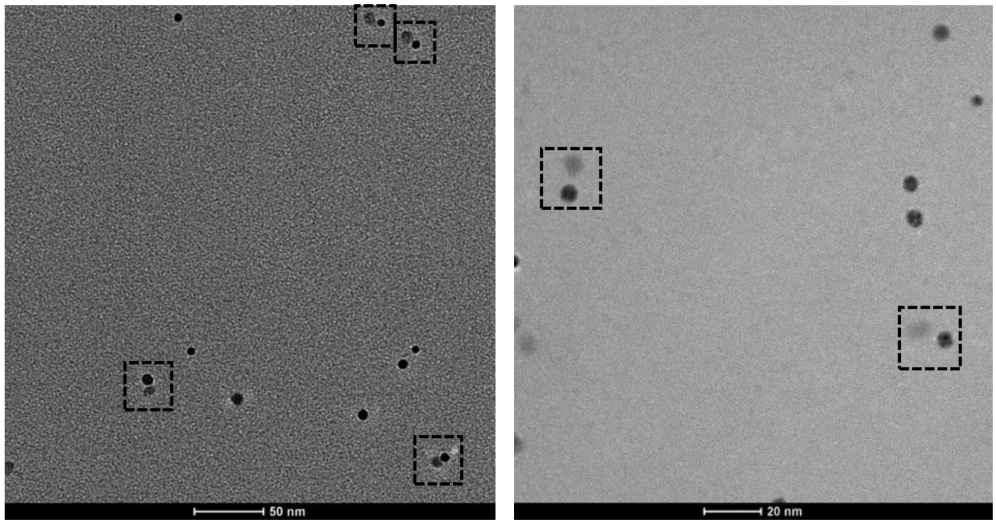


Figure 3.5: Representative TEM images showing QD-Au complexes. Boxes show 1:1 QD:Au binding, indicating monovalency. Bare Au is also seen in the images, as the samples were not purified to remove unbound particles prior to imaging.

cial streptavidin- or antibody-conjugated QDs, which are around 30 nm. Additionally and most importantly, this approach produced monovalent QDs that retained their brightness and stability while binding 1:1 with the protein of interest. This overcomes the limitation with most tagging approaches that have multiple binding sites on the probe surface, potentially leading to cross-linking which could alter the protein mobility dynamics. Finally, the aptamer is highly specific for its target, GFP.

We first transferred the organic phase QDs to the aqueous phase. We mixed thiolated PEG groups and tetrabutylammonium bromide (TBAB) with the organic phase QDs overnight. The TBAB made the solution more polar so that the thiol hydrogen pops off, making the molecule more negative so that it can then bind to the surface of the QD. The PEGs used for this step allowed the QDs to be aqueous but did not bind so strongly that the ptDNA would be excluded. The phase transfer step required optimization from the methods of Farlow et al., with the most significant changes being increased incubation times and altered reagent concentrations. We halved the QD concentration from the original paper to

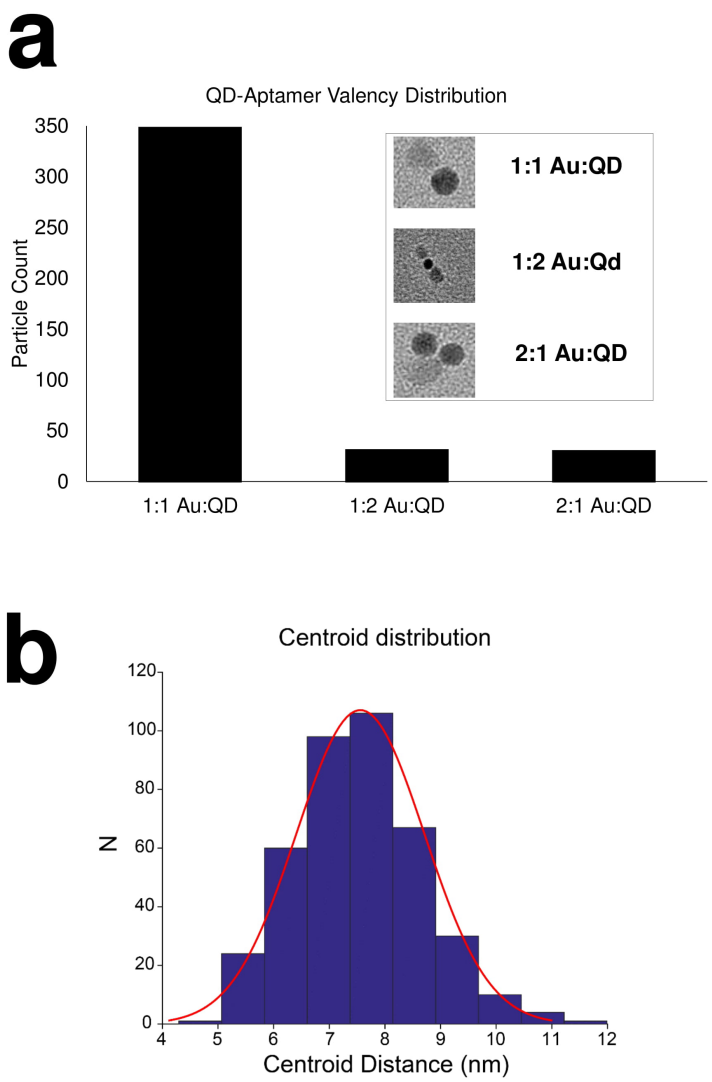


Figure 3.6: (A) Aptamer-QD bound to Au nanoparticles were quantified as either monovalent or divalent. Bound particles were over 95% monovalent with no purification. 1:1 QD:Au and 2:1 QD:Au were both considered monovalent since Au could bind more than 1 QD. (B) Centroid distances were calculated between particles (Centroid graph provided by Dr. Kristina E. Kitko) (Kitko, 2018).

increase the yield of transferred QDs. We then salted out the QDs with sodium hydroxide while stirring and then collected and concentrated the aqueous QDs (Figure 3.2). The excess solvent was removed from the QD solution with a desalt column. These QDs had a net neutral charge, as evidenced by the QDs staying in the wells during gel electrophoresis.

The QDs were then wrapped with the ptDNA, which has a net negative charge, allowing for verification of wrapping by observing a migration in the gel (Figure 3.3 A). ptDNA was added until all of the bare QDs had migrated out of the well and collapsed into a single band.

A custom DNA/RNA aptamer was generated that had a 12 base complementary DNA sequence to the ptDNA single stranded structure, with a 72 base GFP-specific aptamer at the end. Once ptDNA wrapping was confirmed, the aptamer was added dropwise. The QD solution was heated to 55°C to enable strand annealing of the DNA and DNA/RNA aptamer. The original PEG thiols from the phase transfer were then displaced with carboxy-PEG6-alkane thiols to better passivate the surface and decrease nonspecific binding. The original shorter PEGs better facilitated the ptDNA wrapping, but for live cell imaging purposes the longer chain PEGs better passivated the surface to decrease nonspecific binding of the QDs. The QDs retained their optical properties, emitting at 605 nm and showing the same blinking pattern (Figure 3.3 B and C).

While ptDNA wrapping could be confirmed with gel electrophoresis, aptamer binding and monovalency was verified with transmission electron microscopy (TEM). Because the aptamer is specific to GFP, we designed a construct comprised of GFP-bound Au nanoparticles. The Au and QDs were both easily distinguishable in TEM, and quantification of monovalency was thus straightforward. The construct had two parts: the aptamer-QD, which was generated with the same method that was used for live cell imaging; and the GFP-bound Au nanoparticle. The GFP was bound to a biotinylated GFP antibody, which was bound to streptavidin-conjugated Au (Figure 3.4). The two sides of the construct were then incubated together and added to the TEM grid via the dip-dip method.

Monovalency was quantified by analyzing over 300 bound particles from three separate experiments in TEM images (Figure 3.5). A 1:1 QD:Au was considered monovalent, as there was only a single QD bound to the GFP-Au. Because the gold can have more than one binding site due to multiple surface streptavidins, a 2:1 QD:Au was still considered

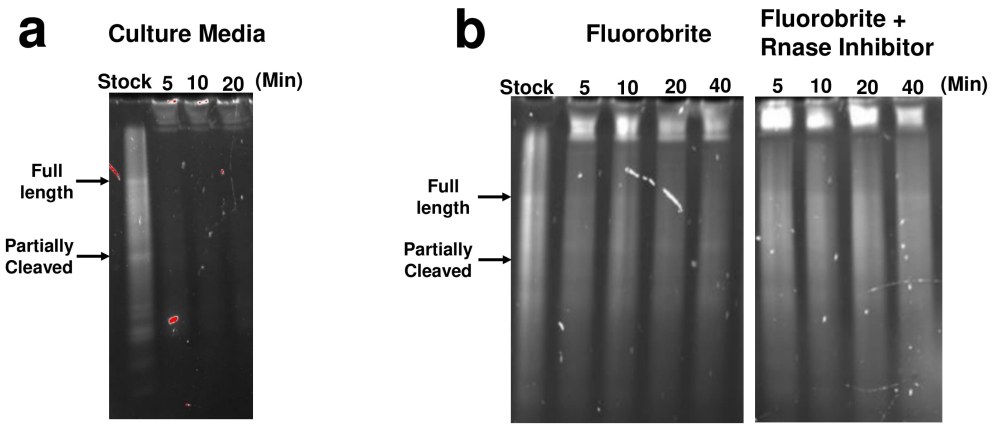


Figure 3.7: (A) In conditioned neuronal media, the RNA aptamer was completely degraded within 5 minutes. (B) In fluorobrite alone, the full length band was still faintly present at 40 minutes. When RNase inhibitor was present, the DNA/RNA aptamer stability significantly increased, with a strong full length band still present at 40 minutes.

monovalent, but a 1:2 QD:Au was not (Figure 3.6 A). Quantification revealed that of the bound particles, about 95% were monovalent, or had a 1:1 binding efficiency with no further purification. This result is comparable to Farlow et al. (Farlow et al., 2013). This is significant because previously reported monovalent QD methods required purification to achieve monovalency, whereas with this method, bound particles were largely already monovalent. To standardize the bound particle analysis, centroid-centroid distances between particles were determined (Figure 3.6 B). A Gaussian distribution was observed, with an average centroid distance of about 8 nm.

Once the aptamer-QD binding distributions were analyzed, the stability of the RNA was investigated to gain insight into how long the aptamer-QDs could be imaged before degradation. Because unmodified RNA aptamers can be unstable, especially in cell culture conditions, the stability was investigated under multiple conditions that would mimic QD tracking conditions. Ribonucleases can be present in the media used to culture the neurons that can then cleave the phosphodiester bond between the units of RNA (Huang et al., 2017). First, the aptamer was incubated with conditioned cell media from neuronal culture. Under these conditions, the aptamer was completely degraded within 5 minutes (Figure

3.7 A). The aptamer-QDs were then incubated in fluorobrite DMEM, which was the QD loading solution. When incubated with fluorobrite alone, much of the aptamer was also degraded by 5 minutes, although a faint band of full length DNA/RNA aptamer was still present. As seen in Figure 3.7 B, when RNase inhibitor was included, the RNA became much more stable in fluorobrite. Even at 40 minutes, a full length band was present. Therefore, for all live cell QD experiments, RNase inhibitor was included to ensure stability in this biological solution. While this is a simple addition to solution, chemically altering the RNA backbone with fluorine or amino groups to make it more stable would be a more permanent solution and something to investigate in the future (Kawasaki et al., 1993). We verified that the RNase inhibitor did not affect neuronal viability with a live/dead cell Trypan blue staining and saw no significant differences between RNase-inhibitor-treated neurons and control. Calcium imaging also showed that the inclusion of RNase inhibitor did not affect responsiveness to electrical stimulation, thus confirming that this method was suitable for use with primary neurons.

Once the probe characteristics were verified, the aptamer-QDs were used in live cell imaging. Synaptic vesicle glycoprotein 2A (SV2A) is a synaptic vesicle protein that is targeted by anti-epileptic drugs, thus making it a target of pharmacological interest. Hippocampal neurons were transfected with SV2A-pHluorin, which is a pH-sensitive form of GFP expressed within the vesicle lumen. The aptamer-QDs were particularly well-suited to synaptic vesicle labeling because of their small size and monovalency. QDs were incubated with neurons for 45 minutes to ensure sufficient vesicle turnover for labeling. Inclusion of RNase inhibitor maintained stability of the aptamer-QDs for this time period and allowed for at least an hour of imaging. Aptamer-QDs were loaded into transfected neurons and imaged at 10 Hz. As seen in the representative images in Figure 3.8, aptamer-QDs are colocalized with SV2A-expressing neurons. These QDs can be used with any protein expressing an extracellular GFP. We also labeled ASAP1-GFP, which is an ADP-ribosylation factor (ARF) GTPase-activating protein, to ensure that the aptamer QDs label other proteins

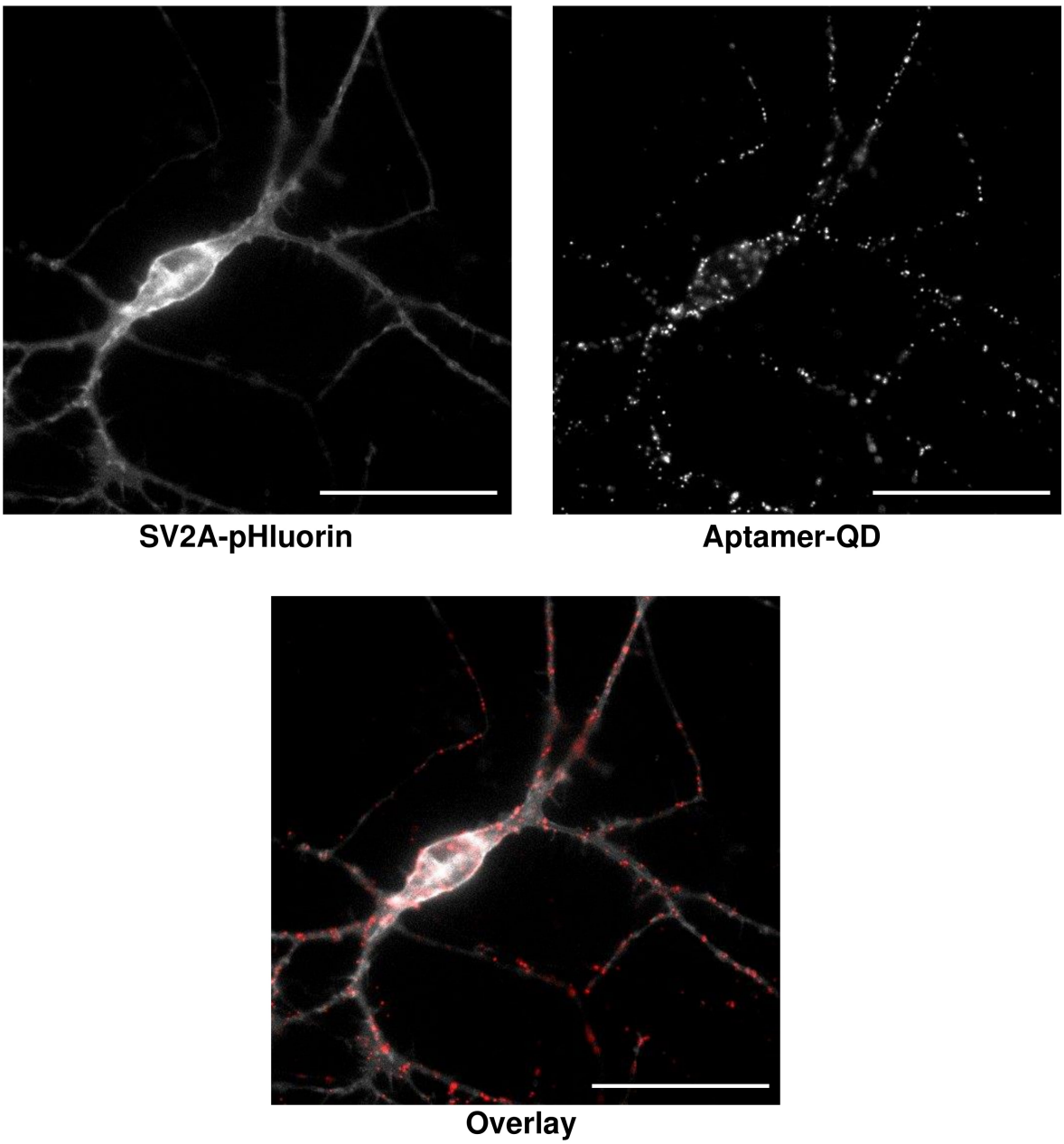


Figure 3.8: Hippocampal neurons were transfected with SV2A-pHluorin and tagged with the aptamer-QDs. As shown by the overlay, the QDs are colocalized with the transfected neurons. Scale bar, 50 μm. Images provided by Dr. Kristina E. Kitko.

encoded with GFP (data not shown).

In conclusion, we have successfully generated a monovalent aptamer-QD probe that can be used for live cell imaging of a variety of targets. Single strand phosphorothioate

DNA was wrapped around 605 nm QDs and bound to a DNA/RNA aptamer hybrid that is specific to GFP. This method did not compromise the fluorescence properties of the QDs. Monovalency was confirmed with TEM image analysis, which showed that over 95% of bound particles were monovalent. Monovalency is especially valuable when many copies of the target protein are in a tight space, such as in the synapse. This method provides another avenue for single molecule imaging, especially when an antibody or ligand is not available. Specific DNA and RNA can be custom synthesized to be adapted for this method. For live cell imaging purposes, RNase inhibitor was included to preserve the full length DNA/RNA aptamer strand to prevent degradation. The aptamer-QDs specifically labeled SV2A-pHluorin transfected hippocampal neurons. While this method does produce a monovalent, generalizable probe, one of the main future directions would be stabilizing the RNA aptamer chemically to increase shelf life. As the method stands, the QDs must be used immediately after the RNA aptamer is added. Overall, this method is a promising technique for imaging a variety of synaptic proteins.

### 3.4 Bibliography

Chang, J. C. and Rosenthal, S. J. (2013). A bright light to reveal mobility: Single quantum dot tracking reveals membrane dynamics and cellular mechanisms. *Journal of Physical Chemistry Letters*, 4(17):2858–2866.

Farlow, J., Seo, D., Broaders, K. E., Taylor, M. J., Gartner, Z. J., and Jun, Y. W. (2013). Formation of targeted monovalent quantum dots by steric exclusion. *Nature Methods*, 10(12):1203–1205.

Germer, K., Leonard, M., and Zhang, X. (2013). Review: RNA aptamers and their therapeutic and diagnostic applications. *Int J Biochem Mol Biol*, 4(1):27–40.

Howarth, M., Liu, W., Puthenveetil, S., Zheng, Y., Marshall, L. F., Schmidt, M. M., Wittrup, K. D., Bawendi, M. G., and Ting, A. Y. (2008). Monovalent, reduced-size quantum dots for imaging receptors on living cells. *Nature Methods*, 5(5):397–399.

Huang, Z., Wen, W., Wu, A., and Niu, L. (2017). Chemically Modified, alpha-Amino-3-hydroxy-5-methyl-4-isoxazole (AMPA) Receptor RNA Aptamers Designed for in Vivo Use. *ACS Chemical Neuroscience*, 8:2437–2445.

Kawasaki, A. M., Casper, M. D., Freier, S. M., Lesnik, E. A., Zounes, M. C., Cummins, L. L., Gonzalez, C., and Cook, P. D. (1993). Uniformly modified 2'-deoxy-2'-fluoro-phosphorothioate oligonucleotides as nuclease-resistant antisense compounds with high affinity and specificity for RNA targets. *Journal of Medicinal Chemistry*, 36(7):831–841.

Kitko, K. E. (2018). *Nanomaterial-based approaches to the study of membrane signaling (Doctoral dissertation)*. PhD thesis, Vanderbilt University.

Liu, H. Y. and Gao, X. (2011). Engineering Monovalent Quantum Dot-Antibody Bioconjugates with a Hybrid Gel System. *Bioconjugate Chemistry*, 22:510–517.

Resch-Genger, U., Grabolle, M., Cavaliere-Jaricot, S., Nitschke, R., and Nann, T. (2008). Quantum dots versus organic dyes as fluorescent labels. *Nature Methods*, 5(9):763–775.

Saxton, M. J. and Jacobson, K. (1997). SINGLE-PARTICLE TRACKING:Applications to Membrane Dynamics. *Annual Review of Biophysics and Biomolecular Structure*, 26(1):373–399.

Sun, M., Bernard, L. P., Dibona, V. L., Wu, Q., and Zhang, H. (2013). Calcium Phosphate Transfection of Primary Hippocampal Neurons. *J. Vis. Exp*, (81):50808.

Uddayasankar, U., Zhang, Z., Shergill, R. T., Gradinaru, C. C., and Krull, U. J. (2014). Isolation of Monovalent Quantum DotNucleic Acid Conjugates Using Magnetic Beads. *Bioconjugate Chemistry*, 25(7):1342–1350.

# CHAPTER 4

## Single quantum dot tracking of endogenous midbrain serotonin transporter

### 4.1 Introduction

The serotonin transporter protein (SERT) controls the amplitude and duration of synaptic serotonin signaling by enabling rapid clearance of the neurotransmitter back into presynaptic terminals. SERT is enriched in the axonal arborizations and accumulates in presynaptic specializations where it sequesters synaptic serotonin by the $Na^+/Cl^-$-dependent alternating access mechanism (Rudnick et al., 2014; Montgomery et al., 2014). SERT is the primary target for selective serotonin reuptake inhibitors (SSRIs), a main class of antidepressants, and is sensitive to psychostimulants and drugs of abuse such as cocaine and 3,4-methamphetamine (Steiner et al., 2008). SERT dysfunction and coding variations have been linked to many psychiatric disorders, including autism spectrum disorder (ASD), depression, anxiety, obsessive-compulsive disorder (OCD), and bipolar disorder (Bermingham and Blakely, 2016). Relevance to brain disorders and therapeutic utility of SERT have led to rigorous investigation of its function and regulation (Bermingham and Blakely, 2016).

These research efforts have been primarily driven by biochemical methods measuring ensembled behavior of many SERTs. Elucidating SERT behavior at the single protein level remains a challenge, especially in endogenous neuronal systems. Quantum dots (QDs), nanometer-sized semiconductor crystals, are excellent candidates for probing single SERT properties due to their unique photophysical characteristics. QDs exhibit broad absorption with narrow, size-tunable Gaussian emission profiles, have high quantum yields, are easily functionalized, and perhaps most importantly, are extremely resistant to photobleaching (Michalet, 2005; Rosenthal et al., 2011). Additionally, QD-tagged proteins can be tracked with 5-10 nm localization accuracy at video rates, making QD-based single particle track-

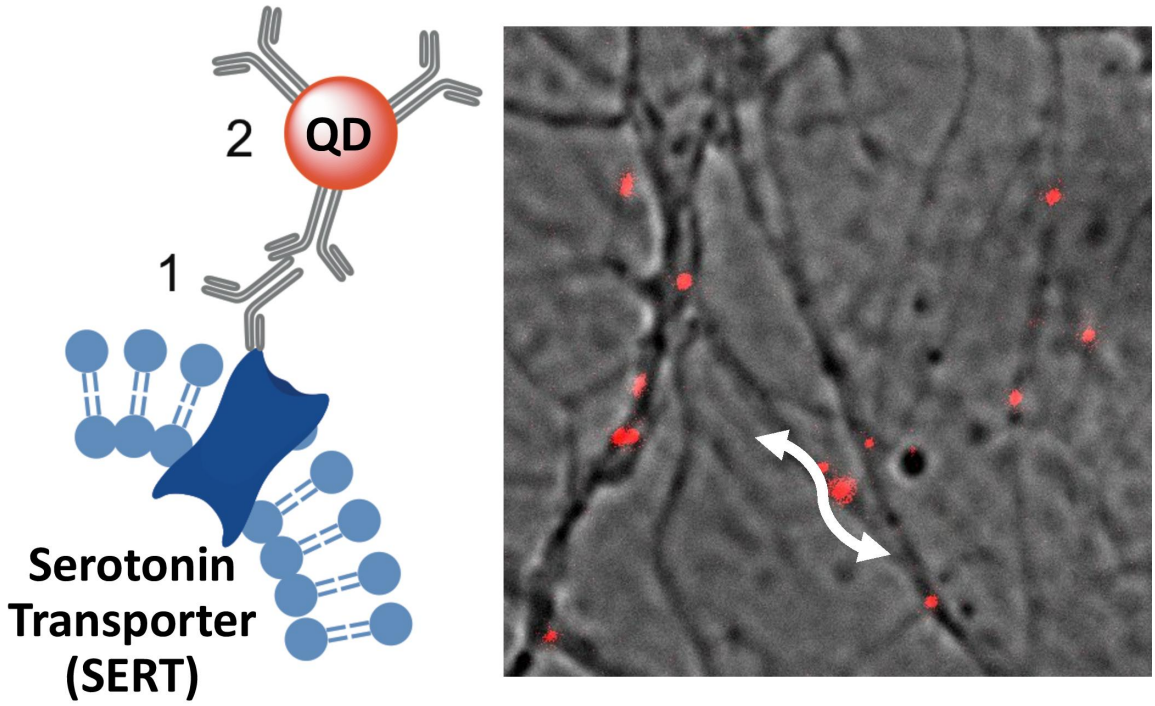


Figure 4.1: SERT was labeled in a two step labeling protocol. First, the primary antibody was bound to SERT (1) after a 6 minute incubation. Secondary antibody-conjugated QDs were then bound to primary antibody (2) and immediately imaged. QDs can be seen moving along the axon. Image stacks were analyzed to determine diffusion coefficients.

ing (SPT) a highly sensitive method (Kovtun et al., 2015). The Rosenthal lab pioneered the use of ligand-conjugated QD SPT for a variety of neuronal proteins, including SERT, norepinephrine transporter (NET), dopamine transporter (DAT), and $\gamma$-aminobutyric acid receptor (GABA) (Kovtun et al., 2015, 2011, 2012; Chang et al., 2012a). In this study, we sought to capture SERT dynamics in an endogenous neuronal system with an antibody specifically targeted to the fourth extracellular loop of SERT along with secondary antibody-conjugated QDs. Since our previous antagonist-based ligand approach could affect intrinsic conformational dynamics of SERT, we chose to use the off-site antibody tag for these experiments. This report offers the first visualization of single SERT diffusion dynamics in living rat midbrain neurons using QD SPT (Figure 4.1).

SERT function and expression are under strict control in part through a variety of biochemical and biophysical events, including phophorylation (Bermingham and Blakely, 2016), membrane microdomain localization (Chang et al., 2012a; Magnani et al., 2004), and conformation shifts (Zhang et al., 2016). Because SERT is a transmembrane protein, the lipid environment, especially cholesterol, plays a crucial role in modulating its activity (Magnani et al., 2004; Scanlon et al., 2001; Hong and Amara, 2010; Bjerregaard et al., 2015). Statins, which inhibit the production of 3-hydroxy-3-methylglutaryl-Coenzyme A reductase (HMG-CoA reductase) in cholesterol synthesis, have been shown to enhance the effects of antidepressants such as imipramine and fluoxetine in behavioral studies, demonstrating the importance of cholesterol for SERT function (Wood et al., 2010; Vevera et al., 2016). At the subcellular level, SERT has been shown to associate with cholesterol-rich lipid rafts and rely on these microdomains for efficient serotonin uptake (Magnani et al., 2004). We have previously shown that SERT appears to be laterally confined within membrane microdomains in an immortalized RN46A cell line, demonstrating that SERT can exist in both confined and more freely diffusing states. These states were found to be sensitive to both cholesterol depletion and protein kinase G (PKG) activation, leading to an increase in diffusion rate (Chang et al., 2012b).

Both experimental evidence and simulations in heterologous expression systems have shown that a conserved cholesterol binding site (CHOL1) appears to be located along SERT transmembrane domain (TM) 1a, TM5, and TM7, and cholesterol binding to CHOL1 promotes the outward-facing conformation, accelerating serotonin uptake (Laursen et al., 2018). When cholesterol binding to CHOL1 was disrupted, the SERT conformation equilibrium shifted toward inward-facing, which provided more accessibility to the PKG-sensitive threonine 276 (Thr276) residue as it lies on the cytoplasmic side of the TM5 helix (Laursen et al., 2018). As such, Thr276 is more susceptible to phosphorylation when inward-facing (Zhang et al., 2016). While several groups have interrogated the contribution of cholesterol and kinase activity to SERT function and regulation, a lack of consensus persists

due to heterogeneity of the SERT molecular phenotype across these studies, which likely stem from differences in expression density and cell host (Bermingham and Blakely, 2016; Scanlon et al., 2001; Laursen et al., 2018; Samuvel, 2005; Zhu et al., 2004). We sought to determine whether lowered cholesterol content affects both lateral mobility and phosphorylation of Thr276 in endogenous SERT in primary midbrain neuron cultures using two different methods of cholesterol manipulation, statins and methyl-beta-cyclodextrin (M$\beta$CD). These alterations in membrane composition might deleteriously impact SERT efficiency as a molecular transducer of antidepressant effects and disrupt proper SERT axonal targeting, compromising brain serotonin homeostasis.

## 4.2 Experimental techniques

### 4.2.1 Cell culture and treatments

All procedures were in accordance with the Vanderbilt University Institutional Animal Care and Use Committee standards. Primary midbrain cultures were prepared as described previously (Bailey et al., 2017). Midbrain was dissected from P1 Sprague-Dawley rats and digested with trypsin-EDTA (Gibco). Tissue was then gently dissociated into single cells in Hanks Buffer Salt Solution (HBSS, Sigma). Dissociated cells were resuspended in Minimal Essential Media (MEM, Life Technologies) containing 27 mM glucose, 2.4 mM $NaHCO_3$, 1.25 µM transferrin, 2 mM L-glutamine, 4.3 µM insulin, and 10% (by volume) fetal bovine serum (FBS, Omega). Neurons were plated onto round 12 mm glass coverslips coated with matrigel (BD Biosciences) and allowed to incubate at 37°C with 5% $CO_2$. After 1 hour, 1 mL media was added to each coverslip. After 24 hours, 1 mL 4-AraC was added in cell media that also contained 1% (by volume) B27 supplement (Sigma) to prevent glia growth. Experiments were performed between DIV 10 and 20.

For acute cholesterol depletion, cells were incubated with 5 µM methyl-$\beta$-cyclodextrin (M$\beta$CD, Fisher Scientific) at 37°C for 30 min. At this concentration, no morphology changes were seen. For chronic cholesterol depletion, cells were incubated with 50 µM

mevastatin (Sigma) for 16 hours according to previously published methods (Shrivastava et al., 2010). Again, at this incubation concentration and time, cell morphology was not compromised. For PKG activation, cells were incubated with 100 μM 8-Br-cGMP (Sigma) for 30 min to 1 hour.

### 4.2.2 Widefield epifluorescence microscopy

Images were obtained on an Olympus IX-81 epifluorescence microscope with an Andor EMCCD camera. Images were collected using a 60X (filipin) or 100X (QD tracking) oil immersion objective lens. QDs and fluorophores were excited with a 405 nm arc lamp. QD 655 signal was collected with a 660/40 nm emission filter. Filipin signal was collected with a 460/50 emission filter. For live cell imaging, cells on coverslips were mounted in an imaging chamber and imaged at 37°C in Tyrodes solution (150 mM NaCl, 4 mM KCl, 2 mM $MgCl_2$, 2 mM $CaCl_2$, 10 mM HEPES buffer, 10 mM glucose in a final volume of 1 L deionized water, pH 7.35) for the duration of the experiment. Single QD tracking was performed at a frame rate of 11-15 Hz for 60 seconds, and data were obtained within 20 minutes of the final wash step after QD labeling.

### 4.2.3 Live cell QD tracking and trajectory analysis

Cells were incubated with 5 μg/mL primary SERT antibody (Advanced Targeting Systems) in warm fluorobrite media (Thermo Fisher) at 37°C and 5% $CO_2$ for 6 minutes. Cells were washed once and incubated with 0.1 nM anti-mouse secondary antibody-conjugated 655 QDs (Invitrogen) in warm 4% bovine serum albumin (BSA, Sigma) fluorobrite media for 4 minutes. Cells were washed 5 times with warm Tyrodes solution and immediately mounted in Tyrodes onto a heated microscope stage.

Analysis was performed on data from at least three separate cultures and at least three separate fields of view per culture. Stacks of individual TIFF images were processed using ImageJ. Positions and trajectories of the QD-labeled SERT proteins were determined using modified MATLAB routines developed by Daniel Blair and Eric Dufresne (The Matlab

Particle Tracking Code Repository). The subpixel localization accuracy of the central QD position was determined to be ±10-15 nm (Chang and Rosenthal, 2012). The uncertainty ($\Delta\ \sigma$) is dependent on the width (which is about wide-field diffraction limit, 250 nm) and the signal to noise ratio (SNR), defined as:

$$SNR = \frac{I_0}{\sqrt{\sigma_{bg}^2 + \sigma_{I_0}^2}} \tag{4.1}$$

where $I_0$ is maximum signal above background, $\sigma_{bg}^2$ is the variance of the background intensity values, and $\sigma_{I_0}^2$ is the variance of the maximum signal intensity above the background, giving $\Delta\ \sigma$ = 250/SNR (nm). All analyzed trajectories were at least 5 seconds in length. Trajectory analysis was performed using custom MATLAB routines to determine mean square displacement (MSD) using the following formula:

$$MSD(n\Delta t) = \frac{1}{N-n}\sum_{i=1}^{N-n}(x_{i+n}-x_i)^2 + (y_{i+n}-y_i)^2 \tag{4.2}$$

where N is the total number of frames, nΔt is the time interval in which the MSD is calculated, and $x_i$ and $y_i$ are positions of the particles in the trajectories. Diffusion coefficients were determined by fitting MSD to the equation $4Dt\alpha$, where D is the diffusion coefficient and $\alpha$ is the anomalous diffusion parameter. Statistical significance for diffusion coefficient analysis was determined with Kolmogorov-Smirnov statistical test. Statistical significance for 5 second radial displacements was determined with Students t-test. To determine the confined and freely diffusing populations, bimodal fitting was performed in MATLAB, and the D threshold value (0.0082 $\mu m^2/s$) was determined to be where the two fits intersected. This D value is consistent with other methods of determining the confined threshold (Constals et al., 2015).

### 4.2.4 Western blot

Cells were washed with cold PBS and lysed with CelLytic M (Sigma) containing protease and phosphatase inhibitors (Sigma) for 15 minutes. The lysate for each condition was collected and centrifuged at 4°C at maximum speed for 10 minutes. Protein concentration of collected supernatant was assayed using Bio-Rad dye reagent (Bio-Rad; #500-0006) on a Beckman Coulter DU 530 spectrophotometer. Samples were then normalized according to their protein concentration, denatured, and subjected to gel electrophoresis using 10% Mini-PROTEAN TGX (polyacrylamide gel electrophoresis) (Bio-Rad) precast gels. Two sets of each sample were run side-by-side in one gel to split later, one for blotting of phospho-SERT, and one for blotting of total SERT. Protein was then transferred to polyvinylidene difluoride membranes (Millipore). Membranes were cut in half vertically to separate the two samples. Antibodies used were polyclonal anti-SLC6A4 (goat; 1:500; Sigma #SAB2502028) to detect total SERT protein and polyclonal serotonin transporter Thr276 antibody (rabbit; 1:500; PhosphoSolutions #P1700-276) to detect phospho-SERT. Monoclonal anti-GAPDH antibody (mouse; 1:6000; Millipore #CB1001) was used as a loading control. After incubation with primary antibodies, IRDye (LI-COR Biosciences) conjugated secondary antibodies were used, and the signals were detected using the Odyssey Infrared Imaging System (LI-COR Biosciences).

The integrated intensity value of each specific band was calculated using the Image Studio Lite 5.2 software (LI-COR Biosciences). Each target bands intensity was normalized to each lanes GAPDH signal, and phospho-SERT levels were calculated as a percentage of the total SERT level from that sample. Data was collected from 7 experiments and at least three separate animal cultures. Statistical analysis was conducted in GraphPad Prism 5. Statistical analyses comparing control and experimental conditions were performed using Students t-test.

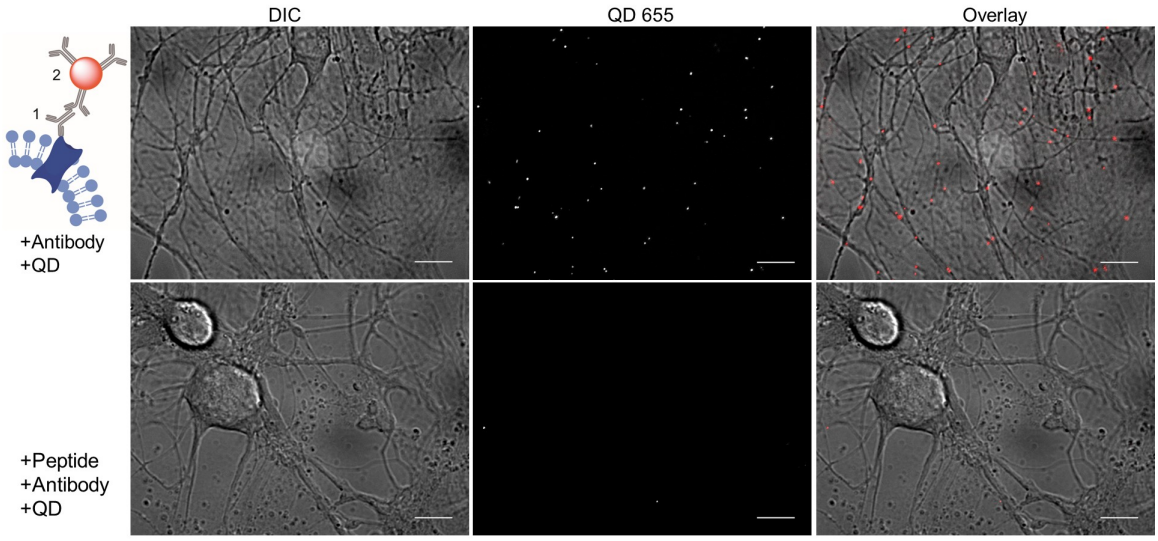


Figure 4.2: QDs are bound to SERT with antibodies in a two-step labeling protocol (antibody and QD size are not to scale). First, primary antibody is bound, followed by secondary antibody-conjugated QDs. QDs are specific to endogenous neuronal SERT as shown with a peptide block (bottom panel). When peptide was present, QD binding was eliminated. Differential interference contrast (DIC) and QD655 channels are overlaid to demonstrate binding along neurites. Scale bar, 10 µm.

### 4.2.5 Filipin staining

Cells were fixed in PBS containing 4% formaldehyde for 30 minutes, washed 3 times with PBS, and stained with 0.05 mg/mL filipin (Sigma) in PBS for 2 hours at room temperature. Coverslips were mounted on slides and imaged on an Olympus IX-81 microscope as described above. Data was collected from three separate coverslips and at least 150 neurons per condition. ROIs containing neurons were manually selected, and average ROI intensities were measured in ImageJ. Background was measured for each image and subtracted from the mean intensity values for the cells. Statistical analyses comparing control and experimental conditions were performed using Students t-test and one-way ANOVA with post-hoc Dunnetts test.

## 4.3 Results and discussion

### 4.3.1 PKG activation mobilizes SERT along the membrane of neurons.

Strong evidence suggests that Thr276 is the cGMP-sensitive phosphorylation site that is activated by a PKG cascade (Zhang et al., 2016; Ramamoorthy et al., 2007; Zhang et al., 2007). This pathway is upregulated in patients with the autism-associated Gly56Ala SERT coding variant, suggesting that phosphorylation of Thr276 is clinically important (Prasad et al., 2005, 2009). However, individual differences in SERT behavior can be missed with traditional ensemble methods. We have found that Gly56Ala, which is hyperphosphorylated and resistant to further 8-Br-cGMP stimulation (Ramamoorthy et al., 2007), displayed increased membrane mobility and diffusion, which led us to examine whether phosphorylation status is linked to membrane mobility (Kovtun et al., 2018). Serotonergic neurons are largely derived from the midbrain raphe nuclei (Imai et al., 1986), thus for these experiments the midbrain was isolated from postnatal day 1 rats, digested, dissociated, and cultured onto coverslips. To examine SERT behavior at the single molecule level, endogenous single neuronal SERT complexes were labeled with QDs using a two-step labeling approach: specifically targeted monoclonal primary antibodies were bound followed by commercial 655 QDs (Figure 4.2). Antibody specificity was confirmed by eliminated QD binding after blocking the antibody binding site with a peptide. QD nonspecific binding was nearly eliminated with the inclusion of 4% bovine serum albumin (BSA). Because we are interested in comparing diffusion between conditions and because previous groups have shown that divalent antibodies do not significantly alter diffusion dynamics, we used full IgG in these studies (Dahan et al., 2003; Groc et al., 2007; Varela et al., 2016). As the QD-IgG conjugates are relatively large compared to the tagged SERT, it is also important to note that the viscous drag on a QD bound to a protein was previously shown to be dominated by the mobility of the target anchored in the membrane (Domanov et al., 2011; Pierobon et al., 2009). QDs provide the distinct advantage of longer imaging timescales, thus time series were taken over the course of 1 minute at 11-15 Hz. To ensure surface SERTs were being

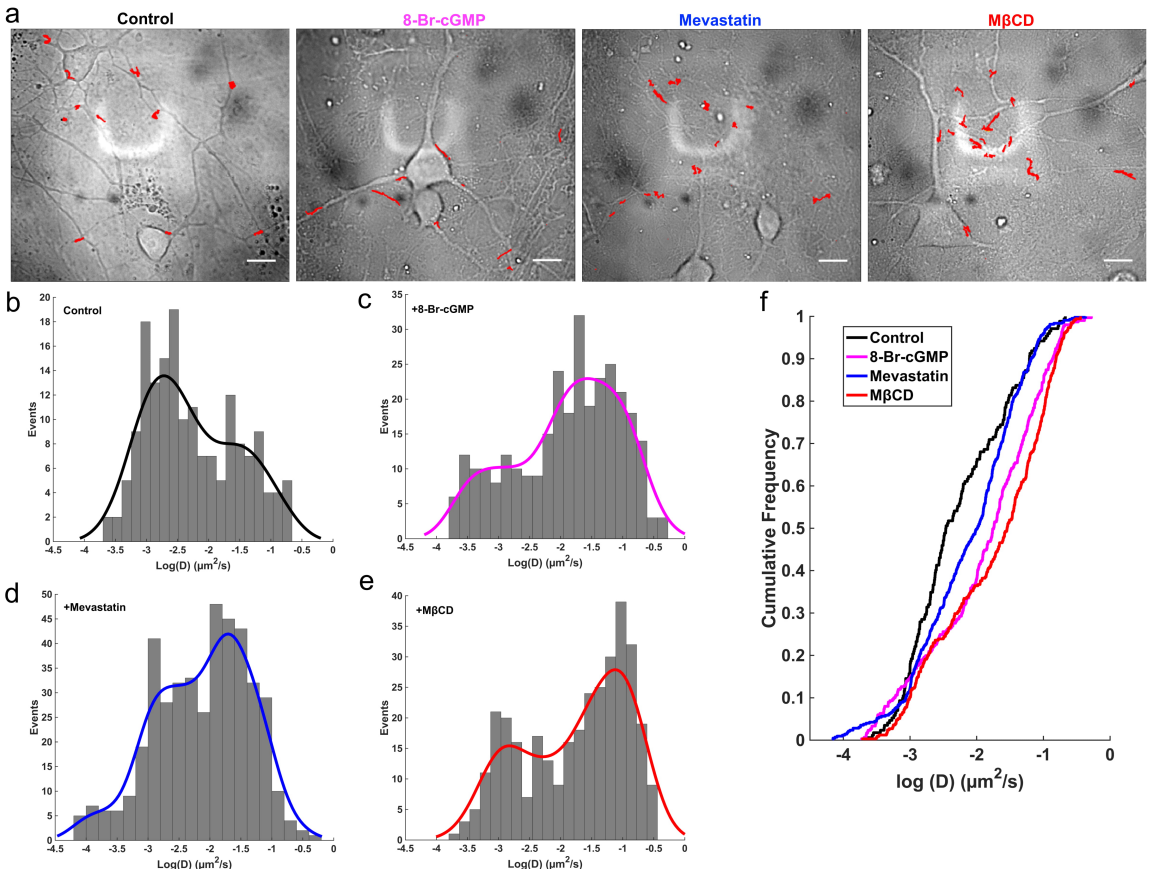


Figure 4.3: Representative trajectories (a) and diffusion coefficients for endogenous midbrain SERT under (b) control, (c) 8-Br-cGMP, (d) mevastatin, and (e) M$\beta$CD treated neurons (scale bar, 10 μm). Diffusion coefficients are significantly higher when neurons are stimulated and cholesterol depleted ($0.0211 \pm 0.0030$ μm$^2$/s for control, $0.0457 \pm 0.0040$ μm$^2$/s for 8-Br-cGMP-treated, $p < 0.0001$, $0.0243 \pm 0.0020$ μm$^2$/s for mevastain-treated, $p < 0.001$, and $0.0569 \pm 0.0038$ μm$^2$/s for M$\beta$CD-treated, $p < 0.0001$, mean$\pm$standard error of the mean (SEM), Kolmogorov-Smirnov (K-S) test). (f) Cumulative frequency plot shows diffusion distributions of each condition, $p < 0.001$ for all conditions, K-S test. Data were collected from at least 3 separate coverslips from at least 3 different animal cultures from at least 10 separate videos (which represent fields of view) for each condition.

tracked, all imaging took place immediately after labeling within 20 minutes of the QD labeling step. Endocytosis was evident in longer imaging experiments through the observation of QD clustering in endosomes, which was also seen in our previous work (Chang et al., 2012b). Blinking was used to verify single QDs were being analyzed.

Under basal conditions, endogenous SERT showed a bimodal mobility distribution with the majority of proteins (62%) falling within the confined regime, likely a manifestation of

SERT partitioning into lipid microdomains. These results are consistent with behavior seen previously in our lab in the RN46A cell line, where SERT colocalized with membrane microdomain-associated GM1 ganglioside (Chang et al., 2012b). Moreover, recent superresolution STORM imaging of the homologous DAT by Gether and colleagues using antibody-dye conjugates showed that DAT is largely clustered (about 60%) along the plasma membrane of midbrain neurons (Rahbek-Clemmensen et al., 2017), consistent with our percentage of confined serotonin transporters. In another endogenous system, clustering of SERT has been observed on the surface of lymphocytes (Romay-Tallon et al., 2017). Next, we examined the effects of PKG activation on cell surface trafficking of SERT in midbrain neurons by applying 8-Br-cGMP. 8-Br-cGMP stimulation significantly increased the diffusion rate of SERT by 2-fold (Figure 4.3A-C). This increase in diffusion rate is also accompanied by a population shift from confined to more freely diffusing (64%). We then analyzed the lateral displacements of single SERTs over 5 seconds, which represents the extent of mobilization for each trajectory. In addition to increased diffusion coefficients, we also observed a significant increase in radial displacement upon 8-Br-cGMP treatment (Figure 4.4). We thus determined that 8-Br-cGMP stimulation led to increased diffusion rate, displacement along membrane, and mobile fraction compared to basal conditions.

### 4.3.2 Mevastatin- and methyl-beta-cyclodextrin-treated neurons exhibit increased SERT mobility.

Membrane cholesterol plays an important role in regulating SERT, along with a variety of transmembrane proteins, and can affect both the membrane fluidity as well as specific protein conformations (Magnani et al., 2004; Scanlon et al., 2001; Hong and Amara, 2010). Molecular dynamics simulations in a lipid raft membrane model revealed six potential SERT cholesterol binding sites that all had functional significance (Ferraro et al., 2016). More recently, experimental evidence validated this notion, showing that cholesterol can bind to a few particular “hot spots” on SERT overlapping with those predicted binding

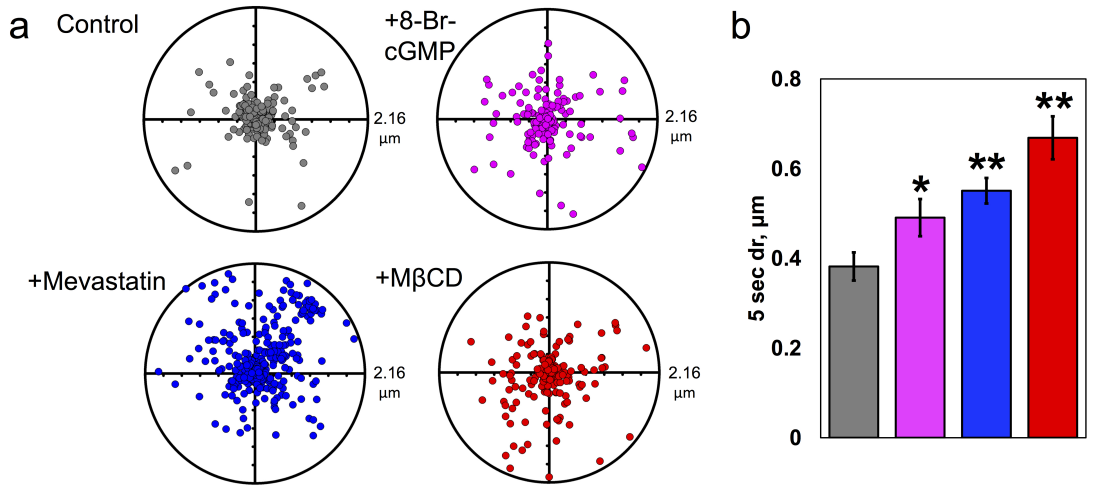


Figure 4.4: (a) Two-dimensional polar plots of 5 second radial displacements (dr) of single QD-SERT complexes, normalized to their starting positions. Radius of a plot is 2.16 μm (12 pixels). (b) Mean dr values show significant increases in radial displacement for treated conditions ($0.38 \pm 0.031$ μm for control, $0.49 \pm 0.041$ μm for 8-Br-cGMP-treated, $p < 0.05$ (Students t-test) and $p = 0.077$ (one-way ANOVA with Dunnetts test), $0.55 \pm 0.028$ μm for mevastatin-treated, $p < 0.001$ (Students t-test) and $p < 0.01$ (one-way ANOVA with Dunnetts test), and $0.67 \pm 0.048$ μm for M$\beta$CD-treated, $p < 0.001$, both Students t-test and one-way ANOVA with Dunnetts test). *denotes $p < 0.05$ (Students t-test), **denotes $p < 0.001$ (Students t-test) compared to control. Data were collected from at least 3 separate coverslips from at least 3 different animal cultures from at least 10 separate videos (which represents fields of view) for each condition.

sites (Laursen et al., 2018). One such site was found to be conformationally-sensitive to cholesterol concentration levels and was near transmembrane domains 1, 5, and 7, which is near the same functional domain that contains Thr276 (Laursen et al., 2018). Reportedly, a more inward-facing conformation was stabilized when cholesterol binding at this site was disrupted. These changes also enhanced ligand binding, which induced a more inward-facing conformation. As the inward-facing conformation favors SERT phosphorylation at Thr276, we hypothesize that lowering cholesterol content will increase lateral mobility and Thr276 phosphorylation (Laursen et al., 2018).

We acutely extracted cholesterol from the membrane with methyl-beta-cyclodextrin (M$\beta$CD), an established method for removing cellular surface cholesterol (Zidovetzki and Levitan, 2007). In addition to direct cholesterol extraction, we also chronically depleted

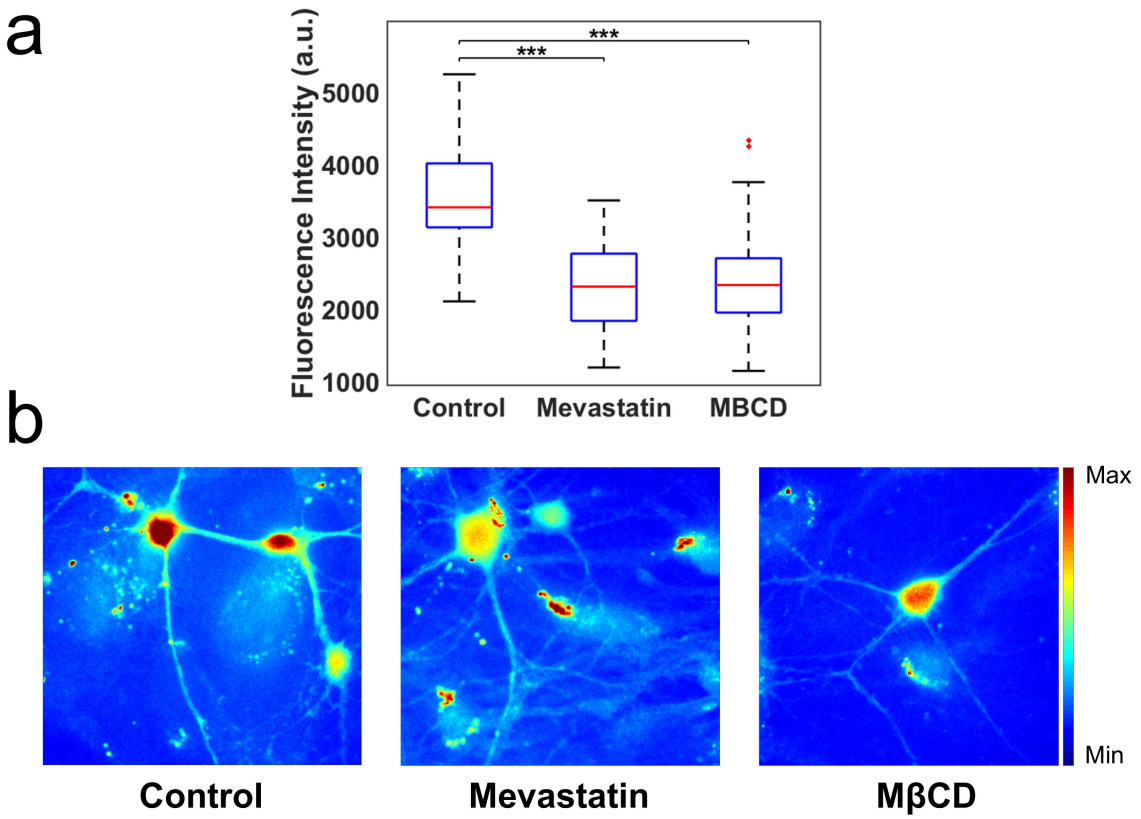


Figure 4.5: Filipin stain confirmed cholesterol depletion by treatments. (a) Relative fluorescence significantly decreased for both mevastatin- and M$\beta$CD-treated neurons. ***denotes $p < 0.0001$, Students t-test and one-way ANOVA with Dunnetts test. (b) Representative images from control, mevastatin- and M$\beta$CD-treated neurons. Data were collected from 3 separate coverslips for each conditions and at least 150 individual neurons for each condition.

cholesterol with mevastatin. Statins are used clinically to reduce the risk of cardiovascular disease by inhibiting production of the HMG-CoA reductase in cholesterol synthesis, which reduces overall cholesterol serum levels (Wood et al., 2010). These findings are particularly relevant as many statins are blood-brain-barrier permeable, and treatment with statins has led to lowered cholesterol levels in the brain, which could have implications for transmembrane proteins regulated by cholesterol (Vevera et al., 2016). In one example, statins have been shown to alter the dynamics of serotonin 1a receptors by increasing the mobile fraction along the membrane (Shrivastava et al., 2010). Additionally, statins were shown to decrease membrane viscosity and overall brain cholesterol content, decrease SERT activ-

ity, as well as induce behavioral changes in rats (Vevera et al., 2016). Thus, we wanted to explore the effects of statins on endogenous neuronal SERT at the single protein level.

Similar to results for 8-Br-cGMP stimulated SERT, both chronic and acute cholesterol depletion significantly increased the diffusion rate of SERT in comparison to control (Figure 4.3). Acute cholesterol depletion had the greatest effect among all conditions, which is expected since M$\beta$CD sequesters cholesterol directly from the membrane, potentially disrupting membrane microdomains and SERT cholesterol binding. Acute cholesterol depletion shifted the SERT populations the most, with 65% of proteins being in the freely diffusing population. Chronic cholesterol depletion caused a subtler population shift than the other treatments, with 47% of proteins still falling in the confined regime and 53% being freely diffusing. Depleting cholesterol also significantly increased cell surface SERT radial displacement along the membrane as seen in 5 second displacement plots for both chronic and acute conditions (Figure 4.4). We ensured that our treatments were depleting cholesterol by the well-accepted filipin staining (Figure 4.5) (Maxfield and Wüstner, 2012). Both conditions had significantly less cholesterol than control.

### 4.3.3 Acute and chronic cholesterol depletion increase phosphorylation of Thr276.

Since these increases in membrane mobility were well aligned with our hypothesis, we then sought to understand if these increases in diffusion coefficient from cholesterol depletion were also coupled with increased Thr276 phosphorylation. With recent evidence showing that the inward-facing conformation of SERT provides access to Thr276, as well as our data showing similar diffusion behavior between PKG-stimulated and cholesterol-depleted conditions, we hypothesized that lowering the cholesterol content would increase Thr276 phosphorylation. To test this, we used western blot to compare Thr276 phospho-SERT levels across conditions. In agreement with our hypothesis, both chronically and acutely depleting cholesterol significantly increased Thr276 phosphorylation levels by over 2.5- and 3-fold respectively (Figure 4.6). 8-Br-cGMP-stimulated conditions were included as

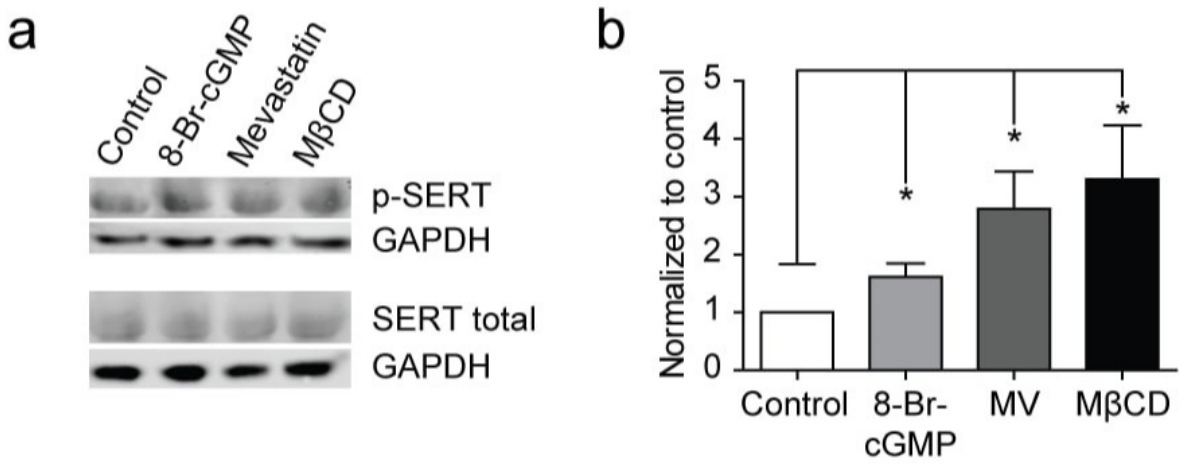


Figure 4.6: Thr276 phosphorylation increases upon cholesterol depletion by both M$\beta$CD and mevastatin. (a) Primary midbrain neurons were treated with 8-Br-cGMP, mevastatin, or M$\beta$CD , lysed for western blot analysis, and probed for phospho-SERT and total SERT. GAPDH was included on both blots for normalization. (b) Analyzed phospho-SERT and total SERT levels are normalized to internal GAPDH. Normalized phospho-SERT was then compared to normalized total SERT, and all data were normalized to the control condition (Fold change increase normalized to control $\pm$ SEM is as follows: $1.62 \pm 0.23$ for 8-Br-cGMP treated, $p < 0.05$ (Students t-test) and $p = 0.08$ (one-way ANOVA with Dunnetts test), $2.93 \pm 0.23$ for mevastatin-treated, $p < 0.05$ (Students t-test and one-way ANOVA with Dunnetts test), and $3.16 \pm 0.92$ for M$\beta$CD-treated, $p < 0.05$ (Students t-test and one-way ANOVA with Dunnetts test). Data were collected from 6 coverslips for each condition per experiment, 6 separate animal cultures total, and 7 replicates.

a positive control, as this treatment is known to increase Thr276 phosphorylation levels and exhibited a 1.62-fold change increase compared to control. These data provide the first evidence that lowered cholesterol content affects a critical regulatory posttranslational pathway that is also coupled with increased SERT membrane mobility.

### 4.4 Conclusions

In conclusion, we have successfully labeled endogenous SERT with QDs to study the surface mobility of individual SERTs in live midbrain neurons. We established that 8-Br-cGMP-mediated PKG activation led to increased SERT surface mobility in its native environment. We also showed that lowering membrane cholesterol, both acutely and chronically, increased SERT surface mobility as well as SERT displacement along the membrane.

In addition, we demonstrated increased phosphorylation of Thr276 in endogenous SERT upon both chronic and acute cholesterol depletion by over 2.5 fold. We hypothesize that cholesterol-sensitive Thr276 activation may either directly drive transporter cell surface reorganization or arise from transporter redistribution away from compartments that restrict phosphorylation. Another possibility is that dynamic destabilization of SERT is a direct consequence of the transporter conformational equilibrium shift that inadvertently provides more access to the Thr276 site. Unraveling the causal relationship between SERT phosphorylation status, membrane microdomain residence, and surface trafficking will be the central goal of our future studies. Overall, this work has provided further understanding of the role of cholesterol in endogenous SERT dynamic membrane organization and has provided a method for visualizing single SERT in this more complex primary neuron system.

**Copyright Permissions**

## 4.5 Bibliography


Bailey, D. M., Catron, M. A., Kovtun, O., Macdonald, R. L., Zhang, Q., and Rosenthal, S. J. (2018). Single Quantum Dot Tracking Reveals Serotonin Transporter Diffusion Dynamics are Correlated with Cholesterol-Sensitive Threonine 276 Phosphorylation Status in Primary Midbrain Neurons. *ACS Chemical Neuroscience*, 9(11):2534–2541.

Bailey, D. M., Kovtun, O., and Rosenthal, S. J. (2017). Antibody-Conjugated Single Quantum Dot Tracking of Membrane Neurotransmitter Transporters in Primary Neuronal Cultures. In *Biomedical Nanotechnology: Methods and Protocols*, volume 726, pages 165–177.

Bermingham, D. P. and Blakely, R. D. (2016). Kinase-dependent Regulation of Monoamine Neurotransmitter Transporters. *Pharmacol. Rev.*, 35559(October):888–953.

Bjerregaard, H., Severinsen, K., Said, S., Wiborg, O., and Sinning, S. (2015). A dualistic conformational response to substrate binding in the human serotonin transporter reveals a high affinity state for serotonin. *Journal of Biological Chemistry*, 290(12):7747–7755.

Chang, J. C., Kovtun, O., Blakely, R. D., and Rosenthal, S. J. (2012a). Labeling of neuronal receptors and transporters with quantum dots. *Wiley Interdisciplinary Reviews: Nanomedicine and Nanobiotechnology*, 4(6):605–619.

Chang, J. C. and Rosenthal, S. J. (2012). Visualization of lipid raft membrane compartmentalization in living RN46A neuronal cells using single quantum dot tracking. *ACS Chemical Neuroscience*, 3(10):737–743.

Chang, J. C., Tomlinson, I. D., Warnement, M. R., Ustione, A., Carneiro, A. M. D., Piston, D. W., Blakely, R. D., and Rosenthal, S. J. (2012b). Single Molecule Analysis of Serotonin Transporter Regulation Using Antagonist-Conjugated Quantum Dots Reveals Restricted, p38 MAPK-Dependent Mobilization Underlying Uptake Activation. *Journal of Neuroscience*, 32(26):8919–8929.

Constals, A., Penn, A. C., Compans, B., Toulmé, E., Phillipat, A., Marais, S., Retailleau, N., Hafner, A. S., Coussen, F., Hosy, E., and Choquet, D. (2015). Glutamate-Induced AMPA Receptor Desensitization Increases Their Mobility and Modulates Short-Term Plasticity through Unbinding from Stargazin. *Neuron*, 85(4):787–803.

Dahan, M., Lévi, S., Luccardini, C., Rostaing, P., Riveau, B., and Triller, A. (2003). Diffusion Dynamics of Glycine Receptors Revealed by Single-Quantum Dot Tracking. *Science*, 302(5644):442–445.

Domanov, Y. A., Aimon, S., Toombes, G. E. S., Renner, M., Quemeneur, F., Triller, A., Turner, M. S., and Bassereau, P. (2011). Mobility in geometrically confined membranes. *Proceedings of the National Academy of Sciences*, 108(31):12605–12610.

Ferraro, M., Masetti, M., Recanatini, M., Cavalli, A., and Bottegoni, G. (2016). Mapping cholesterol interaction sites on serotonin transporter through coarse-grained molecular dynamics. *PLoS ONE*, 11(12):e0166196.

Groc, L., Lafourcade, M., Heine, M., Renner, M., Racine, V., Sibarita, J.-B., Lounis, B., Choquet, D., and Cognet, L. (2007). Surface Trafficking of Neurotransmitter Receptor: Comparison between Single-Molecule/Quantum Dot Strategies. *Journal of Neuroscience*, 27(46):12433–12437.

Hong, W. C. and Amara, S. G. (2010). Membrane cholesterol modulates the outward facing conformation of the dopamine transporter and alters cocaine binding. *Journal of Biological Chemistry*, 285(42):32616–32626.

Imai, H., Steindler, D. A., and Kitai, S. T. (1986). The organization of divergent axonal projections from the midbrain raphe nuclei in the rat. *Journal of Comparative Neurology*, 243(3):363–380.

Kovtun, O., Ross, E. J., Tomlinson, I. D., and Rosenthal, S. J. (2012). A flow cytometry-based dopamine transporter binding assay using antagonist-conjugated quantum dots. *Chemical Communications*, 48(44):5428–5430.

Kovtun, O., Sakrikar, D., Tomlinson, I. D., Chang, J. C., Arzeta-Ferrer, X., Blakely, R. D., and Rosenthal, S. J. (2015). Single-Quantum-Dot Tracking Reveals Altered Membrane Dynamics of an Attention-Deficit/Hyperactivity-Disorder-Derived Dopamine Transporter Coding Variant. *ACS Chemical Neuroscience*, 6(4):526–534.

Kovtun, O., Tomlinson, I. D., Bailey, D. M., Thal, L. B., Ross, E. J., Harris, L., Frankland, M. P., Ferguson, R. S., Glaser, Z., Greer, J., and Rosenthal, S. J. (2018). Single quantum dot tracking illuminates neuroscience at the nanoscale. *Chemical Physics Letters*, 706:741–752.

Kovtun, O., Tomlinson, I. D., Sakrikar, D. S., Chang, J. C., Blakely, R. D., and Rosenthal, S. J. (2011). Visualization of the cocaine-sensitive dopamine transporter with ligand-conjugated quantum dots. *ACS Chemical Neuroscience*, 2(7):370–378.

Laursen, L., Severinsen, K., Kristensen, K. B., Periole, X., Overby, M., Müller, H. K., Schiøtt, B., and Sinning, S. (2018). Cholesterol binding to a conserved site modulates the conformation, pharmacology, and transport kinetics of the human serotonin transporter. *Journal of Biological Chemistry*, 293(10):3510–3523.

Magnani, F., Tatell, C. G., Wynne, S., Williams, C., and Haase, J. (2004). Partitioning of the serotonin transporter into lipid microdomains modulates transport of serotonin. *Journal of Biological Chemistry*, 279(37):38770–38778.

Maxfield, F. R. and Wüstner, D. (2012). Analysis of Cholesterol Trafficking with Fluorescent Probes. *Methods in Cell Biology*, 108:367–393.

Michalet, X. (2005). Quantum Dots for Live Cells, in Vivo Imaging, and Diagnostics. *Science*, 307(5709):538–544.

Montgomery, T. R., Steinkellner, T., Sucic, S., Koban, F., Schuchner, S., Ogris, E., Sitte, H. H., and Freissmuth, M. (2014). Axonal Targeting of the Serotonin Transporter in

Cultured Rat Dorsal Raphe Neurons Is Specified by SEC24C-Dependent Export from the Endoplasmic Reticulum. *Journal of Neuroscience*, 34(18):6344–6351.

Pierobon, P., Achouri, S., Courty, S., Dunn, A. R., Spudich, J. A., Dahan, M., and Cappello, G. (2009). Velocity, processivity, and individual steps of single myosin V molecules in live cells. *Biophysical Journal*, 96(10):4268–4275.

Prasad, H. C., Steiner, J. A., Sutcliffe, J. S., and Blakely, R. D. (2009). Enhanced activity of human serotonin transporter variants associated with autism. *Philosophical Transactions of the Royal Society B: Biological Sciences*, 364(1514):163–173.

Prasad, H. C., Zhu, C.-B., McCauley, J. L., Samuvel, D. J., Ramamoorthy, S., Shelton, R. C., Hewlett, W. A., Sutcliffe, J. S., and Blakely, R. D. (2005). Human serotonin transporter variants display altered sensitivity to protein kinase G and p38 mitogen-activated protein kinase. *Proceedings of the National Academy of Sciences*, 102(32):11545–11550.

Rahbek-Clemmensen, T., Lycas, M. D., Erlendsson, S., Eriksen, J., Apuschkin, M., Vilhardt, F., Jørgensen, T. N., Hansen, F. H., and Gether, U. (2017). Super-resolution microscopy reveals functional organization of dopamine transporters into cholesterol and neuronal activity-dependent nanodomains. *Nature Communications*, 8(1).

Ramamoorthy, S., Samuvel, D. J., Buck, E. R., Rudnick, G., and Jayanthi, L. D. (2007). Phosphorylation of threonine residue 276 is required for acute regulation of serotonin transporter by cyclic GMP. *Journal of Biological Chemistry*, 282(16):11639–11647.

Romay-Tallon, R., Rivera-Baltanas, T., Allen, J., Olivares, J. M., Kalynchuk, L. E., and Caruncho, H. J. (2017). Comparative study of two protocols for quantitative image-analysis of serotonin transporter clustering in lymphocytes, a putative biomarker of therapeutic efficacy in major depression. *Biomarker Research*, 5(1):27.

Rosenthal, S. J., Chang, J. C., Kovtun, O., McBride, J. R., and Tomlinson, I. D. (2011). Biocompatible quantum dots for biological applications. *Chemistry and Biology*, 18(1):10–24.

Rudnick, G., Krämer, R., Blakely, R. D., Murphy, D. L., and Verrey, F. (2014). The SLC6 transporters: Perspectives on structure, functions, regulation, and models for transporter dysfunction. *Pflugers Archiv European Journal of Physiology*, 466(1):25–42.

Samuvel, D. J. (2005). A Role for p38 Mitogen-Activated Protein Kinase in the Regulation of the Serotonin Transporter: Evidence for Distinct Cellular Mechanisms Involved in Transporter Surface Expression. *Journal of Neuroscience*, 25(1):29–41.

Scanlon, S. M., Williams, D. C., and Schloss, P. (2001). Membrane cholesterol modulates serotonin transporter activity. *Biochemistry*, 40(35):10507–10513.

Shrivastava, S., Pucadyil, T. J., Paila, Y. D., Ganguly, S., and Chattopadhyay, A. (2010). Chronic cholesterol depletion using statin impairs the function and dynamics of human serotonin1A receptors. *Biochemistry*, 49(26):5426–5435.

Steiner, J. A., Carneiro, A. M. D., and Blakely, R. D. (2008). Going with the flow: Trafficking-dependent and -independent regulation of serotonin transport. *Traffic*, 9(9):1393–1402.

Varela, J. A., Dupuis, J. P., Etchepare, L., Espana, A., Cognet, L., and Groc, L. (2016). Targeting neurotransmitter receptors with nanoparticles in vivo allows single-molecule tracking in acute brain slices. *Nature Communications*, 7:10947.

Vevera, J., Vales, K., Fisar, Z., Hroudova, J., Singh, N., Stuchlik, A., Kacer, P., and Nekovarova, T. (2016). The effect of prolonged simvastatin application on serotonin uptake, membrane microviscosity and behavioral changes in the animal model. *Physiology and Behavior*, 158:112–120.

Wood, W. G., Eckert, G. P., Igbavboa, U., and Müller, W. E. (2010). Statins and neuroprotection: A prescription to move the field forward. *Annals of the New York Academy of Sciences*, 1199:69–76.

Zhang, Y.-W., Gesmonde, J., Ramamoorthy, S., and Rudnick, G. (2007). Serotonin Transporter Phosphorylation by cGMP-Dependent Protein Kinase Is Altered by a Mutation Associated with Obsessive Compulsive Disorder. *Journal of Neuroscience*, 27(40):10878–10886.

Zhang, Y.-W., Turk, B. E., and Rudnick, G. (2016). Control of serotonin transporter phosphorylation by conformational state. *Proceedings of the National Academy of Sciences*, 113(20):E2776–E2783.

Zhu, C.-B., Hewlett, W. A., Feoktistov, I., Biaggioni, I., and Blakely, R. D. (2004). Adenosine Receptor, Protein Kinase G, and p38 Mitogen-Activated Protein Kinase-Dependent Up-Regulation of Serotonin Transporters Involves Both Transporter Trafficking and Activation. *Molecular Pharmacology*, 65(6):1462–1474.

Zidovetzki, R. and Levitan, I. (2007). Use of cyclodextrins to manipulate plasma membrane cholesterol content: Evidence, misconceptions and control strategies. *Biochimica et Biophysica Acta - Biomembranes*, 1768(6):1311–1324.

# CHAPTER 5

## Diffusion dynamics of autism-associated Gly56Ala SERT

### 5.1 Introduction

Neurotransmitter transporter proteins, such as dopamine transporter (DAT) and SERT, regulate extracellular dopamine and serotonin by recycling the neurotransmitters back into the presynaptic neurons. For these proteins to function properly, they must be able to move to neurotransmitter-releasing sites, associate with various support proteins, and become stabilized in the membrane in order to reuptake these molecules (Chang et al., 2012; Magnani et al., 2004; Steiner et al., 2008). Multiple naturally-occurring, brain disorder-associated coding variants have been identified for the DAT and SERT proteins, fundamentally altering transporter function and regulation (Prasad et al., 2009). Kovtun et al. from the Rosenthal lab investigated the membrane dynamics of one such Attention-Deficit/Hyperactivity-Disorder (ADHD)-associated DAT variant, Arg615Cys (R16C), where the arginine is coded as a cysteine at the 16th position. The R615C variant had increased diffusion rates compared to the wild type transporter, similar to DAT diffusion rates after cholesterol disruption. Importantly, this mobility increase also correlated with loss of DAT mobilization by amphetamine, potentially indicating an altered pharmacological reaction to a common component in ADHD medication (Kovtun et al., 2015). This report was the first to show the altered membrane dynamics of a transporter protein disease-associated variant. Recently, Thal et al. from the Rosenthal lab demonstrated that another DAT coding variant, Ala559Val, also had increased membrane mobility. This result was accompanied by decreased DAT clustering of the variant, likely due to shifts out of membrane microdomains. Increased membrane mobility was also observed when DAT was phosphorylated (Thal et al., 2018). Overall, these variants disrupted the transporters normal membrane diffusion, which may be a common feature of many neuropsychiatric diseases.

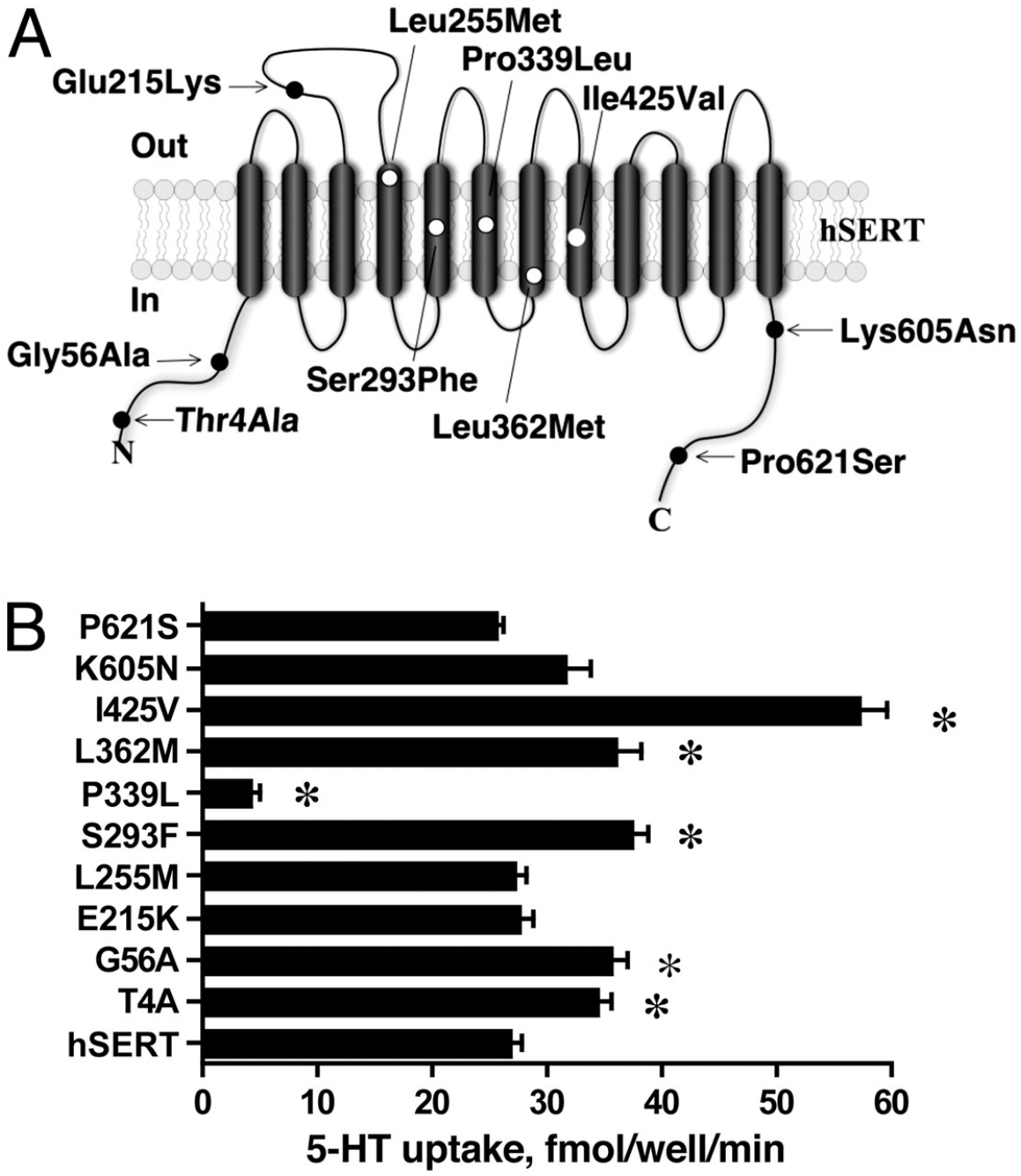


Figure 5.1: (A) Location of hSERT coding variants. Gly56Ala is located on the intracellular facing side along the N terminus. (B) 5-HT transport activity of hSERT coding variants. G56A SERT had significantly higher 5-HT uptake compared to the hSERT wild type. Copyright (2005) National Academy of Sciences, U.S.A. (Prasad et al., 2005).

Many disease-associated variants have also been identified for SERT (Fig. 5.1 A). One such gain-of-function variant, Gly56Ala (G56A) SERT, has been associated with autism

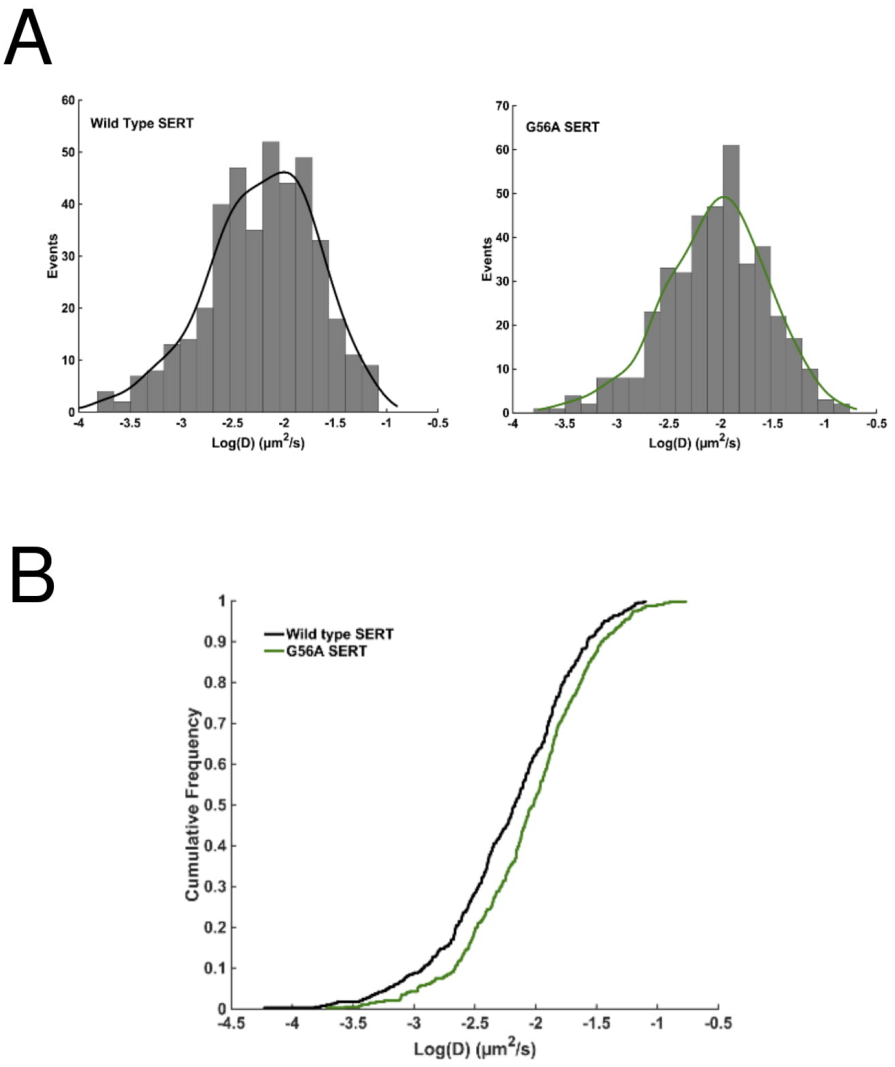


Figure 5.2: Single QD tracking revealed differences in lateral mobility and diffusion between wild type SERT and autism-associated G56A SERT in stably transfected CHO cells ($n > 400$ trajectories per condition from at least three independent experiments). (A) Distributions of diffusion coefficients for wild type SERT and G56A SERT. (B) Cumulative probability plots portraying diffusion coefficient distributions for both conditions; $p < 0.001$, Kolmogorov-Smirnov test.

spectrum disorder (ASD), a highly prevalent brain disorder characterized by impaired social communication and abnormal sensory processing (Prasad et al., 2005). Studies have

shown that elevated blood serotonin is a replicable biomarker present in up to 25% of individuals with ASD (Prasad et al., 2009). In fact, the G56A allele is carried by approximately 1 in 200 Caucasian subjects, representing more than a million Americans. At the molecular level, the G56A SERT mutation lies on the N-terminus. G56A SERT displays an elevated constitutive phosphorylation rate and the complete loss of sensitivity to p38 MAPK-mediated phosphorylation, thus enabling the investigation of the direct link between the transporter phosphorylation status and its lateral mobility (Prasad et al., 2005). For this work, a biotinylated SERT-selective ligand, IDT357, was used in conjunction with streptavidin-conjugated QDs (IDT357 synthesis outlined in Chapter 2) (Tomlinson et al., 2011). The extracellular SERT antibody, specific against the murine SERT epitope, has reduced binding of human SERT (hSERT) in Chinese hamster ovary (CHO) cells, thus a ligand approach is a feasible alternative. Single QDs were tracked and analyzed to compare mobilities of the wild type SERT protein and the G56A SERT variant.

## 5.2 Materials and methods

### Materials

DMEM/F-12K, DMEM fluorobrite, fetal bovine serum (FBS), hygromycin B, and 605 streptavidin-conjugated QDs (SaV-QDs) were purchased from Life Technologies. Poly-d-lysine and bovine serum albumin (BSA) were purchased from Sigma-Aldrich. No. 1.5 glass dishes were purchased from MatTek Corporation. IDT357 was synthesized as previously described.

### 5.2.1 Ligand specificity

To ensure the ligand was specific to SERT, controls were run that included the following: (1) Labeling cells with IDT357 and streptavidin-conjugated QDs. (2) Pre-blocking SERT with 10 μm Paroxetine, followed by IDT357 and streptavidin-conjugated QD labeling. (3) Labeling cells with QD only to assess the degree of nonspecific binding. The results of these controls indicated that IDT357 was specific to SERT (data shown in Figure 2.4 in

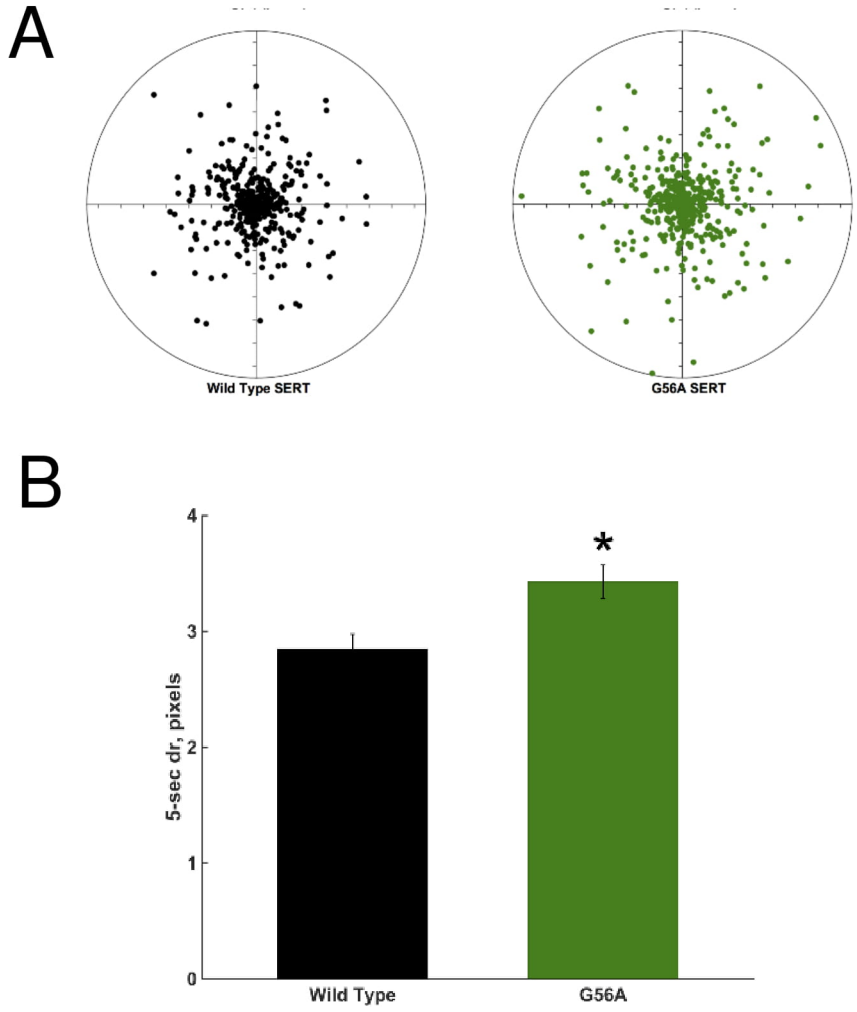


Figure 5.3: (A) Two-dimensional polar plots of five second displacements of single SERT proteins normalized to starting positions for wild type SERT and G56A SERT. Radius of a polar plot is 1.3 µm. (B) Wild type SERT and G56A SERT mean radial displacement values (magnitude of 5-sec vector displacement from the origin); pixel size is 108 nm; $*p < 0.01$, Students t-test.

Chapter 2).

### 5.2.2 Cell culture and imaging conditions

Stably transfected wild type and G56A SERT CHO cells were cultured in complete DMEM/ F-12K media with 10% FBS and 1% pen/strep with 2 mg/mL hygromycin B in a 37°C in-

cubator with 5% $CO_2$.

Cells were plated 48 hours before experiments on poly-d-lysine-coated no.1.5 glass bottom MatTek dishes. Cells were incubated with 500 nM IDT357 ligand in complete medium at 37°C and 5% $CO_2$ for 20 minutes. Following two washes with warm DMEM fluorobrite, cells were incubated with 0.1 nM SaV-QDs in warm DMEM fluorobrite in 2% BSA for 5 minutes. Cells were then washed 4 times with warm DMEM fluorobrite and imaged immediately.

### 5.2.3 High speed widefield microscopy

Images were obtained on a Nikon Multi-Excitation TIRF Microscope and viewed with an Apo TIRF 60x oil immersion objective lens. QDs were excited with a 488 nm diode laser, and fluorescence was collected with a 603/30 bandpass filter. Imaging was performed at 37°C. Single QD tracking was performed at a frame rate of 10 Hz for 60 seconds, and data were obtained within 20 minutes of the final wash step after QD labeling.

### 5.2.4 Trajectory analysis

Raw data files were extracted to generate stacks of individual TIFF images using ImageJ. Positions (x and y coordinates) and trajectories of the QD-labeled SERT proteins were determined using modified MATLAB routines developed by Daniel Blair and Eric Dufresne (Blair and Dufresne, 2017). Trajectory analysis was performed using custom MATLAB routines to determine mean square displacement (MSD). Once MSD for each trajectory was analyzed, diffusion coefficients were determined by fitting MSD to the equation $4Dt\alpha$, where D is the diffusion coefficient and $\alpha$ is the anomolous diffusion parameter. Single QD trajectories were only used if QD blinking lasted for less than 10 consecutive frames and were at least 50 frames in length.

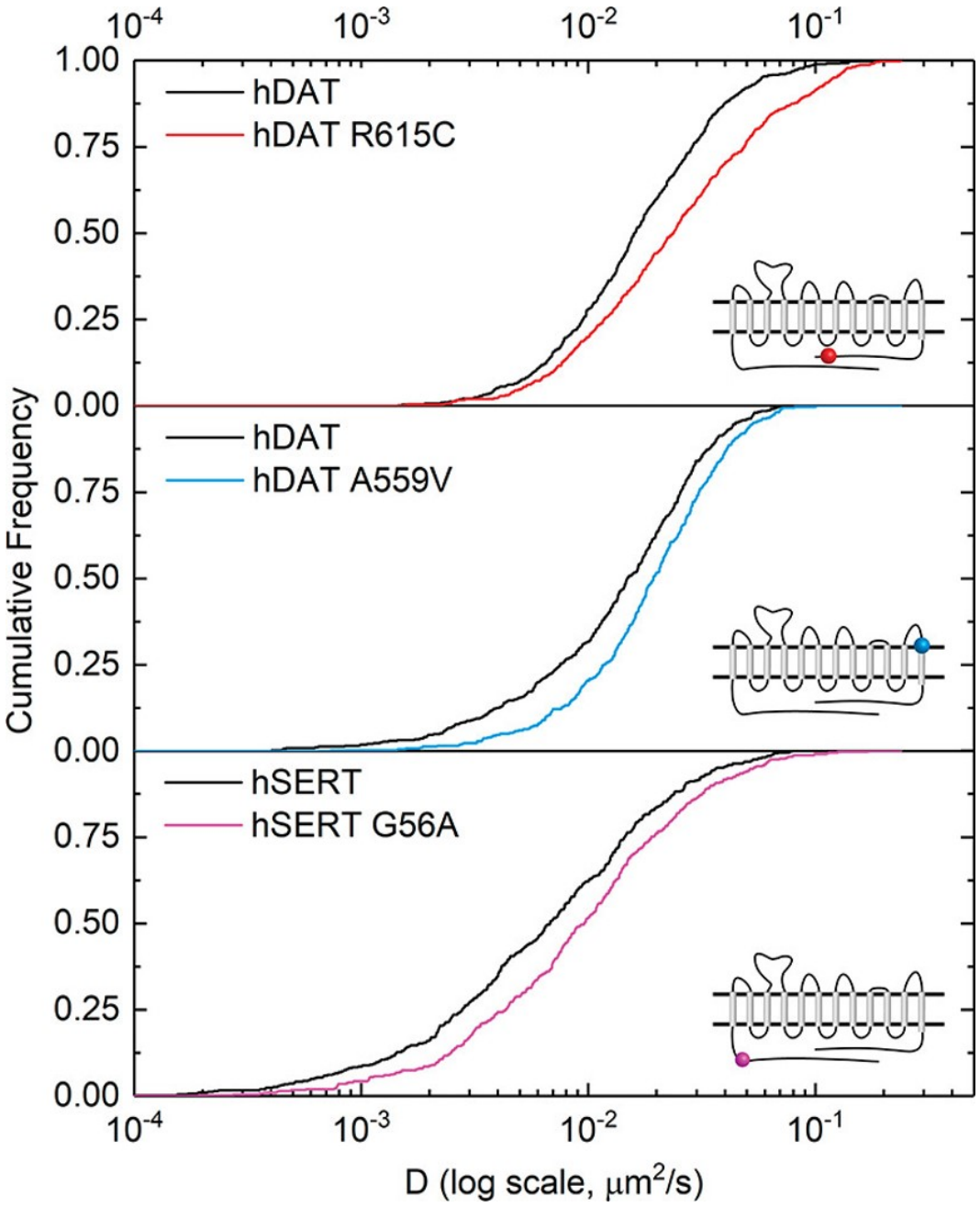


Figure 5.4: Cumulative frequency plots showing diffusion rates for wild type (black lines) and DAT R615C, A559V, and SERT G56A genetic variants (red, blue, and pink lines, respectively). The locations of each variant are shown in the schematics next to each plot. All genetic variants studied displayed increased diffusion coefficients compared to the wild type. Figure reprinted with permission from the American Chemical Society (Rosenthal, 2018).

## 5.3 Results and conclusions

To capture membrane dynamics of G56A and WT SERT in stably transfected Chinese hamster ovary (CHO) cells, a biotinylated, SERT-selective ligand IDT357 was used in conjunction with streptavidin-conjugated QDs as described in Chapter 2. Membrane movement of QD-tagged SERTs was recorded for 1 min at the acquisition rate of 10 Hz, and the motion parameters were then extracted from the obtained trajectories. The hyperphosphorylated G56A SERT mutant showed significantly higher rate of diffusion compared to the wild type SERT ($0.016 \pm 0.001$ μ $m^2$/s versus $0.011 \pm 0.001$ μ $m^2$/s, $p < 0.001$, Kolmogorov-Smirnov statistical test) (Fig. 5.2). To visualize the extent of lateral movement of QD-tagged SERT proteins from the starting position over a 5 s recording interval (5-sec dr), we plotted radial displacement of each variant in Fig 5.3 A. The G56A variant traveled slightly but significantly farther than wild type SERT (one-way ANOVA, $p < 0.01$) (Fig. 5.3 B). We hypothesize that the mutation to alanine disrupts G56A SERT membrane microdomain localization and key associations with the SERT membrane interactome, resulting in a dysregulated dynamic phenotype.

Interestingly, all three variants studied in our lab thus far can be characterized as having increased mobility along the membrane compared to the wild type proteins (Figure 5.4) (Rosenthal, 2018). This finding indicates the relevance of membrane mobility for the proper function of these membrane transporters, as all of these mutants are associated with mental disorders. QDs have enabled these studies by offering a real-time single molecule view of how the genetic makeup of these variants can affect the protein function. Future directions of this work will focus on modeling these mutations to see how they could affect protein-protein interactions, as well as interactions within the membrane. In addition to the abnormal diffusion dynamics exhibited by brain disorder-associated DAT and SERT variants in our studies, Jezequel et al. recently determined that circulating auto-antibodies derived from the blood serum of psychotic patients diagnosed with schizophrenia directly destabilize surface dynamics and nanoscale organization of the synaptic glutamate NMDA

receptors (Jezequel et al., 2017). We believe that spatiotemporal membrane disorganization of neuronal proteins is emerging as a central molecular pathological theme in brain disorder research.

### Copyright Permissions

## 5.4 Bibliography

Blair, D. and Dufresne, E. (2017). The Matlab Particle Tracking Code Repository.

Chang, J. C., Tomlinson, I. D., Warnement, M. R., Ustione, A., Carneiro, A. M. D., Piston, D. W., Blakely, R. D., and Rosenthal, S. J. (2012). Single Molecule Analysis of Serotonin Transporter Regulation Using Antagonist-Conjugated Quantum Dots Reveals Restricted, p38 MAPK-Dependent Mobilization Underlying Uptake Activation. *Journal of Neuroscience*, 32(26):8919–8929.

Jezequel, J., Johansson, E. M., Dupuis, J. P., Rogemond, V., Grea, H., Kellermayer, B., Hamdani, N., Le Guen, E., Rabu, C., Lepleux, M., Spatola, M., Mathias, E., Bouchet, D., Ramsey, A. J., Yolken, R. H., Tamouza, R., Dalmau, J., Honnorat, J., Leboyer, M., and Groc, L. (2017). Dynamic disorganization of synaptic NMDA receptors triggered by autoantibodies from psychotic patients. *Nature Communications*, 8(1791).

Kovtun, O., Sakrikar, D., Tomlinson, I. D., Chang, J. C., Arzeta-Ferrer, X., Blakely, R. D., and Rosenthal, S. J. (2015). Single-Quantum-Dot Tracking Reveals Altered Membrane Dynamics of an Attention-Deficit/Hyperactivity-Disorder-Derived Dopamine Transporter Coding Variant. *ACS Chemical Neuroscience*, 6(4):526–534.

Kovtun, O., Tomlinson, I. D., Bailey, D. M., Thal, L. B., Ross, E. J., Harris, L., Frankland, M. P., Ferguson, R. S., Glaser, Z., Greer, J., and Rosenthal, S. J. (2018). Single quantum dot tracking illuminates neuroscience at the nanoscale. *Chemical Physics Letters*, 706:741–752.

Magnani, F., Tatell, C. G., Wynne, S., Williams, C., and Haase, J. (2004). Partitioning of the serotonin transporter into lipid microdomains modulates transport of serotonin. *Journal of Biological Chemistry*, 279(37):38770–38778.

Prasad, H. C., Steiner, J. A., Sutcliffe, J. S., and Blakely, R. D. (2009). Enhanced activity of human serotonin transporter variants associated with autism. *Philosophical Transactions of the Royal Society B: Biological Sciences*, 364(1514):163–173.

Prasad, H. C., Zhu, C.-B., McCauley, J. L., Samuvel, D. J., Ramamoorthy, S., Shelton, R. C., Hewlett, W. A., Sutcliffe, J. S., and Blakely, R. D. (2005). Human serotonin transporter variants display altered sensitivity to protein kinase G and p38 mitogen-activated protein kinase. *Proceedings of the National Academy of Sciences*, 102(32):11545–11550.

Rosenthal, S. J. (2018). Nanotechnology in Neuroscience Reveals Membrane Mobility Matters. *ACS Chemical Neuroscience*.

Steiner, J. A., Carneiro, A. M. D., and Blakely, R. D. (2008). Going with the flow: Trafficking-dependent and -independent regulation of serotonin transport. *Traffic*, 9(9):1393–1402.

Thal, L. B., Tomlinson, I. D., Quinlan, M. A., Kovtun, O., Blakely, R. D., and Rosenthal, S. J. (2018). Single Quantum Dot Imaging Reveals PKC$\beta$-Dependent Alterations

in Membrane Diffusion and Clustering of an Attention-Deficit Hyperactivity Disorder/Autism/Bipolar Disorder-Associated Dopamine Transporter Variant. *ACS Chemical Neuroscience*.

Tomlinson, I. D., Iwamoto, H., Blakely, R. D., and Rosenthal, S. J. (2011). Biotin tethered homotryptamine derivatives: High affinity probes of the human serotonin transporter (hSERT). *Bioorganic and Medicinal Chemistry Letters*, 21(6):1678–1682.

# CHAPTER 6

## Summary and future directions

The brain is one of the most complex systems known to humankind. To understand both the normal and disease states of the brain at the macro, cellular, and molecular levels is a monumental task, one that will require collaborations between biologists, neuroscientists, chemists, physicists, pharmacologists, and engineers. With the advent of nanotechnology and its use in neuroscience, much progress has been made in understanding basic function of many disease-associated proteins, including SERT and DAT, at the single molecule level. Nanotechnology, especially quantum dots, has opened the possibilities of observing proteins in their native environments in real-time. The overarching theme of this dissertation is to utilize and further develop quantum dot probes to elucidate mechanisms underlying serotonin transporter function in both normal and disease states from a single particle perspective. Alterations in SERT expression, function, and regulation have been implicated as an important risk factor in the etiology of many psychiatric disorders. Although perturbed SERT activity in brain disorders has received continuous attention there have been a lack of opportunities to interrogate endogenous SERT regulation at the level of individual transporters due to the indirect and ensemble nature of conventional approaches. Through their brightness, photostability, and multi-functionality, QDs offer unique characteristics that can provide new insights into neurotransmitter transporter behavior in real-time over longer time scales than traditionally used dyes. The work presented in this dissertation provides new understanding of SERT behavior and its interaction with cholesterol in an endogenous primary system through QD SPT, while also providing new methods for generating a monovalent aptamer-conjugated QD that could be used with any protein with a fused GFP, allowing for the exciting potential for multiplexing using aptamer-QDs, streptavidin-QDs, and antibody-QDs.

## 6.1 Summary

After a literature review in Chapter 1, Chapter 2 covers general methods used throughout this dissertation, including ligand- and antibody-conjugated QD SPT, as well as general analysis for SPT. A two-step labeling protocol is utilized in which the specific ligand or antibody is first bound to the protein of interest followed by either streptavidin- or antibody-conjugated QDs. While this QD labeling method is standard, here we report the first QD SPT protocol for transporter proteins in primary midbrain neurons, which are notoriously difficult to work with and dissect. Being able to track endogenous SERT in these neurons, and uncover a novel regulatory role of cholesterol, is progress towards understanding how these proteins function in the more native environment. Chapter 2 details the methods for SPT in both cell lines and midbrain neurons, as well as the dissection protocols that were optimized for this system.

In Chapter 3, I discuss the generation of a monovalent aptamer-conjugated QD probe. The aptamer-QD exhibited 1:1 binding with extracellular GFP fused to SV2A and ASAP1, making it generalizable and functional for a variety of proteins. These methods were built upon a previously reported method in which ptDNA wraps around a phase transferred aqueous QD, leaving a DNA tail for further functionalization or binding. Chapter 3 outlines the extension of this method by adding a DNA/RNA aptamer hybrid tail that binds to the ptDNA. A construct was designed to test monovalency in which the aptamer-QD binds to GFP-Au nanoparticles, which were then drop casted onto a TEM grid for imaging. The QD and Au are visually distinct due to different electron densities, thus leading to straightforward quantification. The aptamer-QDs were over 95% monovalent and bound specifically to SV2A-pHluorin in live hippocampal neurons. Previous methods to generate monovalent QDs relied on purification methods, such as gel electrophoresis or magnetic bead separation; we achieved over 95% monovalency with no purification. Because these probes do not utilize the commonly used streptavidin- or antibody-conjugated QDs, multiplexing becomes experimentally feasible. The potential for aptamers in nanotechnology is just

starting to be explored, and this method provides an exciting possibility for use of aptamers in SPT applications.

In Chapter 4, we utilize QDs to directly observe the lateral diffusion of individual SERTs in living primary rat midbrain neurons using a generalizable two-step antibody labeling approach. We found that QD-tagged single SERTs exhibit a bimodal diffusion pattern, with 62% of transporters being confined with a mean diffusion coefficient of 0.0211 $\pm$ 0.0030 $\mu m^2/s$ for control conditions. Since perisynaptic SERT localization is critical to effective serotonin reuptake, dysregulated SERT surface trafficking could deleteriously impact brain serotonin homeostasis. Thus, we sought to gain a deeper understanding of endogenous SERT dynamic stability in response to catalytic activation and membrane cholesterol depletion.

SERT associates with cholesterol-rich membrane microdomains, and lowered cholesterol content can shift the transporter conformation equilibrium to inward-facing, possibly impacting phosphorylation of Thr276. This evidence led us to investigate the effects of acute and chronic cholesterol depletion by M$\beta$CD and mevastatin, respectively, on rat neuronal SERT diffusion dynamics. We also examined the effects of 8-Br-cGMP, which is known to stimulate phosphorylation of Thr276, on SERT lateral mobility. Upon stimulating Thr276 phosphorylation with 8-Br-cGMP, the mean diffusion coefficient increased 2-fold. We observed similar trends upon both acute and chronic cholesterol treatments, including faster diffusion rates, larger displacements along the membrane, and greater mobile fractions. Because cholesterol manipulation and SERT Thr276 stimulation induced a similar dynamic transporter response, we then looked at whether these changes were accompanied by a uniform increase in Thr276 phosphorylation across the conditions through western blotting. We observed Thr276 phosphorylation increases of 1.6-fold for 8-Br-cGMP-treated, 2.5-fold for mevastatin-treated, and 3-fold for M$\beta$CD-treated neurons. This approach demonstrated the feasibility and generalizability of QD SPT in visualizing single endogenous neuronal SERT. These findings provided new mechanistic insights into the role

of cholesterol in maintaining SERT lateral membrane stability and, unexpectedly, modulating its Thr276 phosphorylation status. Moreover, this contribution further strengthened the hypothesis that plasma membrane and local lipid microenvironment shape SERT-mediated serotonin reuptake and thus presents an exciting opportunity for therapeutic intervention in psychiatric disorders.

Chapter 5 focuses on the work done with an autism-associated coding variant, Gly56Ala SERT. While multiple naturally-occurring, brain disorder-associated coding variants have been identified for SERT, G56A SERT is of particular interest as it is found in 1 in 200 caucasian subjects and is a gain-of-function variant (Prasad et al., 2009, 2005). Structurally, the G56A SERT mutation lies on the N-terminus. G56A SERT displays a higher phosphorylation rate and is insensitive to p38 MAPK-mediated phosphorylation. These phenotypes thus allow for the investigation of the link between the SERT phosphorylation status and its lateral mobility, providing further evidence for the conclusions in Chapter 4. To track individual wild type or G56A SERT proteins, a biotinylated SERT-selective ligand, IDT 357, was used in conjunction with streptavidin-conjugated QDs. The hyperphosphorylated G56A SERT mutant showed significantly higher rate of diffusion compared to the wild type SERT ($0.016 \pm 0.001$ $\mu m^2$/s versus $0.011 \pm 0.001$ $\mu m^2$/s, $p < 0.001$, Kolmogorov-Smirnov statistical test). The G56A variant also traveled significantly farther than wild type SERT when plotting the lateral movement of the proteins over a 5 second period. It is possible that the mutation from glycine to alanine disrupts membrane microdomain associations, which as shown in Chapter 4, affect SERT mobility along the membrane.

## 6.2 Addressing size limitations

Much of the work in this dissertation utilized antibody-conjugated QDs which are about 15 nm larger than the as-synthesized QD. Thus, one major question is how the size of the biofunctionalized QD affects the protein diffusion dynamics and behavior. While keeping the size of the probe small is especially important in high density membrane regions, the

best way to address possible effects our method may have is to compare our results with studies using small molecule fluorophores. The data we present with our antibody-QD labeling strategy are consistent with the few studies available on monoamine transporter membrane organization in endogenous systems. We have shown that untreated endogenous neuronal SERT displays mostly confined diffusion (62% of transporters fell into the confined regime). Our lab also showed that SERT colocalizes with membrane microdomain-associated GM1 ganglioside in the RN46A cell lines (Chang et al., 2012), again consistent with the slower diffusion coefficient values reported for basal endogenous SERT in our neuronal system. Recent superresolution stochastic optical reconstruction microscopy (STORM) imaging of the homologous dopamine transporter by Gether and colleagues using antibody-dye conjugates has shown that DAT is largely clustered (about 60%) along the plasma membrane of midbrain neurons (Rahbek-Clemmensen et al., 2017), consistent with our percentage of confined serotonin transporters. In another endogenous system, clustering of endogenous SERT has been observed along the surface of lymphocytes (Romay-Tallon et al., 2017). Thus, we believe our bimodal distribution of SERT is in agreement with available data from endogenous systems.

For QD and dye comparison studies, Triller and colleagues investigated how the size of their antibody-conjugated QD probes affected diffusion of glycine receptors in primary neurons compared to the Cy3-labeled Fab fragment of their primary antibody and did not find significant differences (Dahan et al., 2003). Additionally, Groc et al. investigated the effects of probe size and valency on GluR2 AMPA receptors in cultured hippocampal neurons (Groc et al., 2007). They tracked the AMPAR diffusion using antibody-QD, Cy5-Antibody, and Cy5-Bungarotoxin probes. They did not detect any significant differences between instantaneous diffusion coefficients between any of the probes in either extrasynaptic or synaptic compartments, and the median values of the total and mobile receptors were also not significantly different. These studies suggest that the antibody-QD probe used in this work should not significantly affect the diffusion coefficients compared to dye-

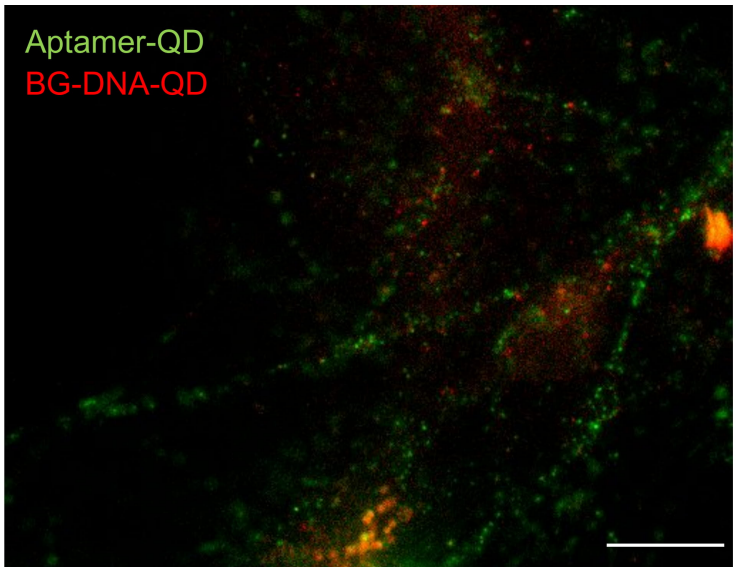


Figure 6.1: As a proof-of-principle demonstration, SV2A-pHluorin and SNAP-tagged endocannabinoid receptor (CB1R) were simultaneously tagged with aptamer-QDs and benzylguanine-DNA-QDs, respectively. Scale bar, 20 μm. Image provided by Dr. Kristina E Kitko (Kitko, 2018).

conjugated antibodies.

Another common concern is the drag effects a QD may have on the mobility of a labeled target. Domanov et al. calculated the 3D diffusion coefficient of 625 nm-emitting QDs at room temperature with a buffer viscosity of $1.2510^{-3}$ Pa·s and found it to be 19.6 $\mu m^2$/s, which is much greater than membrane protein diffusion coefficients (Domanov et al., 2011). They demonstrated with this study that the drag on a QD tagged to a protein is dominated by the mobility of the target anchored in the membrane. Dahan, Cappello, and colleagues also looked at QD drag effects when tagged to myosin V (Pierobon et al., 2009). Like Domanov et al., they found that the size of their probe does not affect the motion of myosin V. They showed that the viscous force of the QD is about 10 times smaller than the stall force of myosin V, thus causing negligible motion effects.

## 6.3 Future directions

### 6.3.1 Monovalent aptamer-QDs

While concerns about how QD size affects protein behavior have been addressed in the previous section, it must be noted that both antibodies and streptavidin add significant bulk to the QD. In addition to that, adding serum to help alleviate nonspecific binding further increases the QD hydrodynamic behavior. Retaining the small size of the QD (about 12 nm) is one main advantage of this aptamer-QD method. Keeping the size small becomes important in multiplexing experiments, especially when the proteins of interest are in tight membrane regions such as the synapse. The main next step for this portion of the dissertation would be to carry out SPT multiplexing experiments with multiple proteins. Farlow et al. showed that the 50 adenosine ptDNA strand can be used for QD wrapping as long as the QD is smaller than 605 QDs (Farlow et al., 2013). Thus, to demonstrate feasibility of this next step, the methods outlined in Chapter 3 were used to generate a ptDNA-wrapped 565 QD. benzylguanine (BG)-DNA with a complementary sequence to the ptDNA was then added. This functional group recognizes a SNAP-tag, which is a polypeptide fused to a protein of interest. The BG covalently attaches to the SNAP tag through the benzyl group, and the guanine is released. Live hippocampal neurons were co-transfected with SV2A-pHluorin and a SNAP-tagged endocannabinoid receptor (CB1R). These proteins were then tagged with aptamer-QDs and BG-DNA-QDs simultaneously (Figure 6.1). While a SNAP tag was utilized for this inital proof-of-principle experiment, future experiments would utilize other aptamers specific to proteins of interest. Another important next step includes optimizing the ptDNA wrapping for larger sized QDs. Right now multiplexing can occur for QDs smaller than 605 QDs, but for this method to have greatest applicability, longer DNA strands would be tested and optimized for use with larger size QDs.

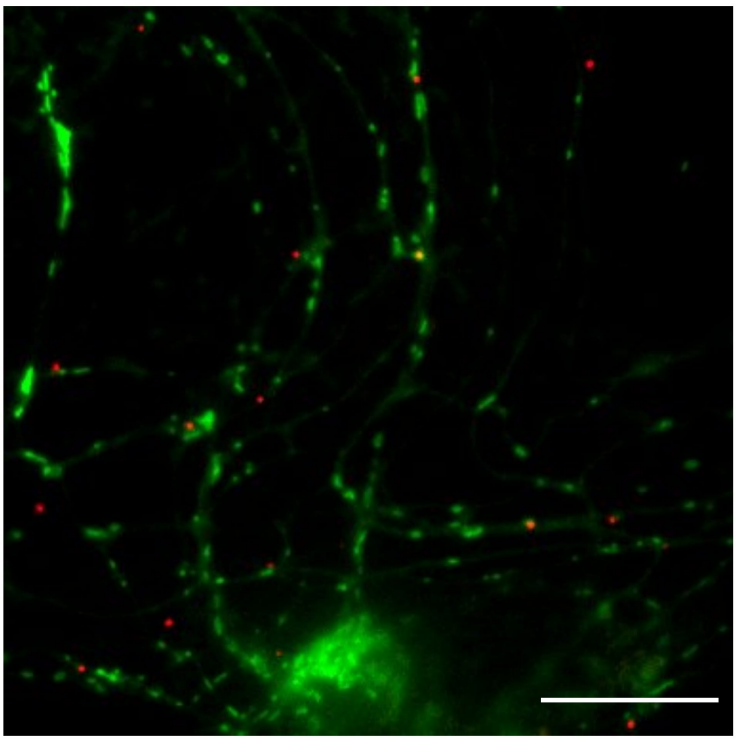

Figure 6.2: Endogenous SERT from midbrain neuronal cultures was tagged with antibody-conjugated QDs (red puncta). MitoTracker Green marked the synapses (green). This dual labeling approach can uncover differences in mobility when SERT is in or out of synaptic regions. Scale bar, 50 μm.

### 6.3.2 Probing SERT dynamics in primary neurons

In Chapter 4, probing the dynamics of SERT mobility along the membranes of primary midbrain neurons provided further understanding of the role of cholesterol in endogenous SERT dynamic membrane organization. Unraveling the causal relationship between SERT phosphorylation status, membrane microdomain associations, and surface trafficking will be the central goal of future studies.

To establish causality between phosphorylation and mobility change, the mobilities of different mutated SERT structures may be investigated that either mimic constitutive phosphorylation or are resistant to phosphorylation at the 276 position. The Thr276Asp mutant could be used to mimic constitutive phosphorylation. This mutant could be transfected into neurons and tagged with QDs to examine whether it also behaves similarly to PKG-

activated SERT. If phosphorylation at this site causes SERT mobility to increase, we would expect to see increased diffusion similar to stimulated SERT conditions. The other important control to be run includes observing mobility of SERT that cannot be phosphorylated at the 276 position to see if it remains confined. To test this, the Thr276Ala mutant could be used. Once these experiments are performed, a better understanding of the relationship between mobility and phosphorylation status will be elucidated.

Another next step would be to establish whether SERT localizes to the site of vesicular serotonin release and examine whether lateral mobility is a key mechanism of SERT delivery to these sites. SERT is the key protein responsible for terminating serotonin signaling near synaptic sites, yet how it is localized and trafficked along the neuronal membrane has yet to be determined (Chang et al., 2012). After intracellular SERT is incorporated into the neuronal membrane, it must still be trafficked in and out of its site of action. Thus, it would be of interest to uncover whether SERT exhibits increased density near synaptic regions in midbrain slices and how SERT localization patterns differ at the soma, dendrite, axon, and synapse in primary midbrain neurons. Because SERT trafficking is a dynamic process, the role of lateral mobility as the key mechanism of SERT delivery in and out of these sites could be examined. I would expect to observe differences in diffusion rates between synaptic and extrasynaptic compartments that correlate with differences in SERT activity.

To approach these questions, it must first be established whether SERT exhibits a heterogenous density distribution on the neuronal membrane using midbrain tissue slices containing raphe nuclei. Tissue could be fixed using 4% paraformaldehyde followed by permeabilization using 0.25% Triton-X in PBS. Tissue could then be stained using extracellular SERT and the serotonergic neuron-marker tryptophan hydroxylase 2 (TPH2) antibodies (immunohistochemistry) or extracellular SERT, synaptophysin and microtubule-associated protein 2 (MAP2) antibodies (immunocytochemistry). Synaptophysin antibodies would mark synapses, while MAP2 antibodies would label dendritic spines. Once SERT distribution is established in tissue labeling, QD labeling methods could be used in live midbrain

neurons. Commercially available 655 QDs could be used in conjunction with MitoTracker Green, which is a fluorescent synaptic marker. SERTs detected within MitoTracker Green positive regions would be considered synaptic, while SERTs outside of these areas would be considered extrasynaptic. The feasibility of these studies has been validated by inital experiments that demonstrate the colocalization of SERT with MitoTracker Green in basal conditions (Fig 6.2). Diffusion coefficients would be analyzed separately for synaptic and extrasynaptic zones to see how localization affects mobility distributions.

These data could build upon prior understanding of SERT regulation through directly visualizing how active SERT is delivered to serotonin-releasing sites to effectively remove excess serotonin. I anticipate that information collected from these studies could offer a more complete understanding of how SERT is functioning in normal and disease states. A potential limitation in these studies could be difficulty resolving multiple targets simultaneously to get a comprehensive view of SERT membrane organization. Super-resolution microscopy using a STORM system can be used to combat this potential problem.

In addition to investigating SERT localization mechanisms in neurons, imaging SERT in the presence of a QD-bound membrane microdomain marker, GM1 ganglioside, could provide more direct understanding of SERT interactions into and out of membrane microdomains. For these studies, it would be valuable to analyze SERT behavior in basal and acute and chronic cholesterol depleted conditions.

### 6.3.3 Mobility of autism-associated Gly56Ala SERT

We previously studied the surface mobility of individual SERTs in live midbrain neurons. We established that 8-Br-cGMP-mediated PKG activation led to increased SERT surface mobility in its native environment and that lowering membrane cholesterol, both acutely with M$\beta$CD and chronically with mevastatin, increased SERT surface mobility as well as SERT displacement along the membrane. Using western blot, we also demonstrated increased phosphorylation of Thr276 in endogenous SERT upon both chronic and acute

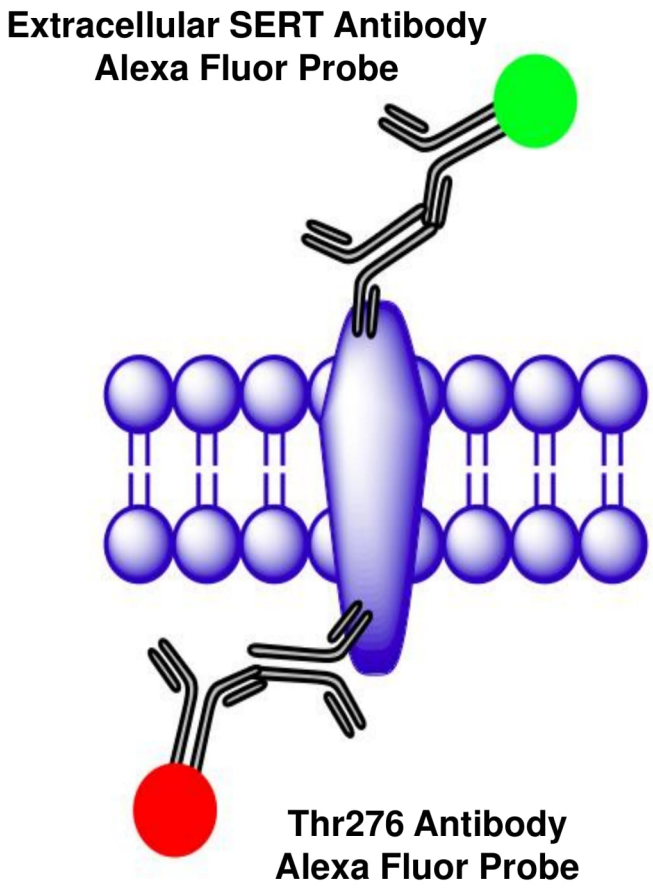


Figure 6.3: Flow cytometry labeling approach. Total SERT fluorescence was measured with an extracellular SERT antibody, while Thr276 SERT fluorescence was measured with an antibody at the Thr276 intracellular site.

cholesterol depletion by over 2.5 fold. In Chapter 5, we established an increase in surface mobility of the hyperphosphorylated SERT Gly56Ala coding variant. Based on the work in midbrain neurons, an immediate next step for the G56A SERT studies is to establish whether the increased mobility in the mutant is also correlated with increased Thr276 phosphorylation and whether G56A SERT is also sensitive to cholesterol manipulation. We showed that SERT phosphorylation status correlated with changes in mobility both in en-

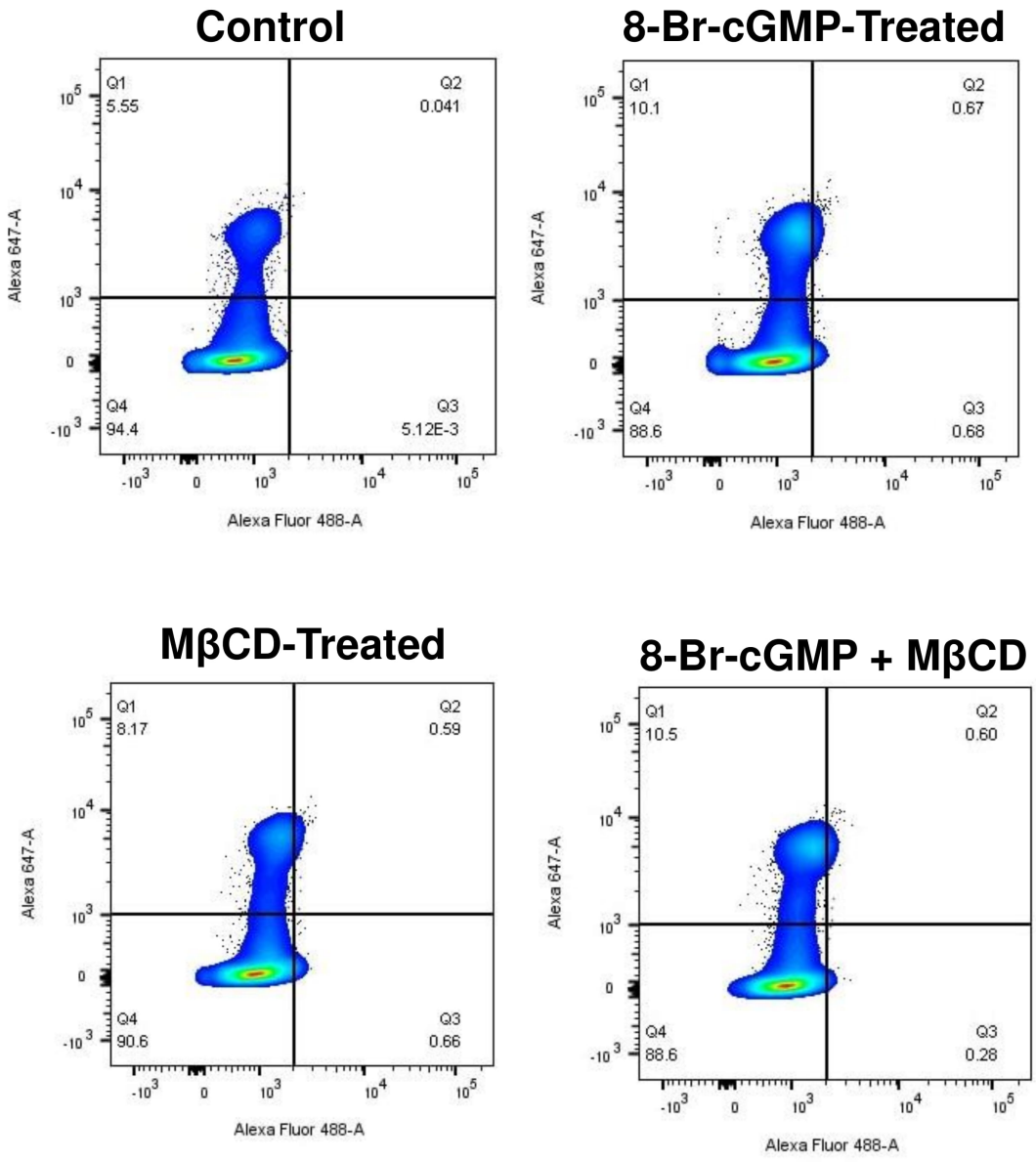


Figure 6.4: Density plots showed that Thr276 fluorescence, detected by Alexa Fluor 488 signal in Q1 and Q2, increased upon cholesterol depletion, 8-Br-cGMP treatment, and simultaneous treatment of both. Total SERT fluorescence was used to normalize phosphorylation events and is represented by Q3 and Q4.

dogenous SERT and in the mutant but the effects of the mutant on membrane microdomain residence is still to be investigated.

While western blot was the method of choice for probing phosphorylation events in

primary neurons, flow cytometry would be utilized for the mutant studies in the stably transfected CHO cell system. Neurons grow on a glial layer and have asymmetrical morphologies, making neuron flow cytometry more challenging. Flow cytometry is a powerful method for probing single cell events with capabilities of detecting up to 17 distinct biomarkers at a time (Thal et al., 2017). I would expect to see increased Thr276 phosphorylation events with the G56A SERT mutant. I also suspect that the coding variant is not susceptible to cholesterol depletion like the wild type SERT is, thus we would not see mobility changes or phosphorylation changes upon cholesterol depletion. I hypothesize that the mutation to alanine disrupts G56A SERT membrane microdomain localization and key associations with the SERT membrane protein-protein interactions, resulting in a dysregulated phenotype. A simulation experiment showing how the mutation affects conformation and SERT interactions with cholesterol in the membrane could be valuable in validating this hypothesis.

To approach these questions, I would utilize the stably transfected wild type and G56A SERT CHO cells used in Chapter 5. To test effects of cholesterol depletion on G56A SERT membrane mobility, cholesterol could be depleted acutely with 5 µM M$\beta$CD, as this treatment should have the most dramatic effect. Once treated, SERT could be tagged with IDT357 and streptavidin-QDs to analyze QD mobility for both G56A and wild type SERT to see if G56A SERT is indeed insensitive to cholesterol depletion.

Flow cytometry would then be performed to probe the effects of the mutation and cholesterol depletion on Thr276 phosphorylation in G56A SERT CHO cells. I demonstrated the capabilities of this approach with wild-type SERT CHO cells but not yet with G56A SERT CHO cells (Fig 6.3). Basal or stimulated cells were incubated with cell stripper for 5 minutes, and cells were dissociated by pipetting up and down. 4% paraformaldehyde was immediately added to the cell suspension to a final concentration of 2% for fixation. After 10 minutes, cells were washed and permeabilized with 100% methanol. Phospho-Thr276 primary antibodies and extracellular SERT antibodies were added to the

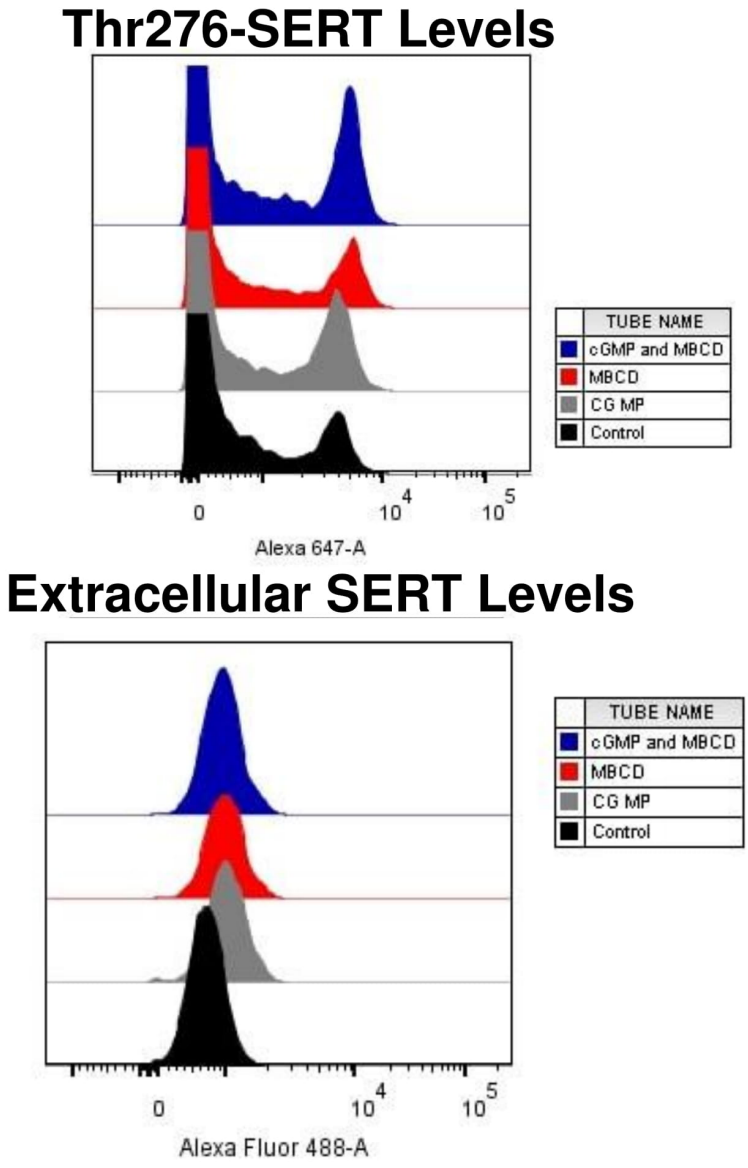


Figure 6.5: Histograms were generated after flow cytometry experiments were performed. The top panel shows phosphorylated Thr276 levels. As can be seen by the size of those histograms, 8-Br-cGMP- and M$\beta$CD-treated cells have the greatest labeling, indicating more phosphorylation. The bottom panel shows total SERT levels.

cells at an optimized concentration of 1:3000. Alexa Fluor 488- (Thr276) or Alexa Fluor 647- (total SERT) conjugated secondary antibodies (1:7000) were then added, and cells

were analyzed by flow cytometry (Fig 6.4). Thr276 fluorescence signal was normalized to total SERT fluorescence to account for any differences in protein amount (Fig 6.5). From these initial experiments, higher phospho-Thr276 labeling was observed in cells treated with 8-Br-cGMP and M$\beta$CD, consistent with western blot data from chapter 4. Normalization to total SERT was included to account for potential differences in SERT expression after treatments. This validated method could be used for the G56A SERT studies as well.

In addition to the flow cytometry studies, cells from each condition could be imaged to quantify levels of phosphorylation visually as well as by flow cytometry. One challenge to note is the fixation process occurs 5-7 minutes after cell stripper has been added, so some phosphorylation events are likely being lost. However, all cells undergo the exact same protocol, so the assumption is made that SERT is being dephosphorylated at roughly the same rate. While the wild type hSERT and G56A SERT CHO cell experiments are useful in elucidating key mechanisms, the ultimate goal is to confirm these mechanisms in the endogenous primary neuronal system. The big challenge for these studies is conducting flow cytometry experiments using primary neurons, as these cells do not exist in single cell suspensions. Western blot is traditionally used to examine phosphorylation events in primary systems, but this method is laborious and ultimately not as sensitive. Thus, another key future direction becomes designing a primary neuron flow cytometry protocol and comparing results with the traditional western blot experimental protocols. Finally, primary neurons are difficult to transfect, but G56A SERT knock in mice have been bred by the Blakely lab (Veenstra-VanderWeele et al., 2009). Thus conducting these studies in neurons dissected from these mice would validate these findings in a primary neuron system.

## 6.4 Final remarks

QDs have become an invaluable tool to the neuroscience community since their first applications in biological labeling and imaging. Because they offer properties ideal for long-

term imaging, including superior photostability, ease of functionalization, large Stokes shift, and narrow emission, they will likely continue to be the probe of choice for biological imaging. I anticipate seeing their popularity rise for tissue and in vivo experiments, where the target of interest can be tracked for long periods of time while retaining brightness and stability in the biological environment. Additionally, I expect to see more efforts be put towards generating monovalent and more compact QDs so that they can be more accessible for 3D imaging in complex environemnts like tissue, as well as tight membrane regions such as the synapse. In summary, QDs have huge potential to shed light on new mechanisms underlying neuropsychiatric diseases, which will hopefully lead to more targeted therapies for millions of affected individuals.

## 6.5 Bibliography

Chang, J. C., Tomlinson, I. D., Warnement, M. R., Ustione, A., Carneiro, A. M. D., Piston, D. W., Blakely, R. D., and Rosenthal, S. J. (2012). Single Molecule Analysis of Serotonin Transporter Regulation Using Antagonist-Conjugated Quantum Dots Reveals Restricted, p38 MAPK-Dependent Mobilization Underlying Uptake Activation. *Journal of Neuroscience*, 32(26):8919–8929.

Dahan, M., Lévi, S., Luccardini, C., Rostaing, P., Riveau, B., and Triller, A. (2003). Diffusion Dynamics of Glycine Receptors Revealed by Single-Quantum Dot Tracking. *Science*, 302(5644):442–445.

Domanov, Y. A., Aimon, S., Toombes, G. E. S., Renner, M., Quemeneur, F., Triller, A., Turner, M. S., and Bassereau, P. (2011). Mobility in geometrically confined membranes. *Proceedings of the National Academy of Sciences*, 108(31):12605–12610.

Farlow, J., Seo, D., Broaders, K. E., Taylor, M. J., Gartner, Z. J., and Jun, Y. W. (2013). Formation of targeted monovalent quantum dots by steric exclusion. *Nature Methods*, 10(12):1203–1205.

Groc, L., Lafourcade, M., Heine, M., Renner, M., Racine, V., Sibarita, J.-B., Lounis, B., Choquet, D., and Cognet, L. (2007). Surface Trafficking of Neurotransmitter Receptor: Comparison between Single-Molecule/Quantum Dot Strategies. *Journal of Neuroscience*, 27(46):12433–12437.

Kitko, K. E. (2018). *Nanomaterial-based approaches to the study of membrane signaling (Doctoral dissertation)*. PhD thesis, Vanderbilt University.

Pierobon, P., Achouri, S., Courty, S., Dunn, A. R., Spudich, J. A., Dahan, M., and Cappello, G. (2009). Velocity, processivity, and individual steps of single myosin V molecules in live cells. *Biophysical Journal*, 96(10):4268–4275.

Prasad, H. C., Steiner, J. A., Sutcliffe, J. S., and Blakely, R. D. (2009). Enhanced activity of human serotonin transporter variants associated with autism. *Philosophical Transactions of the Royal Society B: Biological Sciences*, 364(1514):163–173.

Prasad, H. C., Zhu, C.-B., McCauley, J. L., Samuvel, D. J., Ramamoorthy, S., Shelton, R. C., Hewlett, W. A., Sutcliffe, J. S., and Blakely, R. D. (2005). Human serotonin transporter variants display altered sensitivity to protein kinase G and p38 mitogen-activated protein kinase. *Proceedings of the National Academy of Sciences*, 102(32):11545–11550.

Rahbek-Clemmensen, T., Lycas, M. D., Erlendsson, S., Eriksen, J., Apuschkin, M., Vilhardt, F., Jørgensen, T. N., Hansen, F. H., and Gether, U. (2017). Super-resolution microscopy reveals functional organization of dopamine transporters into cholesterol and neuronal activity-dependent nanodomains. *Nature Communications*, 8(1).

Romay-Tallon, R., Rivera-Baltanas, T., Allen, J., Olivares, J. M., Kalynchuk, L. E., and Caruncho, H. J. (2017). Comparative study of two protocols for quantitative image-analysis of serotonin transporter clustering in lymphocytes, a putative biomarker of therapeutic efficacy in major depression. *Biomarker Research*, 5(1):27.

Thal, L. B., Bailey, D. M., Kovtun, O., and Rosenthal, S. J. (2017). Quantum Dot Toolbox in Membrane Neurotransmitter Transporter Research. In *Membrane Proteins: Chemical and Synthetic Approaches*, pages 219–230.

Veenstra-VanderWeele, J., Jessen, T. N., Thompson, B. J., Carter, M., Prasad, H. C., Steiner, J. A., Sutcliffe, J. S., and Blakely, R. D. (2009). Modeling rare gene variation to gain insight into the oldest biomarker in autism: construction of the serotonin transporter Gly56Ala knock-in mouse. *Journal of Neurodevelopmental Disorders*, 1(2):158–171.